

POLARIMETRIC ROAD ICE DETECTION

by

Krista Drummond

---

Copyright © Krista Drummond 2014

A Thesis Submitted to the Faculty of the

COLLEGE OF OPTICAL SCIENCE

In Partial Fulfillment of the Requirements

For the Degree of

MASTER OF SCIENCE

In the Graduate College

THE UNIVERSITY OF ARIZONA

2014

UMI Number: 1572997

All rights reserved

INFORMATION TO ALL USERS

The quality of this reproduction is dependent upon the quality of the copy submitted.

In the unlikely event that the author did not send a complete manuscript and there are missing pages, these will be noted. Also, if material had to be removed, a note will indicate the deletion.



UMI 1572997

Published by ProQuest LLC (2015). Copyright in the Dissertation held by the Author.

Microform Edition © ProQuest LLC.

All rights reserved. This work is protected against unauthorized copying under Title 17, United States Code



ProQuest LLC.  
789 East Eisenhower Parkway  
P.O. Box 1346  
Ann Arbor, MI 48106 - 1346

## STATEMENT BY AUTHOR

This thesis has been submitted in partial fulfillment of requirements for an advanced degree at the University of Arizona and is deposited in the University Library to be made available to borrowers under rules of the Library.

Brief quotations from this thesis are allowable without special permission, provided that an accurate acknowledgement of the source is made. Requests for permission for extended quotation from or reproduction of this manuscript in whole or in part may be granted by the copyright holder.

SIGNED: Krista M. Drummond

## APPROVAL BY THESIS DIRECTOR

This thesis has been approved on the date shown below:

\_\_\_\_\_  
Russell A. Chipman  
Professor of Optical Science

December 8, 2014  
Date

## ACKNOWLEDGEMENTS

Thanks to Nalux and Omron Corporations for funding this investigation.

Thanks to Dr. Russell Chipman for providing me with the opportunity to work on this project.

And a special thanks to Lisa Li and Karlton Crabtree for their technical support.



## DEDICATION

This thesis is not only the result of a polarization experiment, it is the embodiment of my time spent as a graduate student, and as such should include a note on the people that helped push me forward. These were the people present during my struggle, as either the bellows which heated the fire in which I was being forged, or as the cooling water reminding me that everything was alright; each important in their own way. This is how I will remember their impact.

First, I dedicate this work to my parents. Since the very beginning you were fostering a desire to discover the world around me, in ways that built confidence in my own abilities. You taught me to trust myself, and to never let defeat keep me from my dreams. You gave me strength.

Secondly, I dedicate this work to Dr. Wataru Nakagawa. I blame you for all this. I would never have been capable of surviving graduate school without having learned how to survive your lab first. I will never be able to thank you enough for the experience.

Finally, and perhaps most importantly, I dedicate this to my fellow graduate students. What we go through is hard; it changes us. Without the support of each other, defeat is almost guaranteed. So, it is when one of us succeeds, that we all succeed. I will continue to celebrate all of your triumphs, from afar if I must.

I love you all so very much: Tony, Christine, John, Kelsey, Eric, Shaun, Stacey, Lisa, Jason, Trent

Someday I may look back at this and gasp at my own sappy words, but I refuse to leave this out.

I want to remember exactly how I feel at this moment. When will I again get the chance to show my affection and love for the ones who have helped me get to this point? This is a must.

So future Krista, stop blushing.

Be proud. Remember what it was like as a 24 year old student, sitting in a coffee shop, overwhelmed from trying to do too much in too little time, tired from a night out with friends. Remember that your bread and water back then was laughter and philosophy, late nights and long drives. Remember what it was like to start over. Remember how much you loved every stressed out minute of this crazy struggle. Remember that it was both too much time, and not enough, never enough time.

Love is a funny thing.

## TABLE OF CONTENTS

List of Figures	7
List of Tables	9
Abstract	10
<b>Chapter 1: Introduction</b>	<b>11</b>
1.1 Problem to be addressed	11
1.2 Benefits of Road Ice Detection	13
1.3 Background and Literature Review	14
1.4 New Developments and Principle Results	15
1.5 Research Objective and Method	16
<b>Chapter 2: Methodology</b>	<b>17</b>
2.1 Instruments/Apparatus	18
2.1.1 Visible Polarimeter	18
2.1.2 UV Polarimeter	19
2.1.3 Chiller	21
2.1.4 Liquid Nitrogen Cooling Plate	22
2.2 Subjects/Samples	24
2.2.1 Roadway Samples	24
2.2.2 Surface Conditions	26
2.3 Data Collection/Sampling	28
2.3.1 Complete Muller Matrix Measuring	28
2.3.2 Visible Polarimeter Measurement Angles – Diffuse	34
2.3.3 UV Polarimeter Measurement Angles – Specular and Near Specular	34

<b>2.4</b>	<b>Data Analysis/Statistical Procedures</b>	<b>35</b>
<b>2.4.1</b>	<b>Polarization Properties – Histograms</b>	<b>36</b>
<b>2.4.2</b>	<b>Receiver Operator Curves</b>	<b>38</b>
	<b>Chapter 3: Results</b>	<b>40</b>
<b>3.1</b>	<b>Campaign 1: Visible Polarimeter, Normal Camera Angle of Scatter (0°)</b>	<b>40</b>
<b>3.2</b>	<b>Campaign 2: UV Polarimeter, Specular and Near Specular Angles</b>	<b>53</b>
<b>3.3</b>	<b>Campaign 3: NIR Measurement, Wet Sample Measurement, and System Repeatability</b>	<b>64</b>
<b>3.3.1</b>	<b>NIR Measurement</b>	<b>64</b>
<b>3.3.2</b>	<b>Wet Sample Measurement</b>	<b>66</b>
<b>3.3.3</b>	<b>System Repeatability</b>	<b>73</b>
	<b>Chapter 4: Discussion</b>	<b>75</b>
<b>4.1</b>	<b>Result Implications (Results Viewed in Larger Context)</b>	<b>76</b>
<b>5</b>	<b>Chapter 5: Conclusions</b>	<b>80</b>
<b>5.1</b>	<b>Summary</b>	<b>80</b>
<b>5.2</b>	<b>Future Considerations</b>	<b>81</b>
	<b>Appendix A – Supplemental Data</b>	<b>86</b>
	<b>Bibliography</b>	<b>95</b>

## LIST OF FIGURES

<b>FIGURE</b>	<b>PAGE</b>
<b>Figure 1.1:</b> Hydroplaning	12
<b>Figure 1.2:</b> Refreeze Ice	13
<b>Figure 1.3:</b> The data analysis process	17
<b>Figure 2.1:</b> Visible spectrum polarimeter in the polarization lab, range 400-750 nm	19
<b>Figure 2.2:</b> Ultraviolet spectrum polarimeter in the polarization lab, range 350-550 nm	20
<b>Figure 2.3:</b> Chiller	22
<b>Figure 2.4:</b> Liquid nitrogen cooling plate for UV polarimeter	23
<b>Figure 2.5:</b> Concrete samples which have been mounted to steel plates using epoxy	25
<b>Figure 2.6:</b> Asphalt samples which have been mounted to steel plates using epoxy	25
<b>Figure 2.7:</b> Method to freeze ice	27
<b>Figure 2.8:</b> Iced asphalt sample	28
<b>Figure 2.9:</b> Mueller Matrix Image	31
<b>Figure 2.10:</b> Visible polarimeter angular setup	34
<b>Figure 2.11:</b> UV polarimeter angular setup	35
<b>Figure 2.12:</b> Comparing histograms	36
<b>Figure 2.13:</b> Full Width at Half-Maximum	37
<b>Figure 2.14:</b> Elements of a ROC curve	38
<b>Figure 2.15:</b> Non-Ideal Case ROC Curve	39
<b>Figure 2.16:</b> Ideal Case ROC Curve	39
<b>Figure 3.1:</b> Depolarizaion Index response for asphalt sample A-1 and concrete sample A-1	42
<b>Figure 3.2:</b> ROC curves for the Depolarization Index property for asphalt sample A-1 and concrete sample A-1	44
<b>Figure 3.3:</b> Linear Diattenuation response for asphalt sample A-1 and concrete sample A-1	45
<b>Figure 3.4:</b> ROC curves for the Linear Diattenuation property for asphalt sample A-1 and concrete sample A-1	46
<b>Figure 3.5:</b> Linear Polarizance response for asphalt sample A-1 and concrete sample A-1	47
<b>Figure 3.6:</b> ROC curves for the Linear Polarizance property for asphalt sample A-1 and concrete sample A-1	49
<b>Figure 3.7:</b> ROC curves for the Linear Retardance property for asphalt sample A-1 and concrete sample A-1	50

<b>Figure 3.8:</b> ROC curves for the Circular Diattenuation property for asphalt sample A-1 and concrete sample A-1	51
<b>Figure 3.9:</b> ROC curves for the Circular Polarizance property for asphalt sample A-1 and concrete sample A-1	52
<b>Figure 3.10:</b> ROC curves for the Circular Retardance property for asphalt sample A-1 and concrete sample A-1	53
<b>Figure 3.11:</b> Linear Retardance response for asphalt sample B-1	56
<b>Figure 3.12:</b> ROC curves for the Linear Retardance property for asphalt sample B-1	57
<b>Figure 3.13:</b> Linear Diattenuation response for asphalt sample A-2	58
<b>Figure 3.14:</b> ROC curves for the Linear Diattenuation property for asphalt sample A-2	59
<b>Figure 3.15:</b> Linear Polarizance property for asphalt sample A-2	60
<b>Figure 3.16:</b> ROC curves for the Linear Polarizance property for asphalt sample A-2	61
<b>Figure 3.17:</b> Depolarization Index response for concrete sample A-3	62
<b>Figure 3.18:</b> ROC curves for the Depolarization Index property for concrete sample A-3	63
<b>Figure 3.19:</b> NIR measurement polarization property responses	65
<b>Figure 3.20:</b> Depolarization Index had highest discrimination	66
<b>Figure 3.21:</b> DI and LD responses for wet to dry progression measurement	70
<b>Figure 3.22:</b> LP and LR responses for wet to dry progression measurement	71
<b>Figure 3.23:</b> System repeatability	74
<b>Figure 5.1:</b> Natural environmental light intensity fluctuates over time	83
<b>Figure 5.2:</b> Multiple source, single detector, two-pole system	84
<b>Figure 5.3:</b> Single source, multiple detector, two-pole system	85

## LIST OF TABLES

TABLE	PAGE
<b>Table 3.1:</b> Visible polarimeter measurements	41
<b>Table 3.2:</b> UV polarimeter measurements	54
<b>Table 3.3:</b> The progression measurement from a dry surface state to a wet surface state back to a dry surface state	67
<b>Table 3.4:</b> Progression measurement surface values	73
<b>Table 4.1:</b> Polarization Property as a discriminator	76

## ABSTRACT

Ever since automobiles became affordable for the average American, with the introduction of the Ford Model T in 1908, making driving safer has been a priority. While driver intoxication and distraction are the leading causes of automotive fatalities, poor road conditions increase the frequency and deadliness of these incidents. Monitoring road conditions for thousands of miles of road is a huge undertaking, one too large for human surveillance. Automated systems capable of detecting and reacting to dangerous road conditions would be life-saving. These systems could be mounted to the sides of road and notify an operator of conditions in real-time. Drivers could be warned, action taken, and many lives saved.

This thesis investigated the science behind polarimetric road ice detection systems. Laboratory Mueller matrix measurements of a simulated road under differing surface conditions were collected searching for a discriminatory polarization property. These Mueller matrices were decomposed into depolarization, diattenuation, and retardance. Individual sample surface polarization properties were then calculated from these three unique matrices and compared. Simulated road samples were measured under many wavelengths and angles, which gave us a larger data library from which to observe trends. Specular and off-specular reflection responses of each sample were also collected. Four polarization properties stood out for having high separation between dry and iced measurements: Depolarization Index, Linear Diattenuation, Linear Polarizance, and Linear Retardance.

Through our investigation polarimetric ice detection is possible. Continued research of the polarization properties of road ice can result in the development of a road ice detection system. Proposed deployment methods of such a system have been outlined following the analysis of the data collected in this experiment. Not only is polarimetric ice detection an exciting and novel use of polarization, it has the potential to improve road safety through real-time ice response measures.

## **Chapter 1: Introduction**

This thesis investigated the science behind polarimetric road ice detection systems. Laboratory Mueller matrix measurements of a simulated road under differing surface conditions were conducted in the hopes of finding a discriminatory polarization property. After collecting Mueller matrix images of multiple samples, these Mueller matrices were decomposed into depolarization, diattenuation, and retardance. Depolarization index, linear diattenuation and linear polarizance all discriminated between dry and iced surfaces. Continued research of the polarization properties of road ice can result in the development of a road ice detection system. Proposed deployment methods of such a system have been outlined following the analysis of the data collected in this experiment.

### **1.1 Problem to be addressed**

Ever since automobiles became affordable for the average American, with the introduction of the Ford Model T in 1908, making driving safer has been a priority. Today, this is a world wide effort. While driver intoxication and distraction are the leading causes of automotive fatalities, poor road conditions increase the frequency and deadliness of these incidents. Monitoring road conditions for thousands of miles of road is a huge undertaking, one too large for human surveillance. Automated systems capable of detecting and reacting to dangerous road conditions would be life-saving. These systems could be mounted to the sides of road and notify an operator of conditions in real-time. Drivers could be warned, action taken, and many lives saved.

Such road ice detection systems would need to robustly detect dangerous road conditions, in this case, ice and thin layers of water. By reducing the traction between road and tire, cars slip and drivers lose control. Two of the most dangerous types of ice, known for their smooth surfaces, are melt ice and refreeze ice.



Melt Ice is responsible for automobile hydroplaning or aquaplaning. Hydroplaning occurs when car tires are lifted up onto a thin layer of liquid water because of water pressure in front of the tire. Figure 1.1 diagrams hydroplaning. Aquaplaning occurs when liquid water acts as a lubricant, reducing tire traction, sometimes occurring when a slush mix of ice and water is pressed into tire traction grooves. Melt ice creates traction-reducing conditions similar to a rainstorm. When rain begins to fall onto dry roads, it combines with oils and grease left behind by traffic, drastically reducing traction between road and tire.

Refreeze ice undergoes a melting and refreezing process similar to annealing. This can allow the surface to become much smoother, further reducing traction. Refreeze ice is more commonly known as “Black ice” because of its highly transparent, and thus harder to see, characteristic. Figure 1.2 diagrams the structure of refreeze ice.

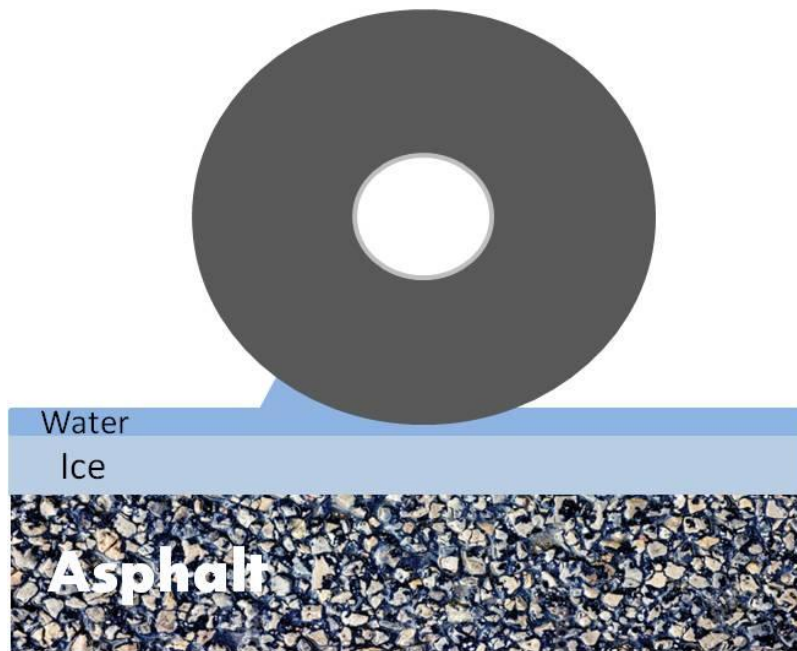


**Figure 1.1: Hydroplaning:** An automobile tire relies on traction to move an automobile forward. When water is present on a road, water pressure in front of a tire can lift up a tire and effectively reduce the traction between the road and the tire to zero, causing hydroplaning.

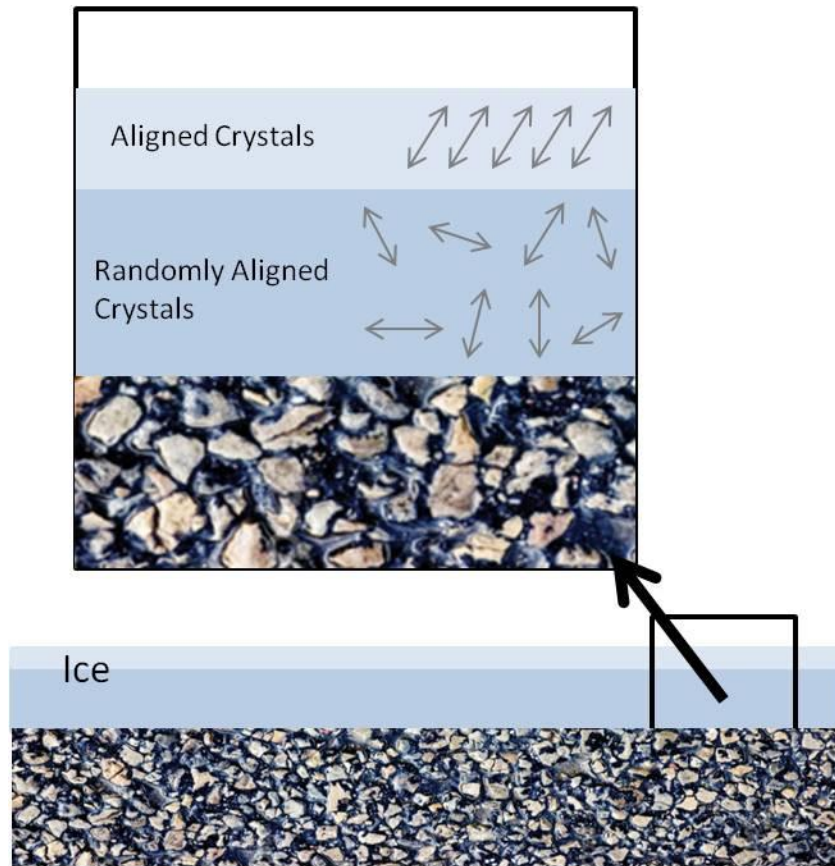


**Figure 1.2: Refreeze Ice:** Refreeze ice occurs when previously frozen water is heated such that the top few millimeters return to liquid form. This water is then refrozen slowly, allowing the water particles to align. These aligned crystals create a much smoother surface than the originally frozen water surface.

## 1.2 Benefits of Road Ice Detection

Road ice detection could be an important technology for many reasons. First, road ice detection reduces environmental and infrastructure harm. Spraying chlorine deicing agent ( $\text{CaCl}_2$ ) to combat the risk of ice based on weather reports, leads to over-use. Excessive spraying of chlorine damages the planting and farmland along roads. Excessive chlorine spraying also damages the steel in construction of bridges, rail guards, etc. Remote sensing, the proposed method of detection, also reduces environmental impact by allowing the device to be small while maintaining the ability to measure vast areas.

Second, road ice detection is projected to be more cost effective than other modes of road surface maintenance. Electric road heating to melt ice is difficult to construct, and has fragile subterranean architecture. Not only is installation costly, but it would require large installation times, and would consume huge amounts of electrical power. More energy is needed to heat ice from  $-1^{\circ}\text{C}$  to  $0^{\circ}\text{C}$ , melting it, than is needed to raise it from  $1^{\circ}\text{C}$  to  $80^{\circ}\text{C}$ . Alternatively, cameras might be easily outfitted with polarization monitoring technology and mounted to observe high ice risk road spots. This would be cheap and requires very small construction or installation time.

Finally, detecting icy roads and providing warning will save human lives. Signaling when and where ice is forming will prod drivers to be cautious and slow down, reducing the probability of an accident. It will also become a powerful feedback system. When ice is detected, the sensor can also signal a request to spray that area with an ice melting agent. When ice is not present, no matter the other weather conditions predicting ice, no melting agent will be sprayed, thus making this a very efficient method of maintaining optimal road conditions while not over compensating when unnecessary.

### **1.3 Background and Literature Review**

Most previous work for optical ice sensing to determine road conditions relied on red light intensity measurements and weather reports. For example, a road would normally scatter and absorb red light leading to low reflectance intensity. However, if frost or snow is present on the road surface the road would brighten, increasing the reflection intensity, allowing the camera operator to sense poor driving conditions. While this red light method works for certain types of precipitation, i.e. clean snow, frost, hail, it is not robust enough to detect more subtle but dangerous road conditions like black ice and rain. It allows for large error, for example, ice can occur in shade (low reflectivity) where a temperature measurement would fail to recognize an ice possibility; also low reflectivity encompasses both the road state with highest traction (dry), and the road state with lowest traction (black ice). This approach is

incomplete and, in the presence of significant polarization-dependent scattering, will encompass much error [Miller]. A polarimetric system would gather more information than a conventional camera system; it would deliver an analysis of the reflected lights' electric field.

Polarization is a successful tool to measure many different aspects of the natural world. Polarization of light comes from the atomic structure and vibrations of a material, thus it contains hard to measure atomic qualities and construction information. Because polarization is a physical property of radiated light, this information can be gathered using remote sensing techniques, allowing for a wide variety of application. Atmospheric aerosol concentration and makeup have been measured using polarimetric remote sensing, aerial mapping can now include land use information due to polarimetric elemental sampling [Najibi], and solvent concentrations can be identified using polarimetry. Polarimetry is also the principal method to measure solar magnetic fields.

Polarimetry is a new avenue to take towards creating a system capable of accurately measuring road surface conditions. Research has investigated polarimetry for sea ice [Miller] and atmospheric ice, however little has been done to investigate thin layers of ice on solid substrates. Since the ice is thin and the substrates below are dark, we expect road ice to be different from solid ice, like sea ice. Reflection from dielectric surfaces such as calm water, wet leaves, or other shiny non-metallic objects is often polarized [Chronin]. We have researched similar polarizing behavior in our road ice experiment.

#### **1.4 New Developments and Principle Results**

Our research explored *Polarization Imaging* for the detection of ice on asphalt and concrete. The presence of ice significantly changes the polarization response of surface-reflected light. It has shown the potential to improve road safety through real-time ice response measures. Polarimetric ice detection is possible. Linear diattenuation, linear polarizance, and depolarization index all consistently showed high quality Receiver Operator Curves (ROC). Measurement of these polarization properties is

promising to distinguish between a safe dry road and a slick iced road. Continued investigation and experimentation should result in a method of polarimetric road ice detection.

## **1.5 Research Objective and Method**

The objective of this research is to determine if thin layers of ice can be detected through polarimetric imaging and polarization metric comparisons. Polarimeters were used to generate polarized light and image the Mueller matrix of simulated road samples. Each Mueller matrix is then decomposed into three unitary matrices: depolarization, retardance, and diattenuation. These three matrices are then used to calculate different polarization properties including:

- Depolarization Index
- Linear Diattenuation
- Circular Diattenuation
- Linear Retardance
- Circular Retardance
- Linear Polarizance
- Circular Polarizance

These polarization properties were recorded as 2D images of the measured surface where each pixel had an individual polarization property value. Each image was broken down into pixels and organized into histograms, grouping same-valued pixels together and creating a distribution of values. Histograms (of the same polarization property) were then compared across surface conditions. Receiver Operator Characteristic (ROC) curves were then used to analytically distinguish between a good and a poor polarimetric ice-dry discriminator. This process is illustrated in Figure 1.3.

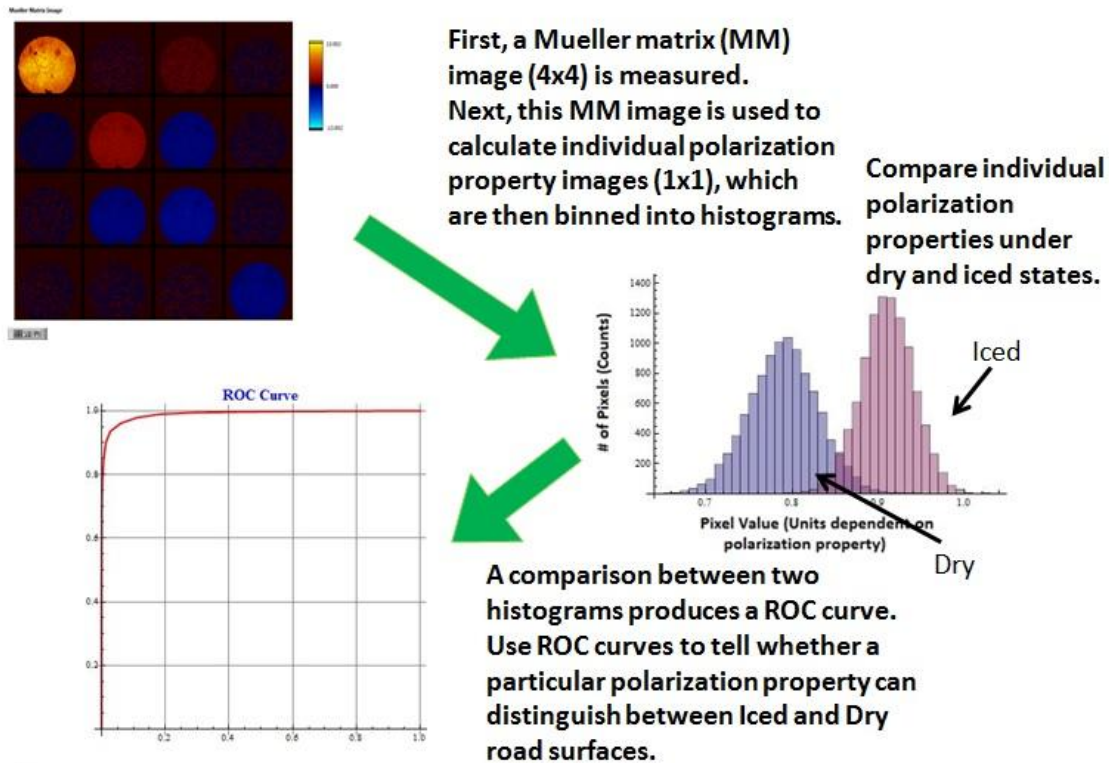


**Figure 1.3: The data analysis process:** First, raw data is collected as Mueller matrix images. These images are then reduced to ten polarization properties. Next, the polarization property images are then broken down into a value distribution, a histogram. Finally, these histograms are compared to each other, resulting in ROC curves which analytically describe the polarization property's ability to discriminate between dry and iced road samples.

## Chapter 2: Methodology

Investigating the use of polarimetry in road ice detection was done with a highly controlled optical scattering experiment to acquire scientific polarization signatures of road materials, water, and ice. This experiment was done in a lab, with well controlled temperature environment. Light source wavelength, angle of incidence, and angle of scatter were monitored and manipulated to gather phenomenology. A complete Mueller Matrix imaging polarimeter was used for data collection. Data collection was done by illuminating a test sample and measuring the effect on scattered polarized light. Multiple measurements of multiple dry and iced samples were made. Finally, data was analyzed for

significant statistical differences between dry and iced measurements. Because of the highly controlled nature of these measurement conditions, they do not represent the varied and non-ideal conditions found on real roads, and do not represent the equipment most likely to be used alongside roads.

## **2.1 Instruments/Apparatus**

A Mueller matrix polarimeter was used to measure the polarization properties of the roadway samples. Testing many different wavelengths for polarization property changes utilized two different polarimeters. Each polarimeter, visible and ultraviolet (UV), was made up of a light source, a camera, and a series of linear polarizers and retarders. Preserving the integrity of the ice samples was also a consideration. Keeping the temperature of the sample at a fixed value below freezing was done using two methods: a temperature controlled chiller and a liquid Nitrogen cooling plate. The liquid Nitrogen cooling plate was used for measurements on both polarimeters, while the temperature controlled chiller was used only for measurements on the visible polarimeter.

### **2.1.1 Visible Polarimeter**

The polarimeter used to collect data in the visible spectrum, contains a polarization generator and a polarization analyzer integrated on a rotating arm. Figure 2.1 shows how this visible polarimeter was mounted to a two armed rotating rail system. One arm, free to rotate about the sample, housed the polarization generator. The polarizer consisted of a narrowband wavelength light source (an Oriel Spectral Illuminator, model 69050), an Ealing Glan-Thompson polarizer (model 43-6949) and a 127° retarder. The second arm, a static rail, housed the polarization analyzer. The analyzer consisted of a 127° retarder, an Ealing Glan-Thompson polarizer (model 43-6949), and a Hamamatsu Photonics CCD camera model C4742-95-12ER.

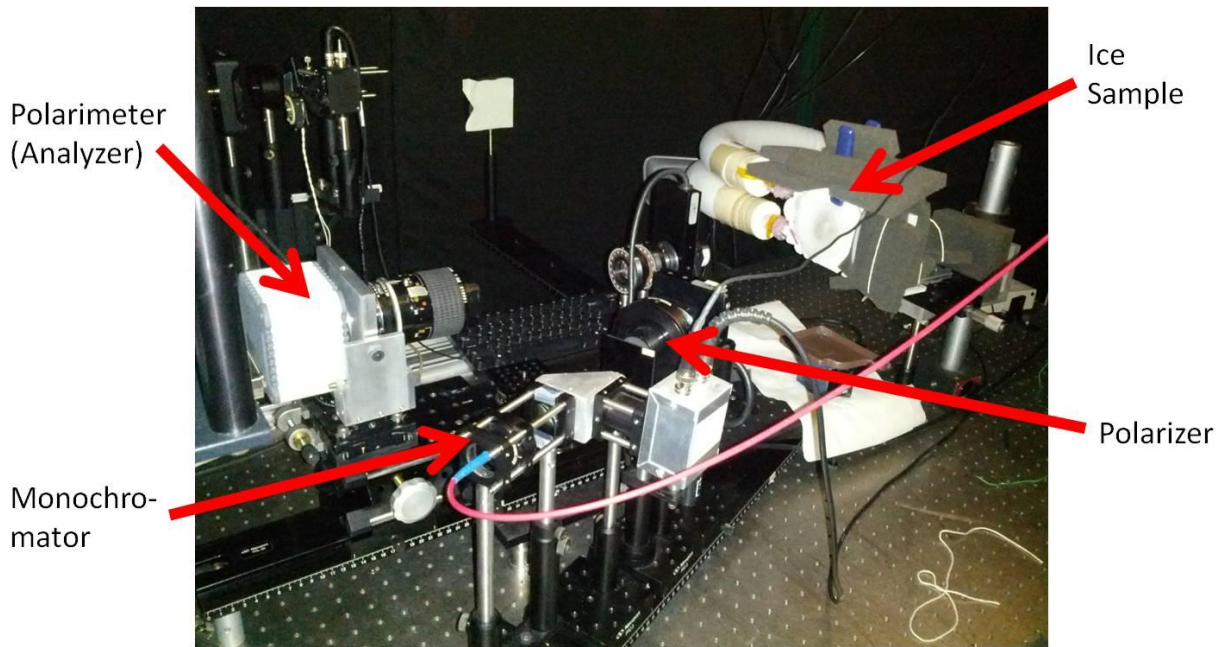


Figure 2.1: Visible spectrum polarimeter in the polarization lab, range 400-750 nm.

A linear rotation stage was used to connect these two arms such that the rotation stage was mounted onto the static arm, and the free to move arm (containing the camera) was mounted on top of the rotation stage. A sample was then mounted to the rail above this crux. The sample was then mounted so that the camera focused on the sample, its back reflection aligned with the source. The camera arm was then rotated to varying angles collecting measurements of diffuse reflections off the sample surface.

Both the polarizing and analyzing  $127^\circ$  retarders were mounted into motorized rotation stages, Newport Stepper Motor model SR50PP; axis of rotation along the light path. Each of these computer controlled rotation stages cycle through eight different positions during a full Mueller Matrix measurement, creating 64 unique retarder combinations, and in turn 64 polarization measurements. These 64 images are then processed to make the Mueller Matrix, which is then used to calculate the polarization properties [Chipman].

### 2.1.2 UV Polarimeter



The polarimeter used to collect the polarization data in the visible and near ultraviolet, UV, was a light source and camera system. Figure 2.2 shows how this UV polarimeter was mounted to a two armed motorized linear rotation stage. One arm, a static rail arm, housed the light polarizer. The polarization generator consisted of a narrowband wavelength light source, (a Spectral Products CM110 1/8 m monochromator), a linear polarizer and a 127° retarder. The second arm, a free to move rail, housed the light analyzer. The polarization analyzer consisted of a 127° retarder, a linear polarizer, and a Hamamatsu EM-CCD digital camera, model C9101-13, controlled using a Newport motion controller, model ESP301.

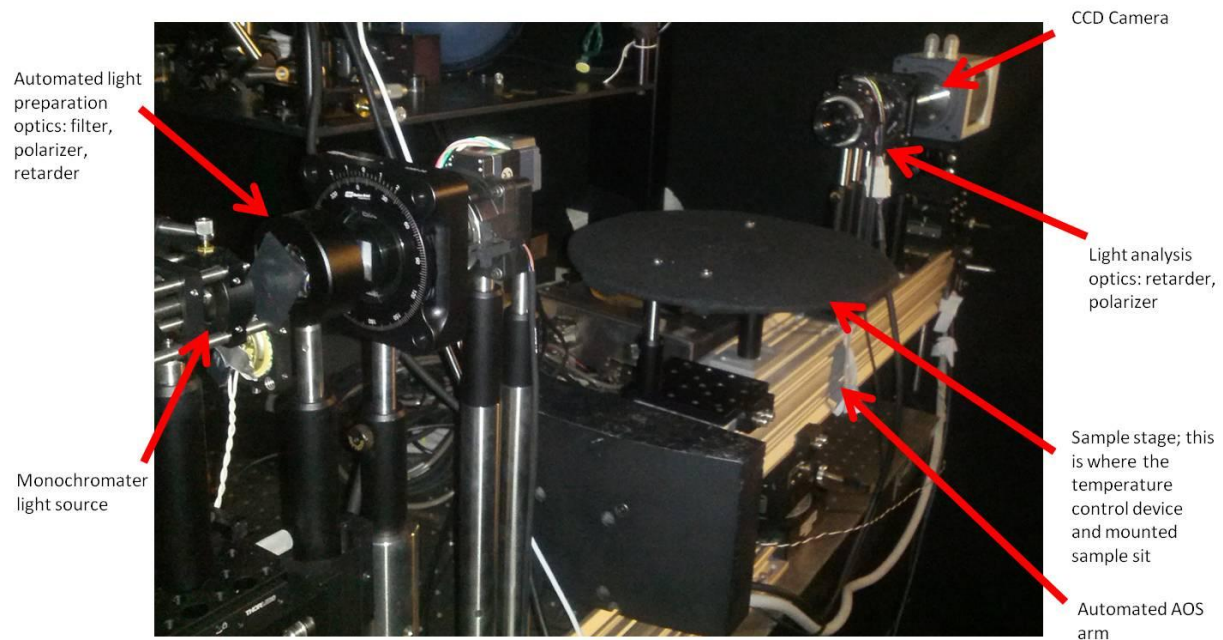


**Figure 2.2: Ultraviolet spectrum polarimeter in the polarization lab, range 350-550 nm.**

A Newport URS100 BPP motorized linear rotation stage rotates the polarization generator such that the rotation stage was mounted onto the static arm, and the free to move arm (containing the camera) was mounted on top of the rotation stage. A stage was then mounted above this crux, and the sample was placed on the stage. This setup allowed for the sample to be mounted so that there is an angle with respect to the sample surface normal and with respect to both the light source and the camera at varying degrees. For example, the motorized linear rotation stage was used to rotate the

camera arm to a value of X degrees. Then the sample was placed on the stage and angled so that it was in focus of the camera and had its back reflection aligned with the source. The camera arm was then rotated to 2X degrees for a specular measurement.

Both the polarizing and analyzing 127° retarders were mounted into motorized rotation stages, Newport Stepper Motor model SR50PP; axis of rotation along the light path. Each of these rotation stages cycle through eight different positions during a full Mueller Matrix measurement, creating 64 unique retarder combinations, and in turn 64 polarization measurements. These 64 images are then processed to make the Mueller Matrix, which is then used to calculate the polarization properties.

### **2.1.3 Chiller**

One method of keeping the temperature of the sample low enough to sustain ice in its solid form was to use a chiller, on loan from the Jet Propulsion Laboratories. The chiller was a large gray control box, with a flexible but stiff arm, the end of which had a flat aluminum cooling plate. Chilled antifreeze was continually cycled through the arm and plate. This machine was capable of keeping the surface of a dry asphalt sample at -5°C for a time period of four hours. This was sufficient for sustaining a 0.6 cm thick ice layer on top of the sample without observing any kind of ice surface degradation.

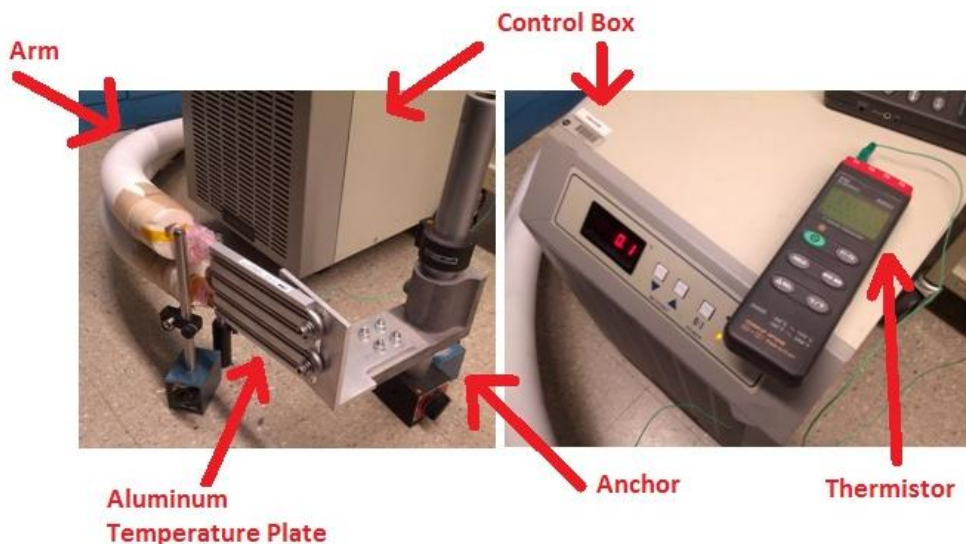


**Figure 2.3: Chiller:** (Right) Close up of the chiller control panel and the thermistor used to monitor surface temperatures; (left) the padded chiller arm is shown here connecting the control box to the aluminum temperature plate. Notice that the temperature plate is secured to an anchoring post to negate the force applied by bending the stiff chiller arm.

The arm of the chiller was secured to the optical table, and extended the flat aluminum temperature plate over the crux of the polarimeter. The temperature plate was then fastened to a 3-D translation stage and mounted to the optical table. Samples were hung from the temperature plate, via the steel mounting plate cutouts, and aligned. Figure 2.3 shows the chiller. Figure 2.1 shows the installed chiller, sample mounted and water containment precautions in place, ready for a measurement.

In order to reduce the amount of energy expended by the chiller and reduce stray light scattering, black insulating foam was tied around all of the exposed portions of the temperature plate. A small brown tray was placed below all iced or wet samples to catch any stray water in case of a chiller malfunction or temperature fluctuation that would cause melting. A paper towel was placed below the tray for a second layer of protection.

#### 2.1.4 Liquid Nitrogen Cooling Plate

Mounting the chiller into the UV polarimeter was not practical due to the tube connecting the control box to the cooling plate, and its associated forces. While the arm was flexible it was very stiff and exerted large reciprocal bending forces, too large for the UV polarimeter arm to balance. A new system for keeping the sample cool was designed and can be seen in Figure 2.4. Utilizing the well below freezing temperature of liquid Nitrogen, a cooling plate was developed. An aluminum plate, acting as a heat sink, was affixed to the side of a large Styrofoam cup using epoxy. The cup was then filled with liquid Nitrogen and a lid was placed over the cup opening to contain any fog. A cable was threaded through holes drilled in the top of the cup and anchored to the opposite side. The sample was then hung from the cable and tied so that the steel plate was held flush with the aluminum heat sink.

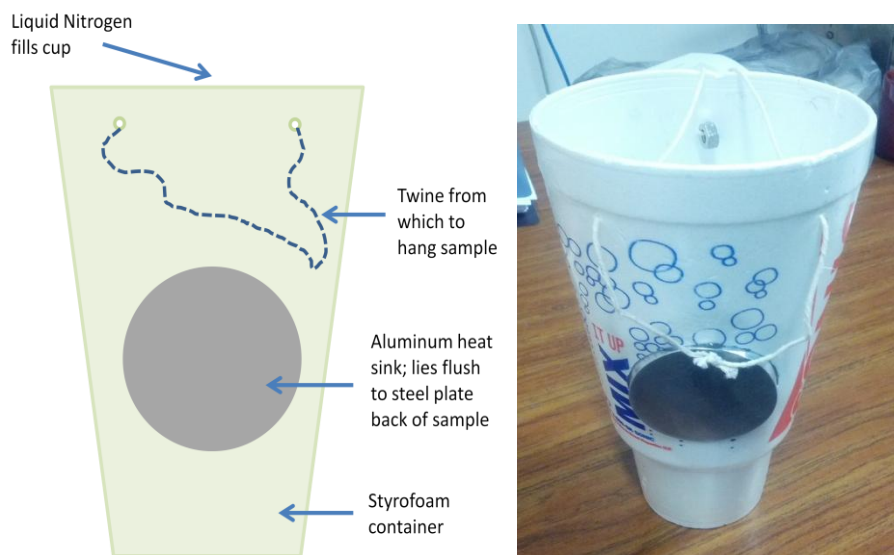


**Figure 2.4: Liquid nitrogen cooling plate for UV polarimeter:** The image above is of the temperature control device used in the measurements on the UV polarimeter.

This cooling method was ideal, because it was compact and could be mounted into the UV polarimeter. It was placed on the sample stage, liquid Nitrogen was added, the sample was hung/mounted, and ready for alignment. The stage was a round plastic dish covered in black felt both to reduce stray light reflections and to catch any water droplets in the event of a temperature fluctuation.

## **2.2 Subjects/Samples**

Simulating a road was done by collecting small samples of actual roadway material, i.e. concrete and asphalt. These samples were then mounted to a steel plate so that they could be installed in the polarimeter. Samples were then frozen, wetted, or measured dry to gather polarimetric information on each sample under each surface condition.

### **2.2.1 Roadway Samples**

Only samples that were deemed good examples of local roadway surfaces were chosen and used during testing. Qualities of a suitable sample were: varying surface geometry (i.e. clearly a non-homogeneous solid, gravel in asphalt and crystals in concrete can be seen with the naked eye), a relatively large flat surface for measurement, a lack of paint or other substances used in road markings, and typical colorings (i.e. gray colored concrete, and black asphalt). These samples, on average, were about 6.5 cm by 4.5 cm, with thicknesses varying from 0.5 cm to 2 cm. Each roadway sample was mounted to a 10 cm X 10 cm steel plate using epoxy, and cured overnight before testing began. Figure 2.5 shows the mounted concrete samples, and Figure 2.6 shows the mounted asphalt samples. Note that the steel plates used for mounting have four hook-like cutouts. These cutouts were used for mounting the sample onto the temperature regulating device, i.e. the chiller or liquid Nitrogen cooling plate.



Figure 2.5: Concrete samples which have been mounted to steel plates using epoxy.



Figure 2.6: Asphalt samples which have been mounted to steel plates using epoxy.

### 2.2.2 Surface Conditions

Each roadway sample was measured under iced and dry conditions, including a few samples measured under wet conditions. For example, a concrete sample was measured when dry, when sprayed with water, and when covered in ice. Each dry measurement became the baseline, so any measured polarization changes are attributed to the surface condition of the sample. The highly variable nature of the surface topography of these roadway materials required that each physical sample is measured in the dry condition. This way, measurements may be zeroed out. In retrospect, smoother samples would have been more scientifically useful; they would have allowed for smaller polarization changes to be observed.

A series of measurements examined the effects different amounts of liquid water on the surface reflection polarization measurement. To obtain different amounts of water on the surface of the vertically mounted sample, a spray bottle filled with deionized water was used. The number of spritzes sprayed onto the surface was small (2 sprays) to measure a small amount of water, and increased incrementally with measurements to analyze the polarization effects vs. liquid water thickness. Along with moderating the number of sprays, a measurement of the surface resistivity was conducted. Due to the conductive nature of liquid water, higher resistances indicate minimal amounts of water while lower resistances (within  $k\Omega$  range) indicate larger amounts of water.

To create ice on the surface of these road samples, each sample was individually suspended in a tray of liquid water and then placed in a freezer overnight. Once the ice has frozen solid, the samples are removed from the trays in a fashion similar to popping ice cubes out of an ice tray. If any cracks formed from this popping motion the sample was cleaned off and refrozen. This ice creating system is depicted in Figure 2.7.



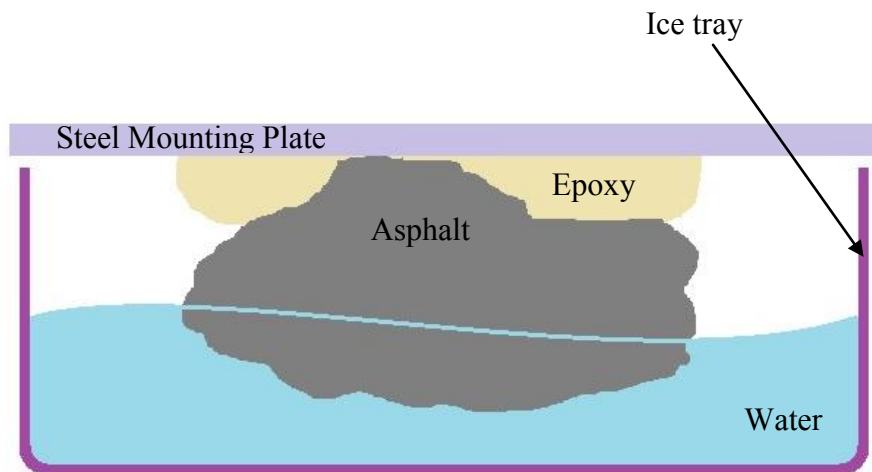


**Figure 2.7: Method to freeze ice:** Ice is formed on the surface of a sample by partially submerging the mounted sample in an ice tray filled with deionized water. After the water has solidified, the sample is popped out of its tray and mounted into a polarimeter.

These ice trays form a very flat ice surface for measuring. This is ideal because a flat surface has minimal friction, the case of most interest for measuring the safety of roadways. These ice samples, while having a very controlled growing process, had their own unique internal structures and imperfections which could have an effect on polarized light. For example, in Figure 2.8 one can clearly see air bubbles trapped at the surface of the sample, lateral cracks which permeate from the top of the ice to the asphalt surface, and cloudiness (loss of clarity) due to either surface ice crystals or internal crystal lattice impurities. However, because of the highly variable nature of natural road ice formation, these imperfections were not corrected.





**Figure 2.8: Iced asphalt sample:** The spherical white-ish shapes are frozen trapped air bubbles, and the long sweeping lines (one of which can be seen on the bottom left section of the image) are fissures in the ice. Note there are sections of high and low clarity which occur naturally

### **2.3 Data Collection/Sampling**

The polarized scattering information collected from a measurement came in the form of a Mueller Matrix (MM) image. These Mueller matrices were then compared with each other to find differences which would indicate the presence of ice. These comparisons were done using Receiver Operator Characteristic (ROC) curves which indicate the degree of “sameness” of two data sets.

#### **2.3.1 Complete Muller Matrix Measuring**

Light from a monochromator, with a 5 nm bandwidth, is shone through a linear polarizer to polarize the light in a single direction. Then the light travels through a variable axis retarder (retarder

mounted in a motorized rotation stage) which controls the polarization state of the light output, i.e. circularly, elliptically, or linearly polarized. Light is then sent through a non-polarizing beam splitter, which siphons off a percentage of the light to a reference detector. This allows for any intensity fluctuations from the source to be measured and removed from the final intensity measurements at the analyzer.

The prepared polarized light illuminates and is reflected off of the sample and collected by a polarization analyzer (camera plus linear polarizer and 134° retarder). The analyzer uses a variable axis retarder (retarder mounted in a motorized rotation stage), and then through a linear polarizer. This stationary linear polarizer allows for any polarization sensitivities on the analyzer’s detector array (camera) to be avoided. The light illuminates the camera detector, and an intensity measurement is made. After 64 different retarder position combinations (both retarders in combination) are measured, these 64 intensity measurements are then converted into a Mueller Matrix image in LabView. A Mueller matrix is a 4x4 matrix used to describe the polarization state of an element when illuminated by unpolarized or partially polarized light. In its symbolic form it appears as shown as Equ. 2.1. Polarization change is indicated by deviations from the identity matrix.

$$\text{Mueller Matrix} = \begin{bmatrix} M_{0,0} & M_{0,1} & M_{0,2} & M_{0,3} \\ M_{1,0} & M_{1,1} & M_{1,2} & M_{1,3} \\ M_{2,0} & M_{2,1} & M_{2,2} & M_{2,3} \\ M_{3,0} & M_{3,1} & M_{3,2} & M_{3,3} \end{bmatrix} \quad [\text{Equ. 2.1}]$$

$$\text{Normalized Mueller Matrix} = M = \frac{1}{M_{0,0}} \begin{bmatrix} 1 & m_{0,1} & m_{0,2} & m_{0,3} \\ m_{1,0} & m_{1,1} & m_{1,2} & m_{1,3} \\ m_{2,0} & m_{2,1} & m_{2,2} & m_{2,3} \\ m_{3,0} & m_{3,1} & m_{3,2} & m_{3,3} \end{bmatrix} \quad [\text{Equ. 2.2}]$$

Figure 2.9 shows an example of a typical Mueller matrix image. This Mueller matrix was collected from a dry concrete sample under 550 nm light at an angle of incidence of 22.5° and a 0° angle of scatter. A Mueller matrix is used to describe all the polarizing and de-polarizing properties of an optical element. Diattenuation, retardance, polarizance and depolarization, in both circular and linear

orientations are contained in the Mueller matrix. Each Mueller matrix has 16 degrees of freedom: one degree of freedom in intensity, three degrees of freedom in retardance (x, y, and z), three degrees of freedom in diattenuation (x, y, and z), and nine degrees of freedom in depolarization.

Each normalized Mueller matrix, Equ. 2.2, can also be described using diattenuation, and polarizance vectors, Equ. 2.3. The diattenuation vector, Equ. 2.5, is given by the first row of the Mueller matrix. The polarizance vector, Equ. 2.6, is given by the first column of the Mueller matrix.

$$M = \begin{bmatrix} 1 & \vec{D}^T \\ \vec{P} & m \end{bmatrix} \quad [\text{Equ. 2.3}]$$

$$m = \begin{bmatrix} m_{1,1} & m_{1,2} & m_{1,3} \\ m_{2,1} & m_{2,2} & m_{2,3} \\ m_{3,1} & m_{3,2} & m_{3,3} \end{bmatrix} \quad [\text{Equ. 2.4}]$$

$$\vec{D} = \begin{bmatrix} m_{0,1} \\ m_{0,2} \\ m_{0,3} \end{bmatrix} \quad [\text{Equ. 2.5}]$$

$$\vec{P} = \begin{bmatrix} m_{1,0} \\ m_{2,0} \\ m_{3,0} \end{bmatrix} \quad [\text{Equ. 2.6}]$$

Each normalized Mueller matrix is then decomposed (Lu-Chipman Decomposition) into three 4x4 matrices: a diattenuation matrix,  $M_D$ , a retarder matrix,  $M_R$ , and a depolarization matrix,  $M_\Delta$ , as described in Equ 2.7.

$$M = M_\Delta M_R M_D \quad [\text{Equ. 2.7}]$$

The diattenuation matrix,  $M_D$ , is found using Equ. 2.8 and Equ. 2.9, where  $I_3$  is a 3x3 identity matrix, and  $a$  and  $b$  are scalars derived from the norm of the diattenuator (Equ. 2.10).

$$M_D = \begin{bmatrix} 1 & \vec{D}^T \\ \vec{D} & m_D \end{bmatrix} \quad [\text{Equ. 2.8}]$$

$$m_D = aI_3 + b(\vec{D} \cdot \vec{D}^T) \quad [\text{Equ. 2.9}]$$

$$D = |\vec{D}|, a = \sqrt{1 - D^2} \text{ and } b = \frac{1-a}{D^2} \quad [\text{Equ. 2.10}]$$

The retarder matrix,  $M_R$ , is found using Equ. 2.11 and 2.12, where  $\vec{0}$  is a vector of zeroes.

$$M_R = \begin{bmatrix} 1 & \vec{0}^T \\ \vec{0} & m_R \end{bmatrix} \quad [\text{Equ. 2.11}]$$

$$m_R = \frac{1}{a} [m - b(\vec{P} \cdot \vec{D}^T)] \quad [\text{Equ. 2.12}]$$

The depolarization matrix,  $M_\Delta$ , has nine degrees of freedom and is much more complicated to calculate.

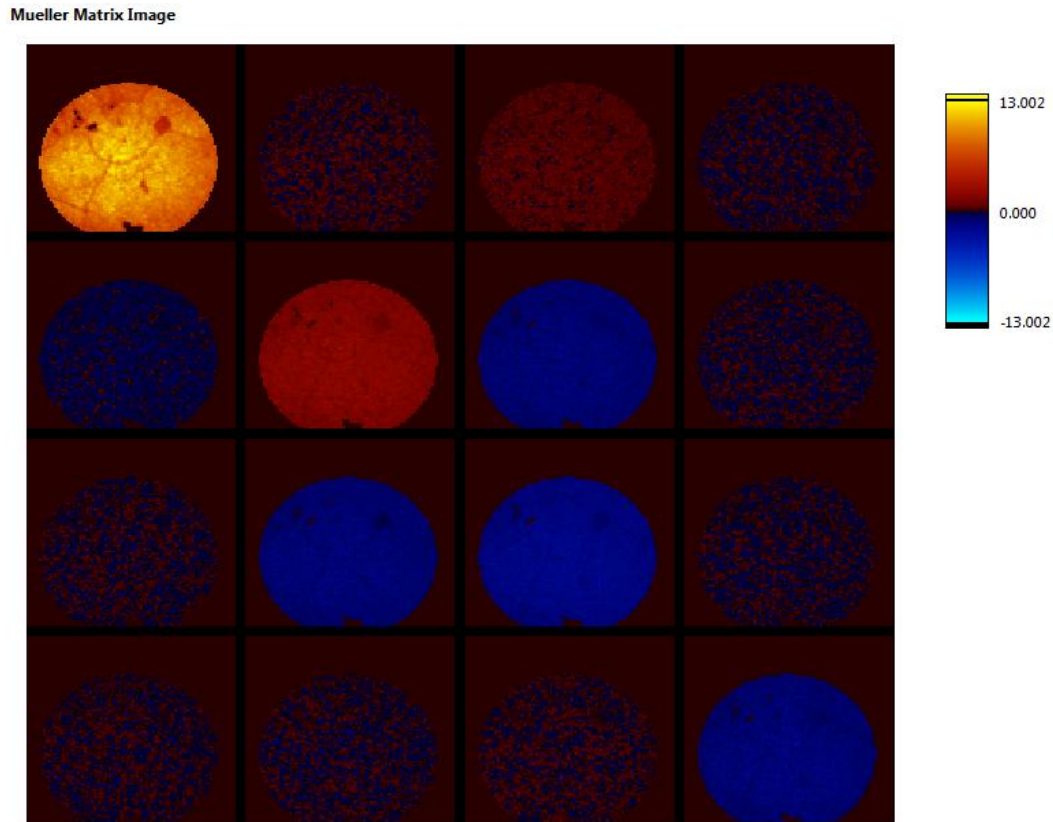


**Figure 2.9: Mueller Matrix Image:** Mueller matrix for a dry concrete sample under 550nm light at an angle of incidence of 22.5° and a 0° angle of scatter; notice the physical cracks and pits in the concrete are visible in the Mueller matrix calculation

Diattenuation refers to the difference in attenuation between two orthogonal polarization states, or can be described as the difference in reflected intensity from the surface of the target between different incident polarized states. Diattenuation is calculated from the diattenuation matrix,  $M_D$ , using Equ. 2.13. A “perfect” polarizer has a diattenuation magnitude of one [Chipman].

$$\text{Diattenuation of } M_D = \frac{R_{max} - R_{min}}{R_{max} + R_{min}} = \frac{\sqrt{m_{0,1}^2 + m_{0,2}^2 + m_{0,3}^2}}{m_{0,0}} \quad [\text{Equ. 2.13}]$$

$$\text{Linear Diattenuation of } M_D = LD = \frac{\sqrt{m_{0,1}^2 + m_{0,2}^2}}{m_{0,0}} \quad [\text{Equ. 2.14}]$$

Diattenuation has three degrees of freedom which can be expressed as the diattenuation magnitude, fast axis orientation, and ellipticity, or alternatively can be expressed as horizontal-vertical LD, 45°-135° LD, and circular diattenuation. Linear diattenuation, calculated from the Mueller matrix using Equ. 2.14, encompasses all of the linear polarization states, i.e. H-V and 45°-135°. The horizontal-vertical diattenuation component describes the difference in reflected intensity between horizontal and vertical polarized states. Zero values mean horizontal and vertical polarized light scatter with the same intensity. Positive values mean horizontal light is reflected more than vertical, and negative values mean vertical light is reflected more than horizontal [Chipman]. High magnitude values, near 1, are expected with specularly reflective media, i.e. water surface, smooth ice. Low magnitude values, near 0, are expected with diffuse reflections, i.e. rough surfaces like concrete and asphalt.

Retardance is the difference in phase accumulation between two polarization states. The retardance has three degrees of freedom which can be expressed as the retardance magnitude, fast axis orientation, and ellipticity, or alternatively can be expressed as horizontal-vertical LR, 45°-135° LR, and left and right circular retardance [Chipman]. Birefringence occurs when one axis of the electromagnetic signal travelling through a media experiences an index of refraction different than that of the orthogonal axis. Since ice is slightly birefringent, it is expected to have a non-zero value of retardance. Asphalt and concrete on the other hand are not expected to transmit light very deep into its surface, and is not conductive (like a metal) so it is expected to have near zero retardance. Retardance is calculated from the retarder matrix,  $M_R$ , using Equ. 2.15.

$$\text{Retardance of } M_R = 2\pi - \cos^{-1} \left( \frac{\text{Tr}(m_R) - 1}{2} \right),$$

where  $Tr(m_R)$  is the Trace of the retardance submatrix  $m_R$  [Equ. 2.15]

The linear retardance magnitude is the maximum difference in phase between linearly polarized states. We describe a commercial quarter wave retarder by saying it has 90° of linear retardance with a certain orientation of the fast axis. This linear retardance magnitude includes the horizontal-vertical retardance and 45°-135° linear retardance components. Linear retardance represents the averaged birefringence of the sample [Chipman].

$$Polarizance = \frac{\sqrt{m_{1,0}^2 + m_{2,0}^2 + m_{3,0}^2}}{m_{0,0}} \quad [Equ. 2.16]$$

$$Linear Polarizance = \frac{\sqrt{m_{1,0}^2 + m_{2,0}^2}}{m_{0,0}} \quad [Equ. 2.17]$$

Polarizance is the coupling of completely unpolarized light into polarized light. Polarizance is calculated from the diattenuation matrix,  $M_D$ , using Equ. 2.16, and linear polarizance is calculated using Equ. 2.17.

Depolarization is the property of coupling polarized light into partially-polarized or un-polarized light. Depolarization/polarizance has nine degrees of freedom. An isotropic depolarizer has equal elements along the diagonal of the matrix which means all incident polarized states are depolarized the same amount [Chipman].

$$Depolarization Index = DI = 1 - \frac{\sqrt{\sum_{i,j=0}^3 M_{i,j}^2 - M_{0,0}^2}}{\sqrt{3}M_{0,0}} \quad [Equ. 2.18]$$

Depolarization index, Equ. 2.18, is the depolarization of the reflected and scattered light averaged for all possible incident polarized states. The depolarization index for light exiting an optical element ranges from +1 for light that remains completely polarized, to 0.5 for light that is 50% depolarized, to 0 for light that is completely depolarized. Rough surfaces tend to have large depolarization, so asphalt and concrete are expected to have smaller depolarization indices than smooth iced surfaces.

### 2.3.2 Visible Polarimeter Measurement Angles – Diffuse

Figure 2.10 shows graphically the angular range of measurements taken by the visible polarimeter. Note that the camera was always positioned at a  $90^\circ$  angle from the sample, looking down its normal, and the source was positioned at varying angles of incidence. With this geometry specular measurements are not taken. The amount of light reflected towards the camera should increase as the angle of incidence approaches  $0^\circ$  and the system approaches the specular condition.

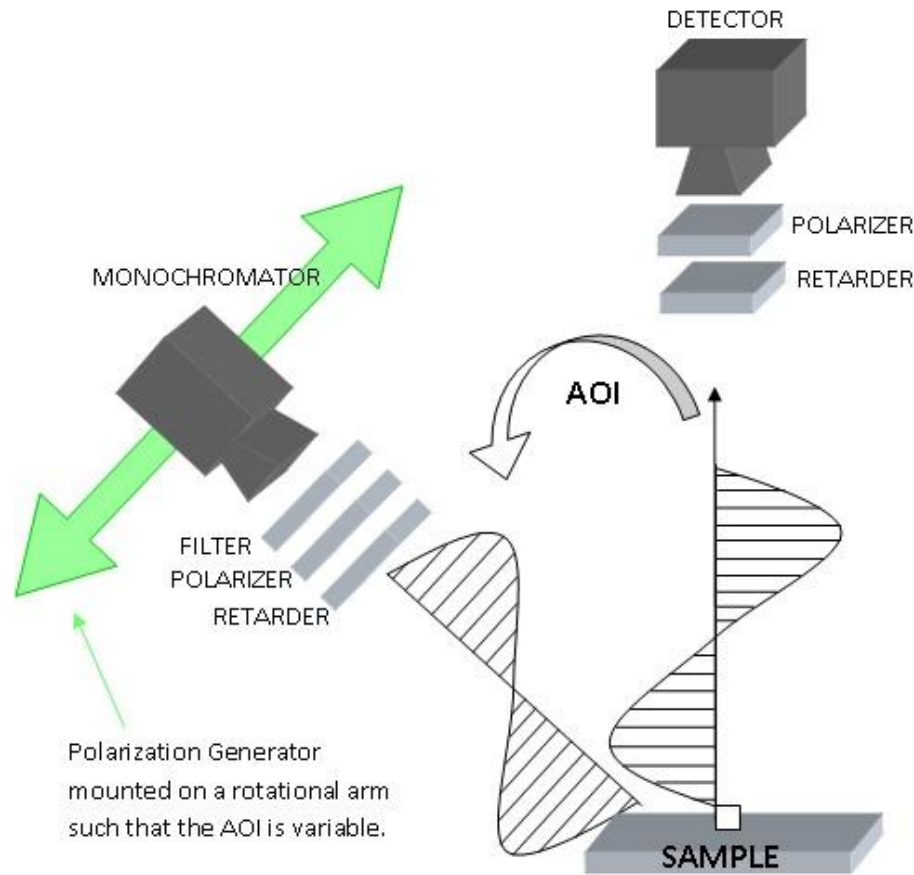


**Figure 2.10: Visible polarimeter angular setup:** A graphical representation of the angular range of the visible polarimeter. The visible polarimeter collected Mueller Matrix measurements for normal reflectance responses for multiple incident angles

### 2.3.3 UV Polarimeter Measurement Angles – Specular and Near Specular

Specular reflection is the mirror-like reflection of light from a surface, i.e. angle of scatter = angle of incidence. Scattered irradiance is usually highest near specular reflectance; placing a detector at the specular reflectance angle usually provides the maximum light collection. Scanning the angles near specular, i.e.  $\pm 5^\circ$  and  $\pm 10^\circ$ , map out the irradiances reflected near specular. Examination of this range studies different polarization responses. The UV polarimeter had a motor which allowed for automated angle of incidence changes; greatly speeding up the measurement process. Figure 2.11 shows graphically the angular range of measurements taken by the UV polarimeter.

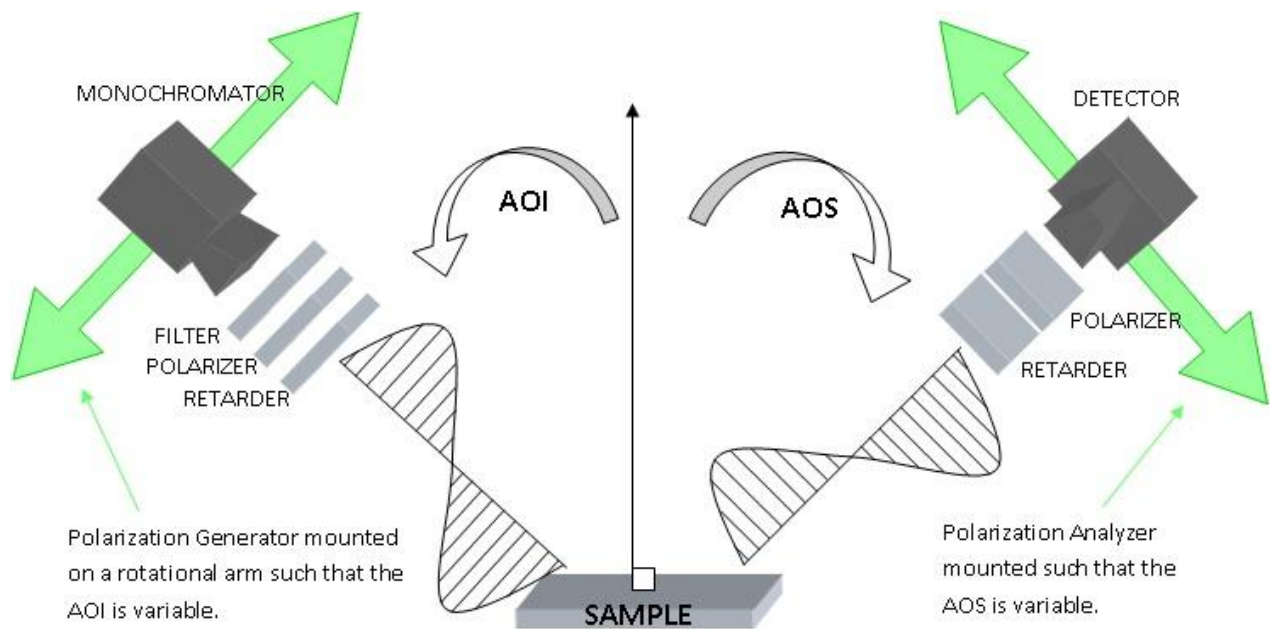


**Figure 2.11: UV polarimeter angular setup:** A graphical representation of the angular range of the UV polarimeter. The UV polarimeter collected Mueller Matrix measurements for an angular reflectance scan which encompassed specular and near specular responses. Two incidence angles were examined, a small angle of incidence and a large angle of incidence.

## 2.4 Data Analysis/Statistical Procedures

Analysis adapted these Mueller Matrices into histograms, populated by pixels of single Mueller matrix images, of various polarization properties and allowed for direct comparison in the form of a Receiver Operating Characteristic (ROC) curve.



### 2.4.1 Polarization Properties – Histograms

Data reduction is performed on each pixel of a measured Mueller Matrix, resulting in ten histogram plots of various polarization properties, Linear Retardance, Linear Diattenuation, Linear Polarizance, Circular Retardance, Circular Diattenuation, Circular Polarizance, Retardance Orientation, Diattenuation Orientation, Polarizance Orientation, and Depolarization Index.

A histogram plots the number of samples (height) in a set of bins (x-axis). The histogram in Figure 2.12 compares the depolarization index histograms for a dry (blue) and iced (purple) image illuminated with 550nm light at an angle of incidence of 22.5° and measured at a 0° angle of scatter. This is a desirable pair of histograms; they have small overlap, and can be easily distinguished from one another.

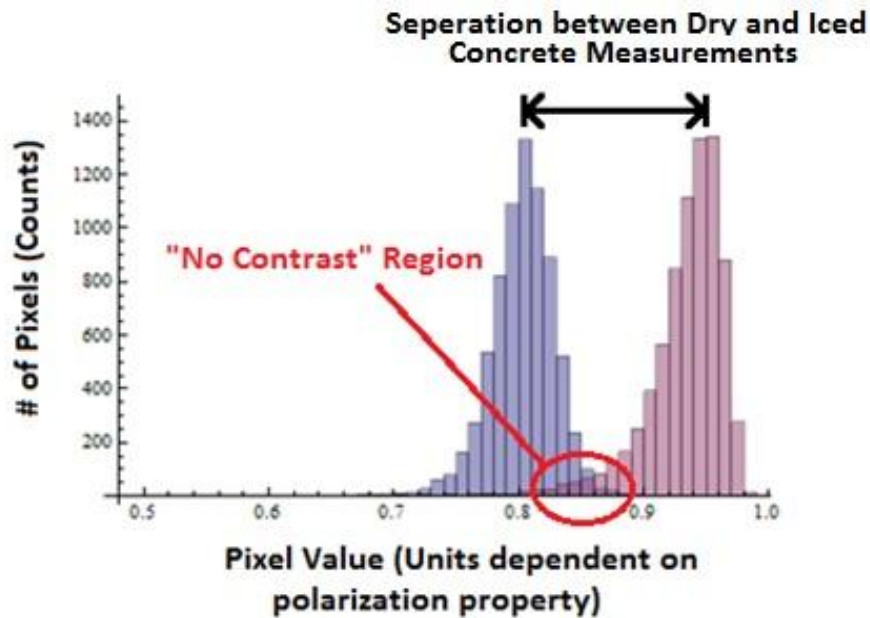


**Figure 2.12: Comparing histograms:** Histogram example of a high contrast measurement, specifically a comparison of the depolarization index for a dry (blue) and iced (purple) concrete sample oriented at 22.5° AOI and 0° AOS, and illuminated with 550 nm. The small region of overlap between 0.8 and 0.9 is the only place where the dry histogram cannot be distinguished from the iced.

A useful measurement, one that discriminates between dry and iced roads, requires a large change in a property between dry and iced sample, i.e. “Classification requires contrast”. Optical properties with overlapping histograms provide low contrast and do not help in discerning sample surface conditions. In conclusion, curves that are well separated have high contrast. Polarization properties that consistently demonstrate high contrast between iced and dry measurements should be subjected to further testing. Since these histograms are for only samples taken in the laboratory, an “ideal situation”, this classifier (contrast between measurements) may or may not work on roads, an uncontrolled environment. Histograms need to be accumulated over many samples under many conditions to demonstrate a credible measurement strategy.

The Full Width at Half Maximum (FWHM) is a metric used in determining the range of values measured on a histogram. FWHM means the full width of the distribution function of data at half of the maximum value as shown in Figure 2.13. Different FWHM’s for iced and dry measurements may allow for better discrimination, without enhancing the quality of the ROC curve for that comparison.

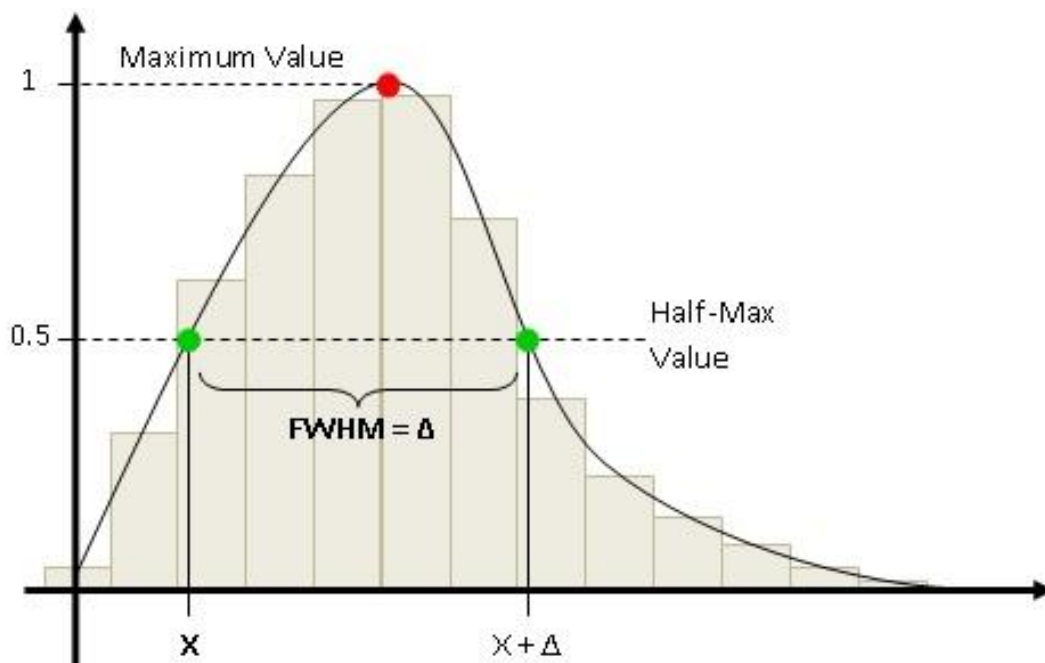
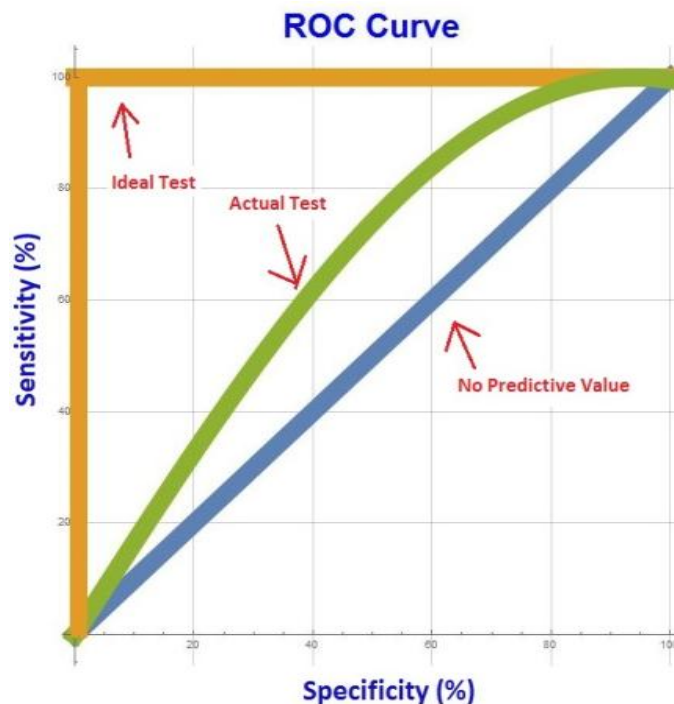


Figure 2.13: Full Width at Half-Maximum: A diagram of how the FWHM is calculated from a histogram.

## 2.4.2 Receiver Operator Curves

A “Receiver Operating Characteristic”, or ROC curve is a comparison of two different measurements. Each histogram is summed (integrated) from its left side. The resulting values are plotted such that one histogram's summation becomes the x value, and the other histogram's summation becomes the y value. In other words, the x and y coordinates of the ROC curve become the fraction of each histogram that are found below a certain x-axis value; each x,y coordinate pair is created as you step in increments across the x-axis of the two-histogram graph from left to right. Histograms with no overlap yield a sharp right angle, known as the “Ideal test” curve. The “Ideal test”, or discriminating measurement, is explained in Figure 2.16. Identical histograms grow in x and y at the same rate, yielding the diagonal “No Predictive Value”. This non discriminating measurement is explained in Figure 2.15. Typical ROC curves fall between these two extremes. The closer the curve is to the Ideal Test, the better the classifier polarization property is as a discriminant. Figure 2.14 outlines the different ROC classifications.



**Figure 2.14: Elements of a ROC curve:** The No Predictive Value line describes a comparison of two very similar data sets. The Ideal Test line describes a comparison of two data sets which do not share any same-values [Sprawls].

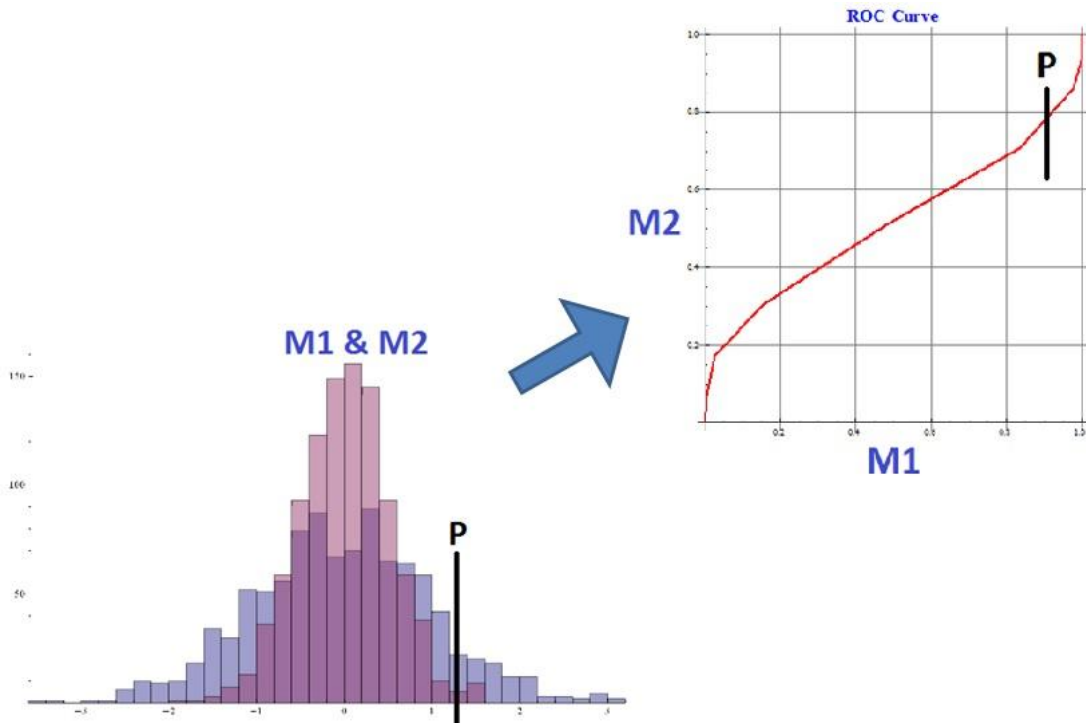


**Figure 2.15: Non-Ideal Case ROC Curve:** Shows little contrast between measurements M1 and M2. Point P on the histogram corresponds to point P on the ROC curve.

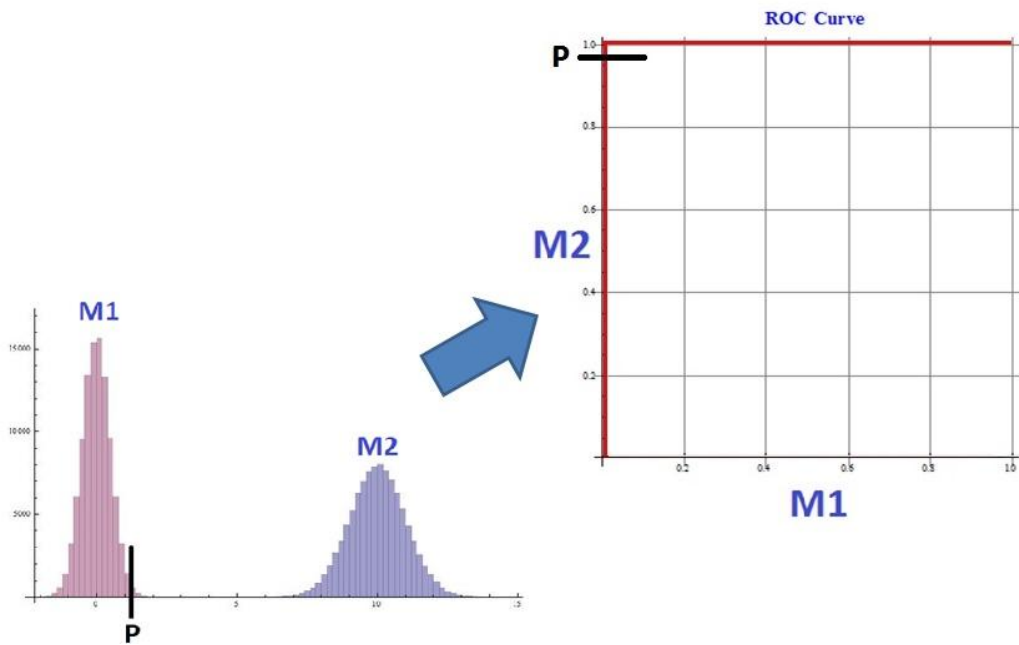


**Figure 2.16: Ideal Case ROC Curve:** Shows most contrast between measurements. This is the discriminating case we are searching for. Point P on the histogram corresponds to point P on the ROC curve.

## Chapter 3: Results

During the experimental portion of this investigation, three different campaigns of measurements were conducted. Campaign one, the first campaign, consisted of measurements taken by the visible polarimeter. Campaign two began with creating a new mode of temperature control, and consisted of measurements taken by the ultraviolet polarimeter. Finally, campaign three consisted of special interest measurements taken on the ultraviolet polarimeter.

Each campaign investigated the effects of changing a different variable in search of interesting polarization effects, and a good combination of wavelengths and angles for predictive measurements. Campaigns one and two investigate the sensitivity of polarization properties to changes in wavelength, angle of incidence, angle of scatter, and, of course, sample surface conditions. Campaign three looked at the polarization properties of liquid water being present on the road surface, multiple different water volumes. It also looked at the polarimeter system repeatability, and the stability of the ice while being cooled by liquid nitrogen.

### 3.1 Campaign 1: Visible Polarimeter, Normal Camera Angle of Scatter (0°)

Campaign one focused on many Mueller matrix images of samples quickly and efficiently. This allowed for the formation of a “game plan” for the following campaigns. For this exploratory imaging, the most available polarimeter where the chiller could be easily mounted was chosen, i.e. the visible polarimeter. The sample was mounted into the polarimeter such that the surface was perpendicular to the detector, i.e. AOS fixed at 0°. The angle of incidence stepped to 22.5°, 30°, 45°, and 60°. The monochromator stepped to 500 nm, 550 nm, 650 nm, and 750 nm. Each wavelength was measured at

all four angles of incidence, creating 16 Mueller matrix measurements as seen in Table 3.1. The following series of data shows the histograms from some of the more interesting polarization properties seen from measuring two samples, one concrete and one asphalt.

**Table 3.1: Visible polarimeter measurements:** The 16 Mueller matrices measured for a sample surface; four measurements for each of four wavelengths.

Measurement Number	Wavelength (nm)	Angle of Scatter (AOS, sample surface normal to camera)	Angle of Incidence (AOI, sample surface normal to light source)
1	500	0°	22.5°
2	500	0°	30°
3	500	0°	45°
4	500	0°	60°
5	550	0°	22.5°
6	550	0°	30°
7	550	0°	45°
8	550	0°	60°
9	650	0°	22.5°
10	650	0°	30°
11	650	0°	45°
12	650	0°	60°
13	750	0°	22.5°
14	750	0°	30°
15	750	0°	45°
16	750	0°	60°

Orientation of polarization properties (diattenuation orientation, polarizance orientation, and retardance orientation) were excluded from the analysis due to noisy measurement values. When polarization property values are close to zero the values congregate around the origin. When they are close to the origin, the calculations are very noisy and may appear to show false trends. The other polarization properties are enough to prove that polarimetric road ice detection is possible.

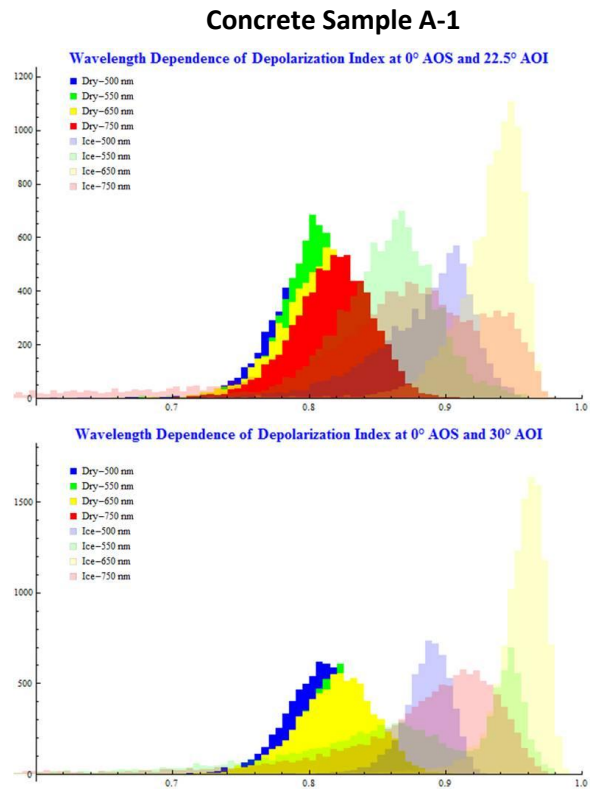
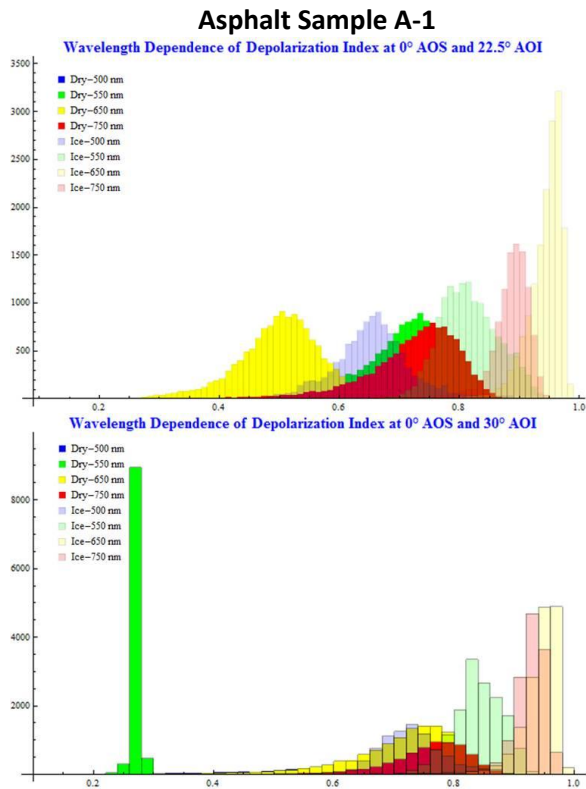
Three polarization properties that showed the most discrimination between different sample surface conditions; in order of decreasing discrimination:

- Depolarization index (DI)

- Linear diattenuation (LD)
- Linear polarizance (LP).

**Depolarization Index**

Depolarization index (DI) is a single number metric for characterizing the overall depolarization of a Mueller matrix. The DI equals one for non-depolarizing Mueller matrices; when only polarized light exits a system illuminated by polarized light. A perfect retarder would have a DI value of 1. The DI equals zero for an ideal depolarizer; when only unpolarized light exits a system illuminated by polarized light.



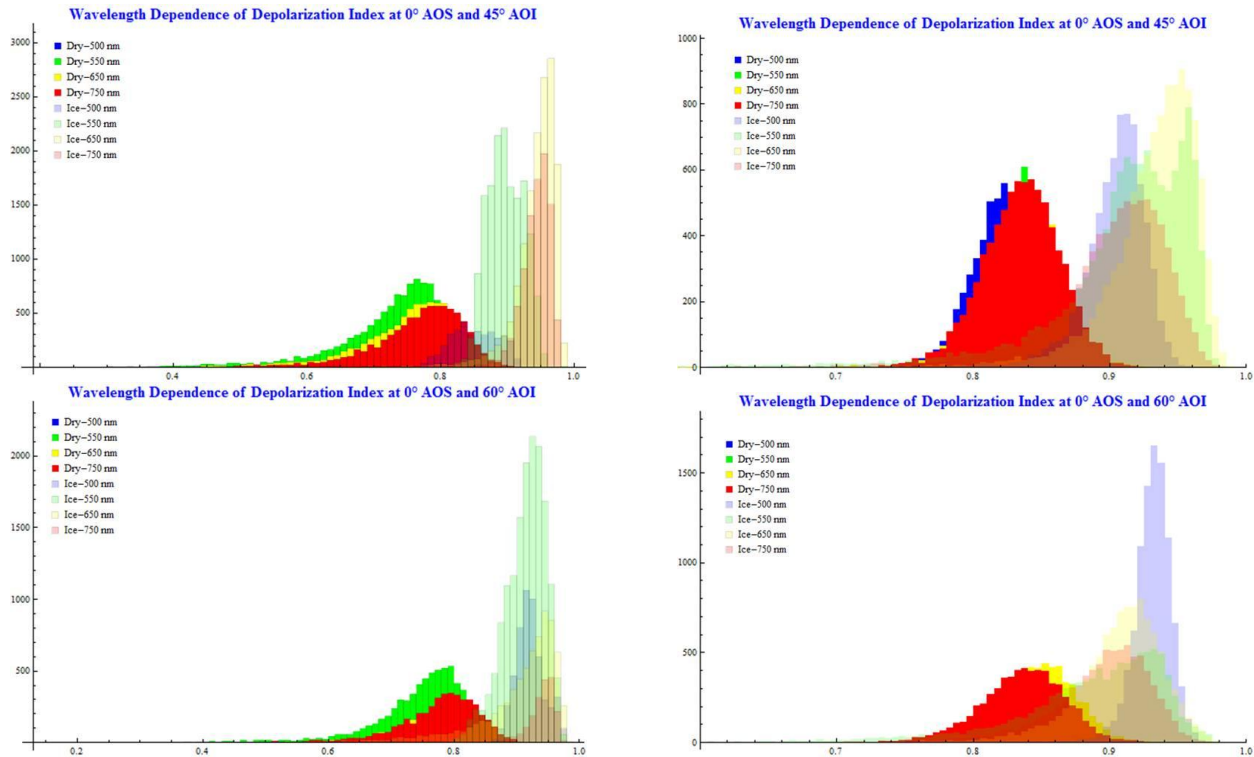


**Figure 3.1: Depolarization Index response for asphalt sample A-1 and concrete sample A-1:** Asphalt A-1 (left column) and Concrete A-1 (right column) Depolarization Index responses as the angle of incidence is increased (moving from top to bottom). Only a small amount of overlap is seen between the dry (bright colors) and the iced (pastel colors) measurements. This large amount of separation between responses results in a good quality ROC curve. [An anomalous measurement is seen in the 30°AOI histogram for dry asphalt at 550 nm]

In this data, shown in Figure 3.1, it is clear that iced samples are less depolarizing than dry samples, since iced asphalt has a higher DI than dry asphalt, and iced concrete has a higher DI than dry concrete. Measurements for the dry asphalt are constant at  $\sim 0.78$ ; DI is weakly dependent on the angle of incidence (AOI). Measurements for the dry concrete increase in magnitude slightly as AOI increases, meaning there appears to be a small DI dependence on AOI.

DI measurements for the dry asphalt decrease as wavelength decreases. DI measurements for the iced asphalt increase as the angle of incidence (AOI) increases. DI measurements for the iced concrete increase as the angle of incidence (AOI) increases, causing the different wavelengths to group together. DI measurements for the dry concrete slightly decrease as wavelength decreases, indicating a slight direct relationship between DI and wavelength.



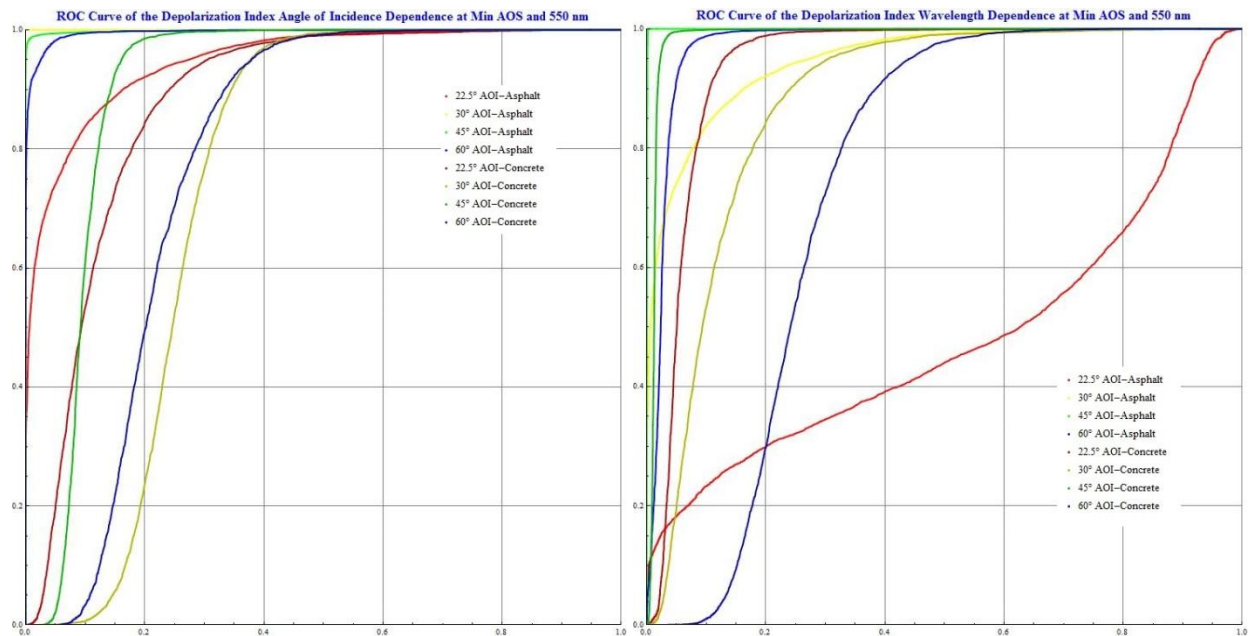


**Figure 3.2: ROC curves for the Depolarization Index property for asphalt sample A-1 and concrete sample A-1: DI angle of incidence dependence (left) at 500 nm, and DI wavelength dependence (right) at AOI = 22.5°, AOS = 0°. Asphalts 500 nm line (red, right) could be an outlier; a better understanding comes with more data. [\* 650 nm – Asphalt measurement is incorrect due to a corrupted reference measurement; \* 30° AOI – Asphalt measurement was not plotted due to a corrupted reference measurement]**

Examining the ROC curves against AOI and wavelength dependencies, DI had the best ROC curves of campaign one. Concrete and asphalt curves match well across all measured AOI and wavelengths. ROC curve quality increases as AOI increases, as well as peaking at about 650 nm for both asphalt and concrete. The best ROC curve, showing the best iced to dry distinction, is 45° AOI at 650 nm, seen as the green lines on Figure 3.2.

### Linear Diattenuation

Linear diattenuation (LD) is the dependence of the intensity transmittance on the polarization state of the incident linearly polarized light. A perfect linear diattenuator has a LD value of 1; linear polarizers have LD values close to 1.

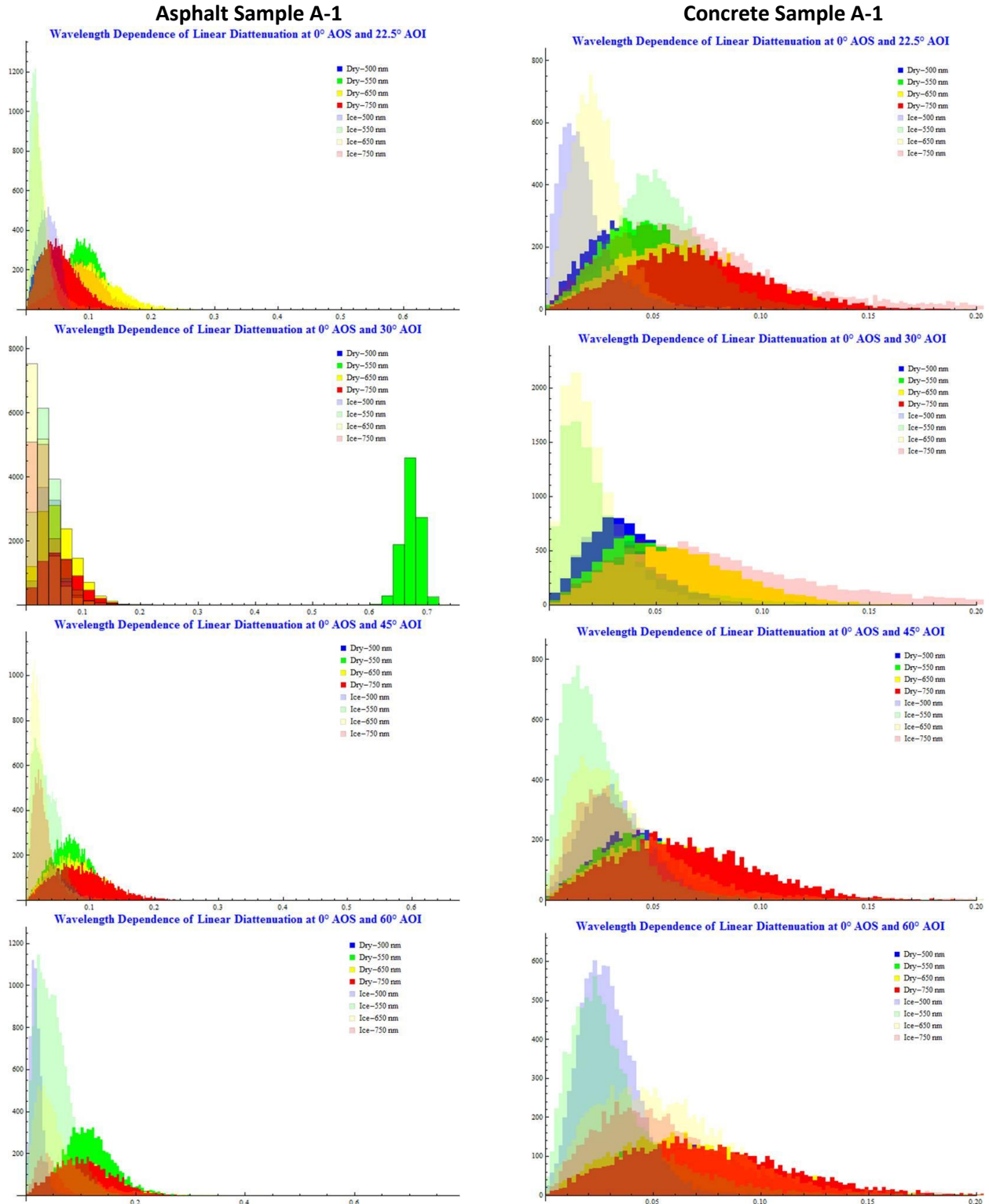


**Figure 3.3:** Linear Diattenuation response for asphalt sample A-1 and concrete sample A-1: Asphalt A-1 (left column) and Concrete A-1 (right column) linear diattenuation responses as the angle of incidence is increased (moving from top to bottom).

Note the very low values of linear diattenuation, x axis. [An anomalous measurement is seen in the 30°AOI histogram for dry asphalt at 550 nm]

From the graphs presented in Figure 3.3 linear diattenuation for the dry asphalt increases as the AOI increases; the LD shows significant angular dependence. The Full Width at Half Maximum (FWHM) difference between iced and dry measurements, FWHM meaning the full width of the distribution function of data at half of the maximum value. Iced asphalt has a lower LD than dry asphalt, and has about half of the FWHM (in LD) than dry asphalt.

Measurements for the dry concrete stay fairly constant at about ~ 0.06 across the full AOI spectrum, showing little LD dependence on AOI. Iced concrete has a lower LD than dry concrete, and has about half of the FWHM (in LD) than dry concrete. Concrete LD values are all much smaller than asphalt, but follow the same ice-dry relationships relative to each other.

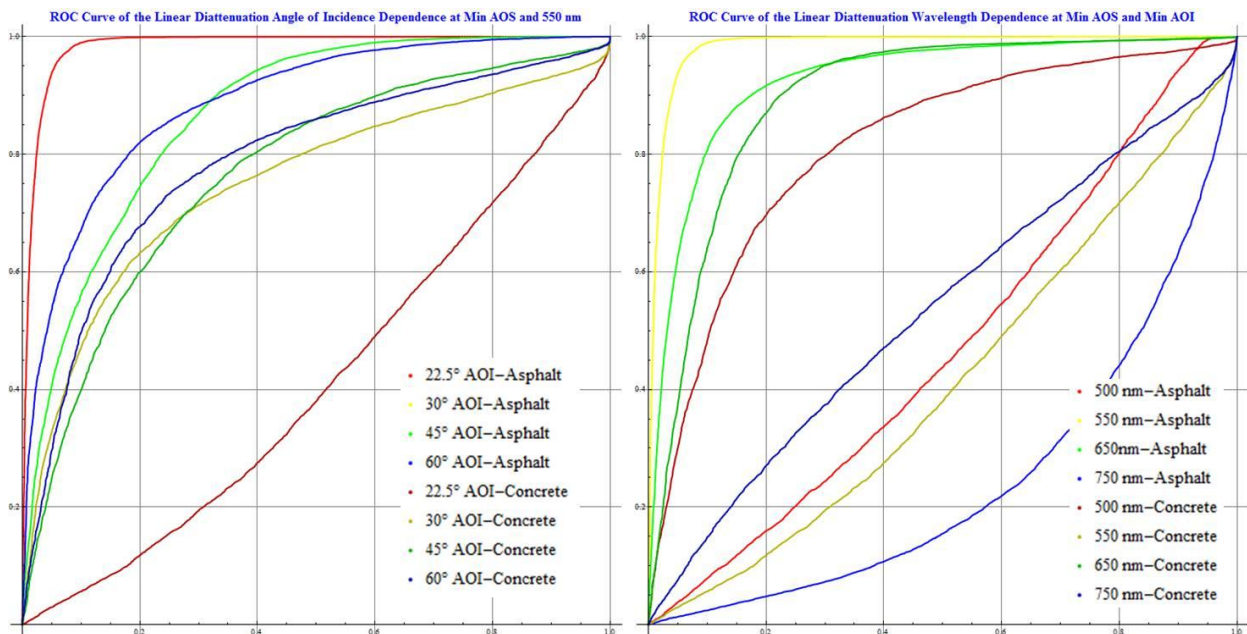


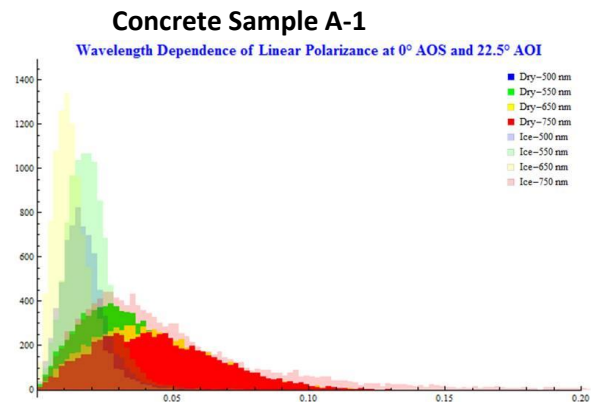
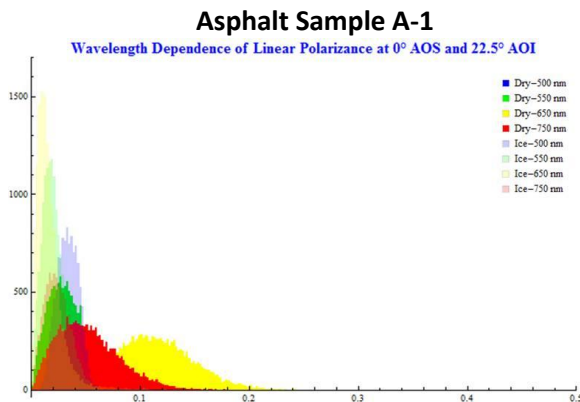
**Figure 3.4: ROC curves for the Linear Diattenuation property for asphalt sample A-1 and concrete sample A-1: LD angle of incidence dependence (left) at 500 nm, and LD wavelength dependence (right) at AOI = 22.5°, AOS = 0°. [\* 30° AOI – Asphalt measurement was not plotted due to a corrupted reference measurement]**

The concrete and asphalt linear diattenuation curves are very different. While the ROC curve quality is fairly uniform over all AOIs, the quality of the concrete curves is measurably worse than

asphalt. The worst ROC line, 22.5° AOI-Concrete, could be an outlier; a better understanding comes with more data. Great ROC curves are seen at 650 nm for both concrete and asphalt. Because of the seemingly random distribution of responses (Figure 3.4 , right), for example 550 nm asphalt ROC being of better quality than both 500 nm and 650 nm, ROC curve quality dependence on wavelength is not clear.

### Linear Polarizance

Linear polarizance (LP) is the degree of linear polarization of the transmitted light when unpolarized light is incident. A LP value of 1 is consistent with a perfect linear polarizer, in this case the DI cannot be zero. Usually linear polarizance is very similar to linear diattenuation. We are interested if significant differences appear because that would indicate whether modulating the polarization generator or polarization analyzer generates more or comparable amounts of information. For example, if the linear polarizance is large and linear diattenuation small, then the performance of the road ice detection might be better with an unpolarized light source.



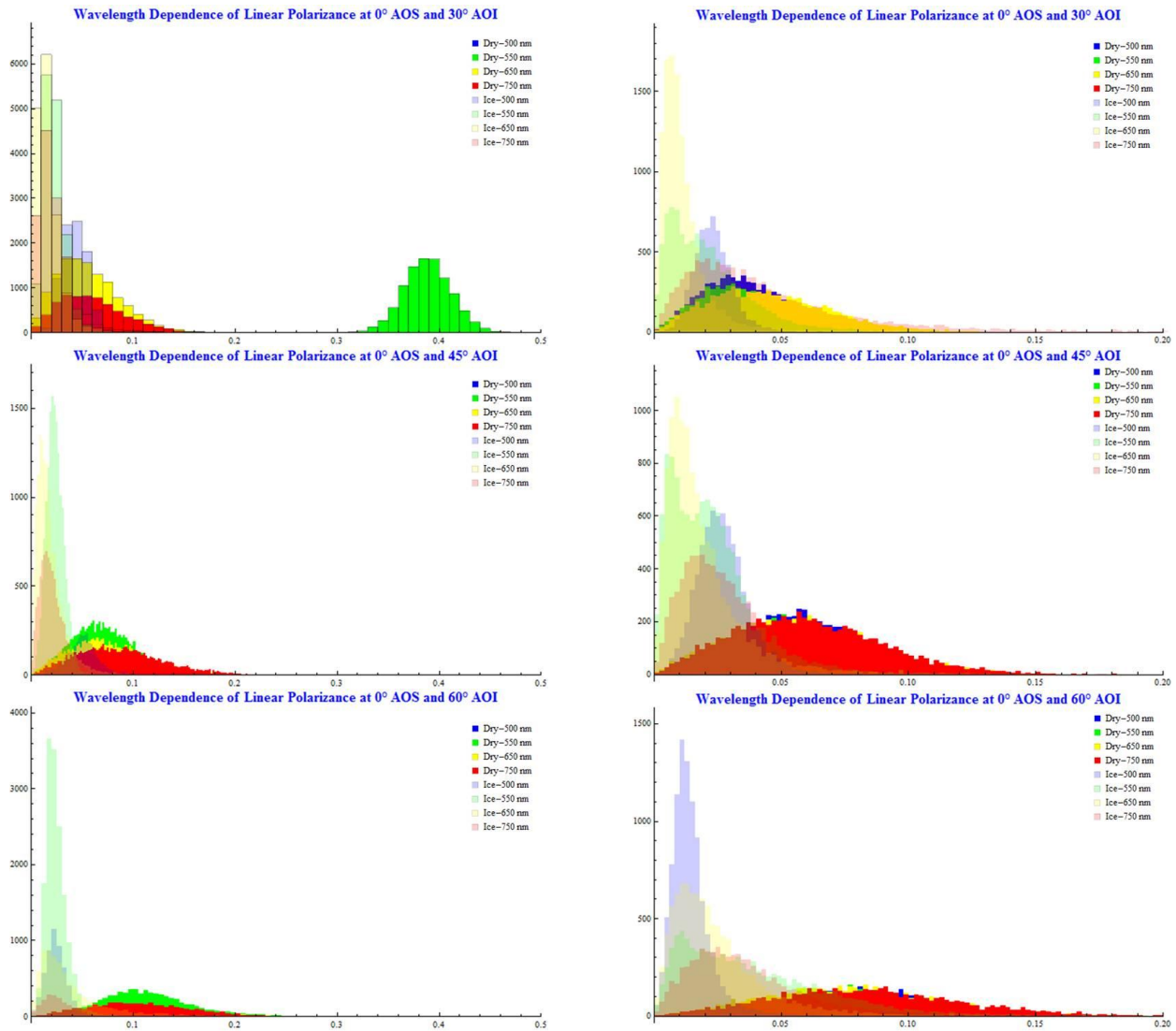


**Figure 3.5:** Linear Polarization response for asphalt sample A-1 and concrete sample A-1: Asphalt A-1 (left column) and Concrete A-1 (right column) linear diattenuation responses as the angle of incidence is increased (moving from top to bottom).

[An anomalous measurement is seen in the 30°AOI histogram for dry asphalt at 550 nm]

Measurements for the dry asphalt also increase in FWHM as the AOI increases. Iced asphalt has a lower LP than dry asphalt, and has about half of the FWHM (in LP) than dry asphalt. Figure 3.5 shows these trends in LP data.

The average value for the dry concrete LP increases as the AOI increases, meaning the LP appears to have a small angular dependence. LP Measurements for the dry concrete increase in FWHM

as the AOI increases. Iced concrete has a lower LP than dry concrete, and has about half of the FWHM (in LP) than dry concrete.

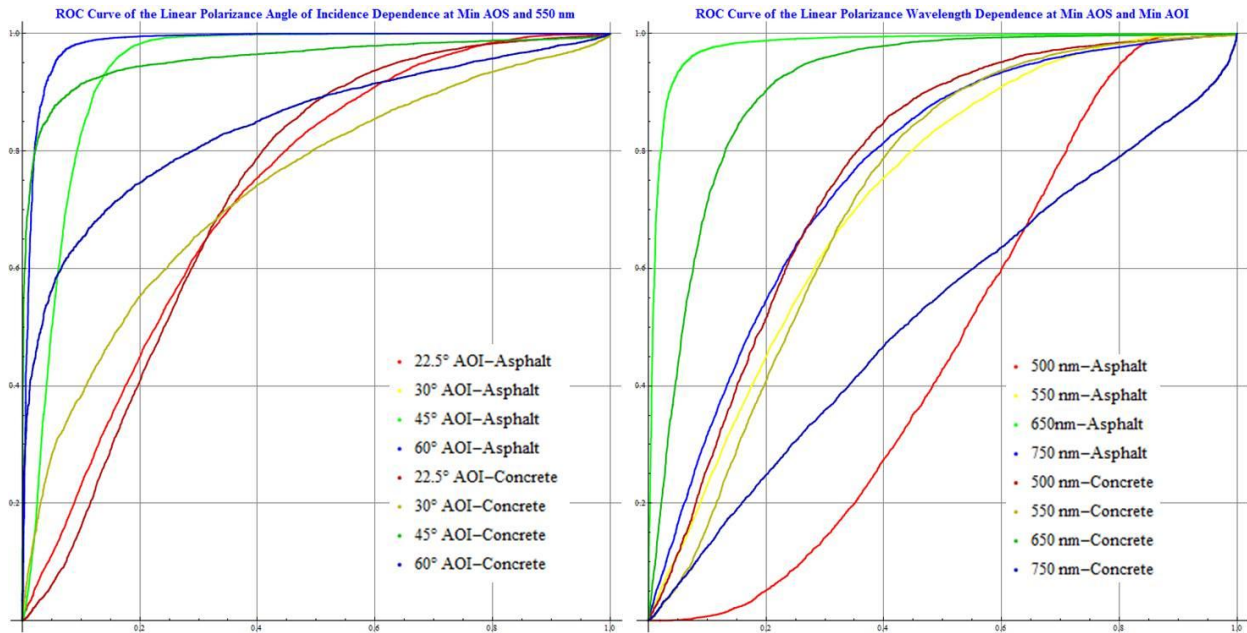


**Figure 3.6: ROC curves for the Linear Polarization property for asphalt sample A-1 and concrete sample A-1: LP angle of incidence dependence (left) at 550 nm, and LP wavelength dependence (right) at AOI = 22.5°, AOS = 0°. [\* 30° AOI – Asphalt measurement was not plotted due to a corrupted reference measurement]**

The concrete and asphalt curves match well across all measured angles of incidence; 22.5° AOI asphalt overlaps 22.5° AOI concrete (Fig. 3.6, dark red and bright red lines), 45° AOI asphalt overlaps 45° concrete (Fig.3.6, dark green and bright green lines), etc. ROC curve quality increases as AOI increases. ROC curve quality increases as wavelength increases, peaking at about 650 nm. The best ROC curve is seen at 45° AOI and 650 nm.

### Linear Retardance

Linear retardance (LR) is the linear polarization-dependent phase change associated with the surface interaction; the phase of the output beam depends upon the polarization state of the incident light. Linear retardance is cyclical, meaning a value of 360° is equal to a value of 0° (i.e. LR period is 360° or  $2\pi$ ).



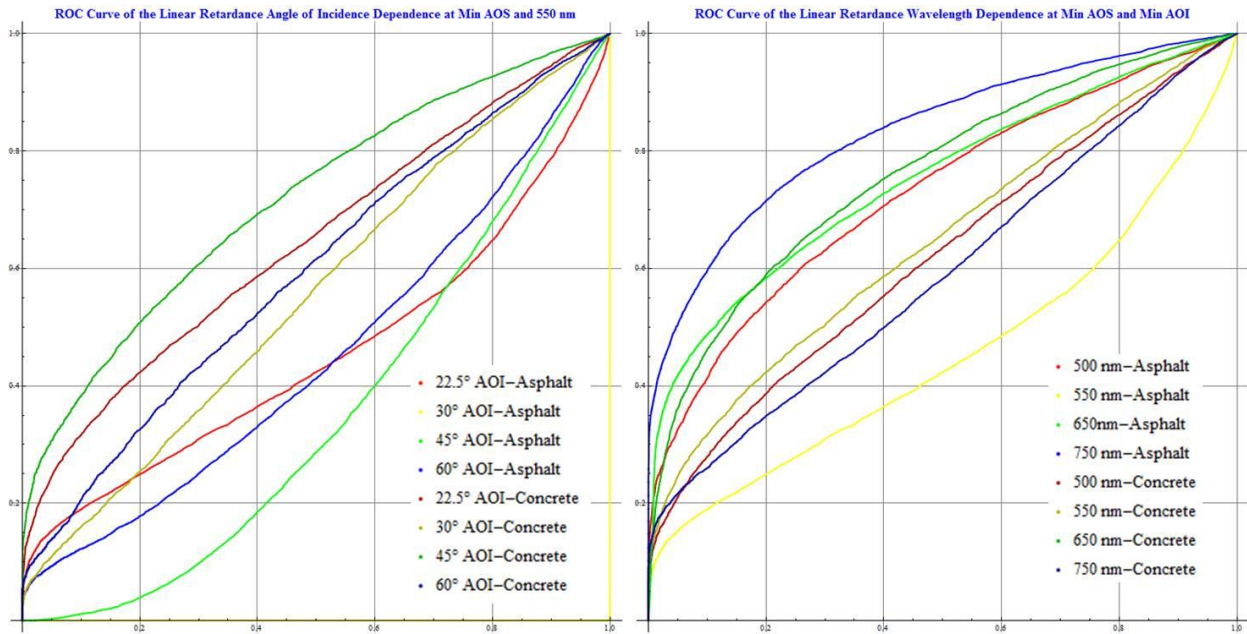


**Figure 3.7: ROC curves for the Linear Retardance property for asphalt sample A-1 and concrete sample A-1: LR angle of incidence dependence (left) at 500 nm, and LR wavelength dependence (right) at AOI = 22.5°, AOS = 0°. [\* 30° AOI – Asphalt measurement was not plotted due to a corrupted reference measurement]**

Both the dry and iced samples behave like mirrors; both have a linear retardance (LR) close to 180° ( $\pi$  radians), and are highly reflective in specular. An iced sample has a much broader FWHM, or spread of values, in the higher wavelengths (650 nm and 750) than a dry sample. There is no strong LR AOI dependence apparent for both dry and iced samples; Figure 3.7 shows weak AOI dependencies for LR. Because of large histogram overlap, the ROC curves for LR responses are poor. Concrete and asphalt ROC curves match very well across all measured AOI. ROC curve quality increases as AOI increases; however ROC curves are poor everywhere.

Linear retardance data is very noisy and, like other samples, of limited usefulness for highly scattering samples. It has been included here for completeness in case it shows a valuable behavior.

### **Circular Diattenuation**

Circular diattenuation (CD) is the dependence of the intensity transmittance on the circular polarization state of the incident light, specifically the circular nature of the incident light. A perfect

circular diattenuator has a circular diattenuation (CD) value of 1; circular polarizers have circular diattenuation (CD) values close to 1.

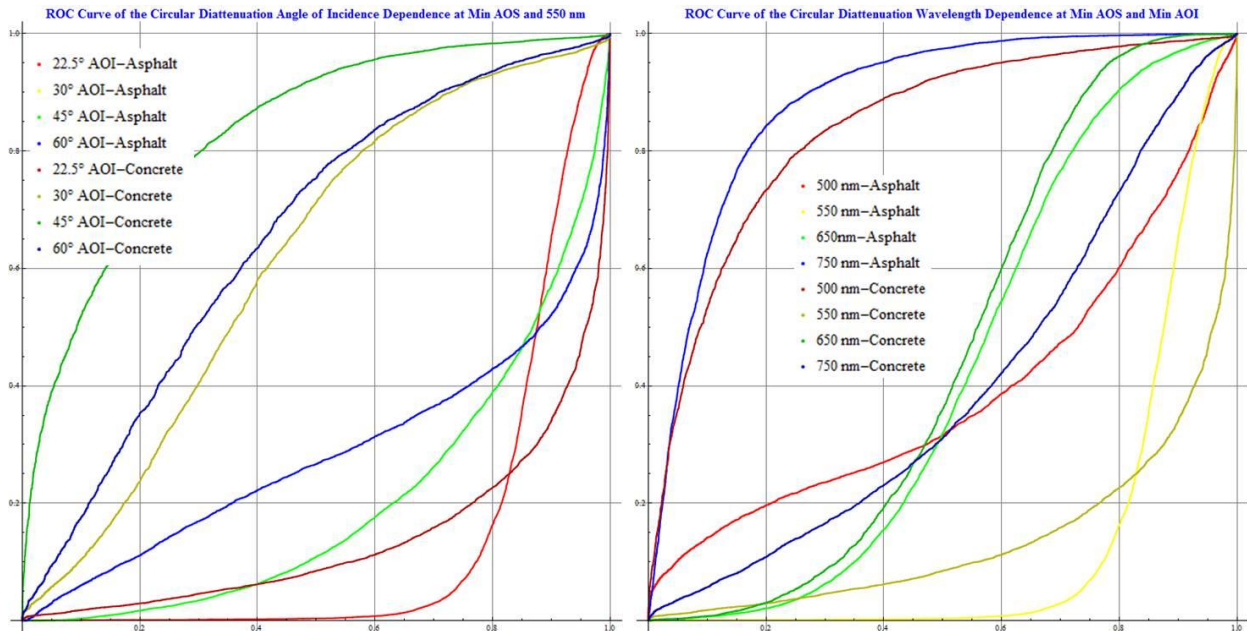


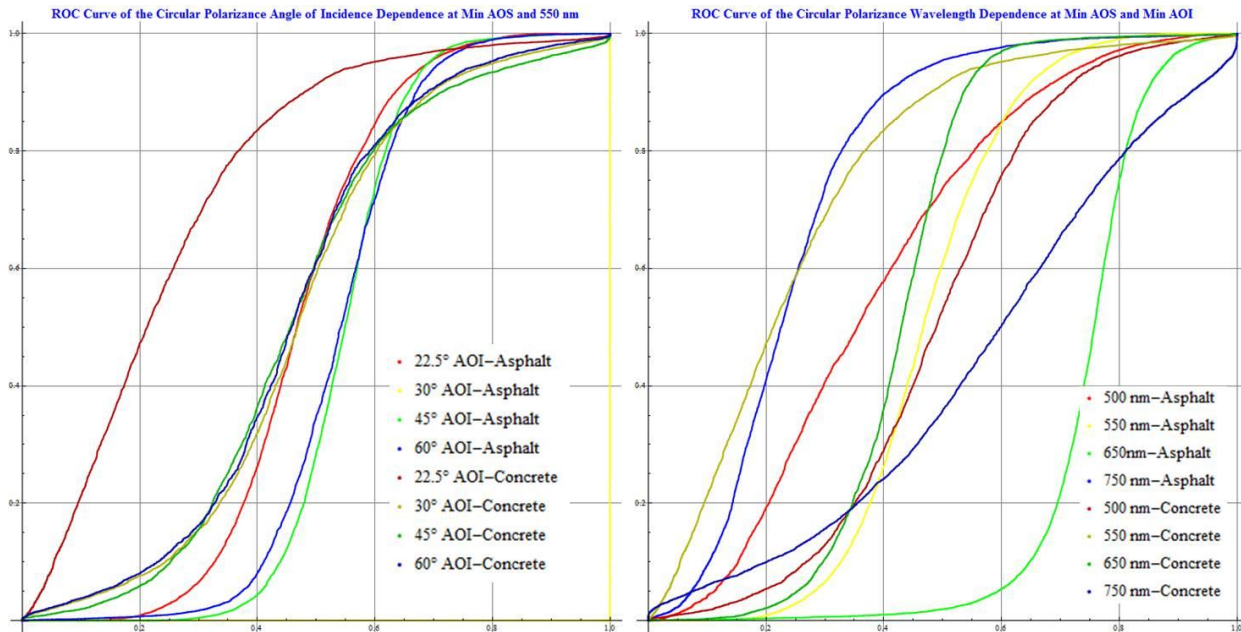
**Figure 3.8: ROC curves for the Circular Diattenuation property for asphalt sample A-1 and concrete sample A-1: CD angle of incidence dependence (left) at 500 nm, and CD wavelength dependence (right) at AOI = 22.5°, AOS = 0°. [\* 30° AOI – Asphalt measurement was not plotted due to a corrupted reference measurement]**

Little differentiation is seen between iced and dry asphalt with CD, distribution width (FWHM), and distribution height. Concrete and asphalt curves match well across all measured angles of incidence; 22.5° AOI asphalt and 22.5° AOI concrete overlap (Fig. 3.8, dark red and bright red lines), etc. ROC curve quality decreases as AOI increases, however, all ROC curves are poor. No strong assessments can be made from this data.

### **Circular Polarizance**

Circular polarizance (CP) is the degree of circular polarization of the transmitted light when unpolarized light is incident. A CP value of 1 is consistent with a perfect circular polarizer, in this case the DI cannot be zero.





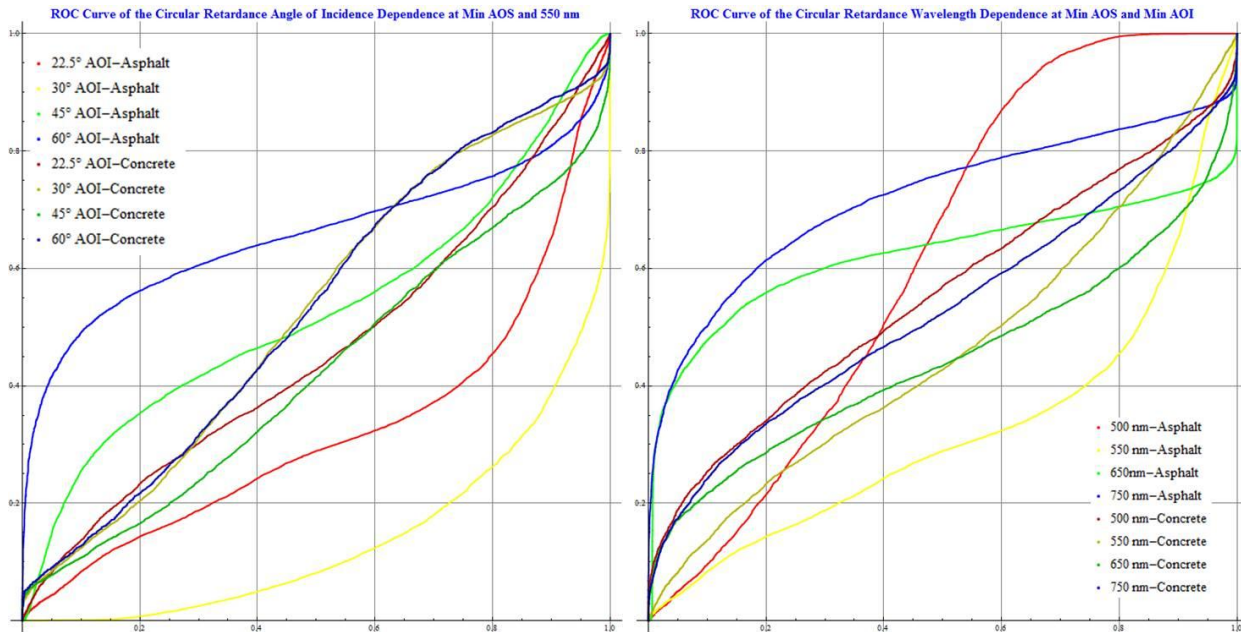
**Figure 3.9: ROC curves for the Circular Polarization property for asphalt sample A-1 and concrete sample A-1: CP angle of incidence dependence (left) at 500 nm, and CP wavelength dependence (right) at AOI = 22.5°, AOS = 0°. [\* 30° AOI – Asphalt measurement was not plotted due to a corrupted reference measurement]**

Figure 3.9 shows the CP response for asphalt and concrete. Dry samples have a much broader FWHM than iced; dry asphalt has a CP FWHM ~5x larger than iced asphalt, while dry concrete has a CP FWHM ~3x larger than iced concrete. No strong CP AOI dependence apparent for both dry and iced samples. No strong CP wavelength dependence apparent for both dry and iced samples.

ROC curve quality appears to be independent of AOI or wavelength. Because of the high overlap between iced and dry measurements (FWHM being the main distinguisher) the ROC curves are poor for all CP data.

### **Circular Retardance**

Circular retardance (CR) is the circular polarization-dependent phase change associated with the surface; the phase of the output beam depends upon the polarization state of the incident light. Note that this circular retardance is cyclical, meaning a value of 360° is equal to a value of 0° (i.e. CR period is 360° or  $2\pi$ )



**Figure 3.10: ROC curves for the Circular Retardance property for asphalt sample A-1 and concrete sample A-1: CR angle of incidence dependence (left) at 550 nm, and CR wavelength dependence (right) at AOI = 22.5°, AOS = 0°. [\* 30° AOI – Asphalt measurement was not plotted due to a corrupted reference measurement]**

Distinction between iced and dry samples is difficult in value of CR, distribution width (FWHM), and distribution height. No strong CR AOI dependence apparent for both dry and iced samples, illustrated in Figure 3.10. No strong CR wavelength dependence apparent for both dry and iced samples. ROC quality is poor for all CR data.

### 3.2 Campaign 2: UV Polarimeter, Specular and Near Specular Angles

Following the success of finding discriminatory polarization properties in campaign one, campaign two developed a more in-depth image as to what polarization manipulations are occurring in roadway ice. This was done by implementing a new setup to investigate polarization changes near specular reflection. The new test bed was the UV polarimeter (Range 350-550 nm), and 400, 450, 500, and 550 nm were measured. The light source was designed to rotate horizontally about the surface normal of the vertically mounted sample. This made the angle of incidence a controllable variable. Measurements were made at specular, AOI = AOS, then several angle of incidences near specular, AOI =

AOS  $\pm 5^\circ$  & AOS  $+10^\circ$ . The detector would stay at a fixed angle with respect to the sample, either  $30^\circ$  or  $60^\circ$ . For example, an AOS =  $30^\circ$  would require four AOI measurements of  $25^\circ$ ,  $30^\circ$ ,  $35^\circ$ , and  $40^\circ$ . Each of these eight measurements would be measured for each of the four wavelengths tested, resulting in 32 Mueller matrices for each sample under a single surface condition.

**Table 3.2: UV polarimeter measurements:** The 32 Mueller matrices measured for a sample surface; eight measurements for each of four wavelengths.

Measurement Number	Wavelength (nm)	Angle of Scatter (AOS, sample surface normal to camera)	Angle of Incidence (AOI, sample surface normal to light source)
1	400	$30^\circ$	$25^\circ$
2	400	$30^\circ$	$30^\circ$
3	400	$30^\circ$	$35^\circ$
4	400	$30^\circ$	$40^\circ$
5	400	$60^\circ$	$55^\circ$
6	400	$60^\circ$	$60^\circ$
7	400	$60^\circ$	$65^\circ$
8	400	$60^\circ$	$70^\circ$
9	450	$30^\circ$	$25^\circ$
10	450	$30^\circ$	$30^\circ$
11	450	$30^\circ$	$35^\circ$
12	450	$30^\circ$	$40^\circ$
13	450	$60^\circ$	$55^\circ$
14	450	$60^\circ$	$60^\circ$
15	450	$60^\circ$	$65^\circ$
16	450	$60^\circ$	$70^\circ$
17	500	$30^\circ$	$25^\circ$
18	500	$30^\circ$	$30^\circ$
19	500	$30^\circ$	$35^\circ$
20	500	$30^\circ$	$40^\circ$
21	500	$60^\circ$	$55^\circ$
22	500	$60^\circ$	$60^\circ$
23	500	$60^\circ$	$65^\circ$
24	500	$60^\circ$	$70^\circ$
25	550	$30^\circ$	$25^\circ$
26	550	$30^\circ$	$30^\circ$
27	550	$30^\circ$	$35^\circ$
28	550	$30^\circ$	$40^\circ$
29	550	$60^\circ$	$55^\circ$
30	550	$60^\circ$	$60^\circ$

31	550	60°	65°
32	550	60°	70°

Four polarization properties showed best discrimination between different sample surface conditions. These four polarization properties were the same highly discriminatory properties seen in campaign one:

- Depolarization index (DI)
- Linear diattenuation (LD)
- Linear polarizance (LP)
- Linear retardance (LR)

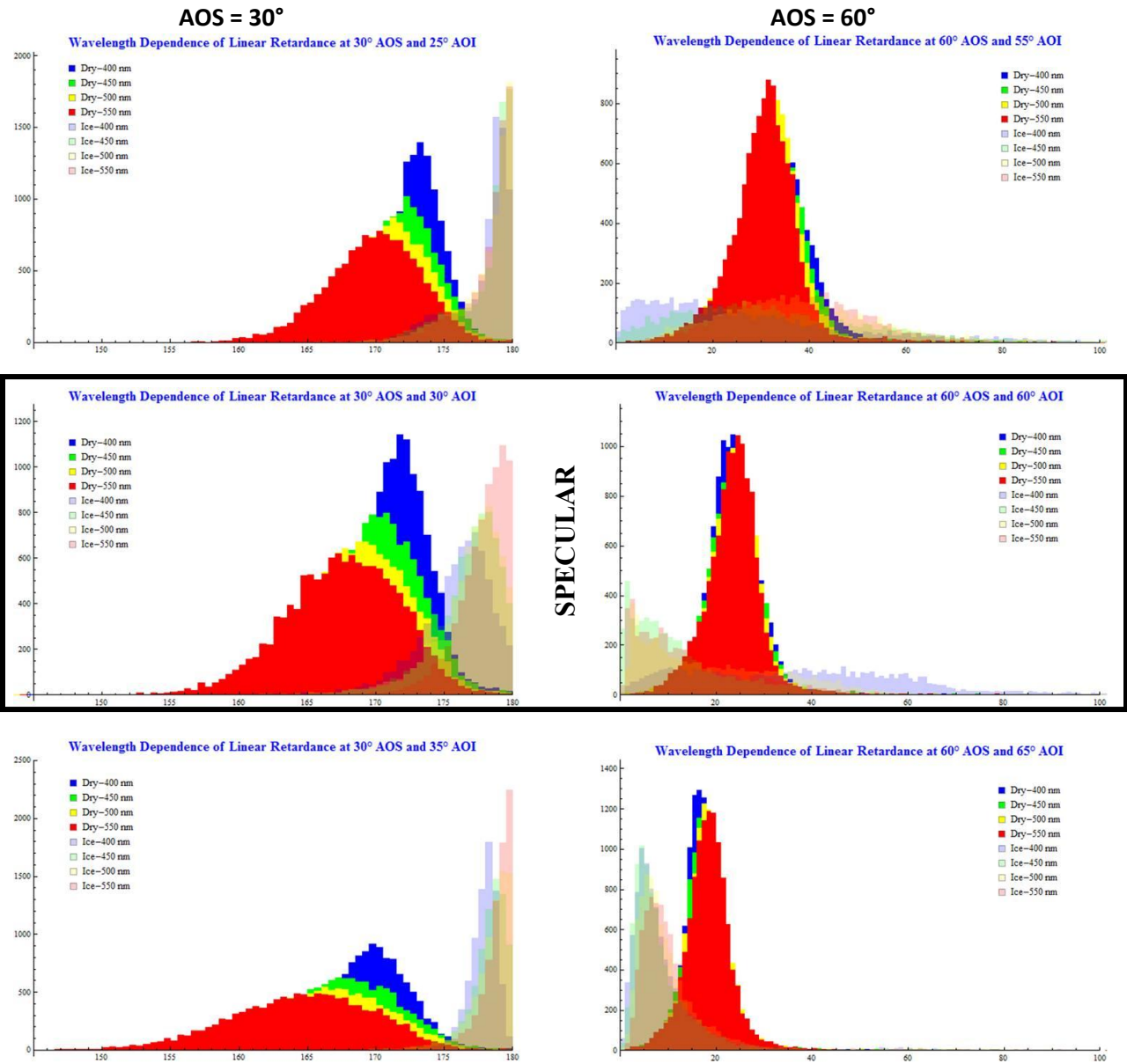
While linear retardance was not a very good dry-ice separator in earlier experiments, this data saw stronger LR responses. Each of these four polarization properties are reported on in detail, and the Orientation dependent polarization properties will be disregarded. Due to the similar nature the final three polarization (circular) properties had with campaign one, these will not be reported on in this section.

Each histogram plot shows a comparison between dry (bright colors) and ice (pastel colors) polarization measurements. Progressions of angles of incidence (AOI) are shown by multiple graphs, the top most being the minimum AOI, and the bottom being the largest AOI. Also note that the data for each of the following polarization properties may be from differing sample measurements. Each data set was chosen from the library because it is the clearest depiction of each particular polarization property response.

**Linear Retardance**

Linear retardance measurements for the dry asphalt decrease in average magnitude as the AOI increases. This means the LR appears to have an inverse relationship with AOI. As AOI increases, dry asphalt LR FWHM increases, while iced asphalt LR FWHM decreases. LR measurements for the dry

asphalt increase in magnitude as wavelength decreases, meaning there appears to be an inverse relationship between LR and wavelength; LR measurements appear to be a direct relationship between LR and wavelength for iced asphalt (see AOS 30°, AOI 30° & AOS 30°, AOI 40°).



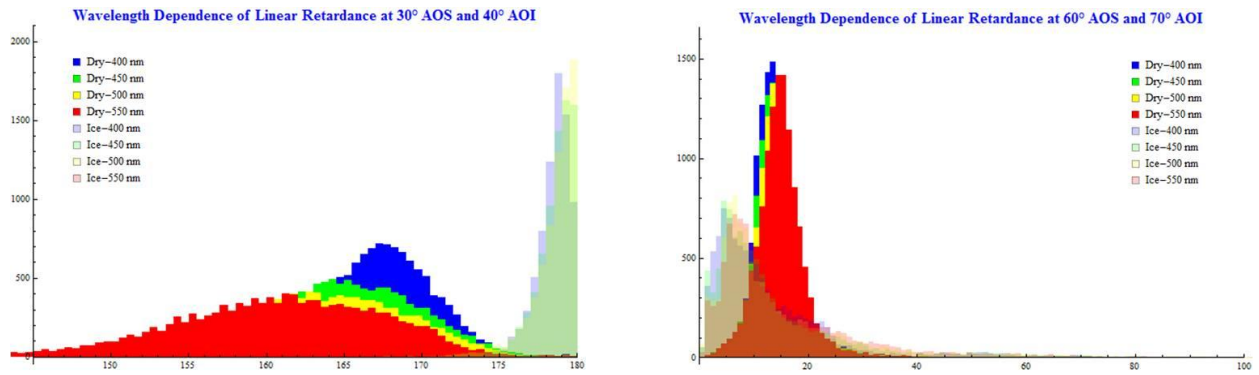


**Figure 3.11: Linear Retardance response for asphalt sample B-1:** Asphalt sample B-1's Linear Retardance property responses as the angle of incidence is increased (moving from top to bottom) for a 30° angle of scatter (left column) and a 60° angle of scatter (right column).

LR measurements inside specular (AOI 55°) for the dry asphalt increase in magnitude as wavelength decreases, meaning there appears to be an inverse relationship between LR and wavelength in this region. Outside of specular (AOI 65° & AOI 70°), for the dry asphalt, the LR measurements decrease with a decrease in wavelength. This means there appears to be a direct relationship between LR and wavelength in this region. LR measurements appear to have a direct relationship between LR and wavelength for iced asphalt (Figure 3.11 see AOI 65° & AOI 70°).

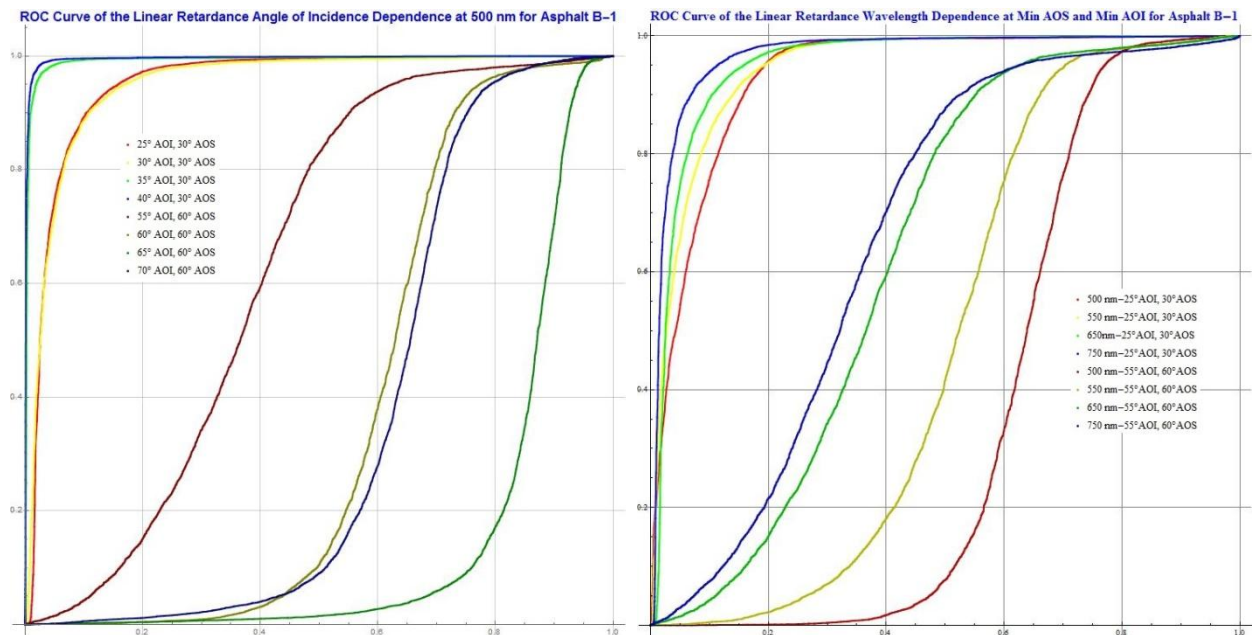
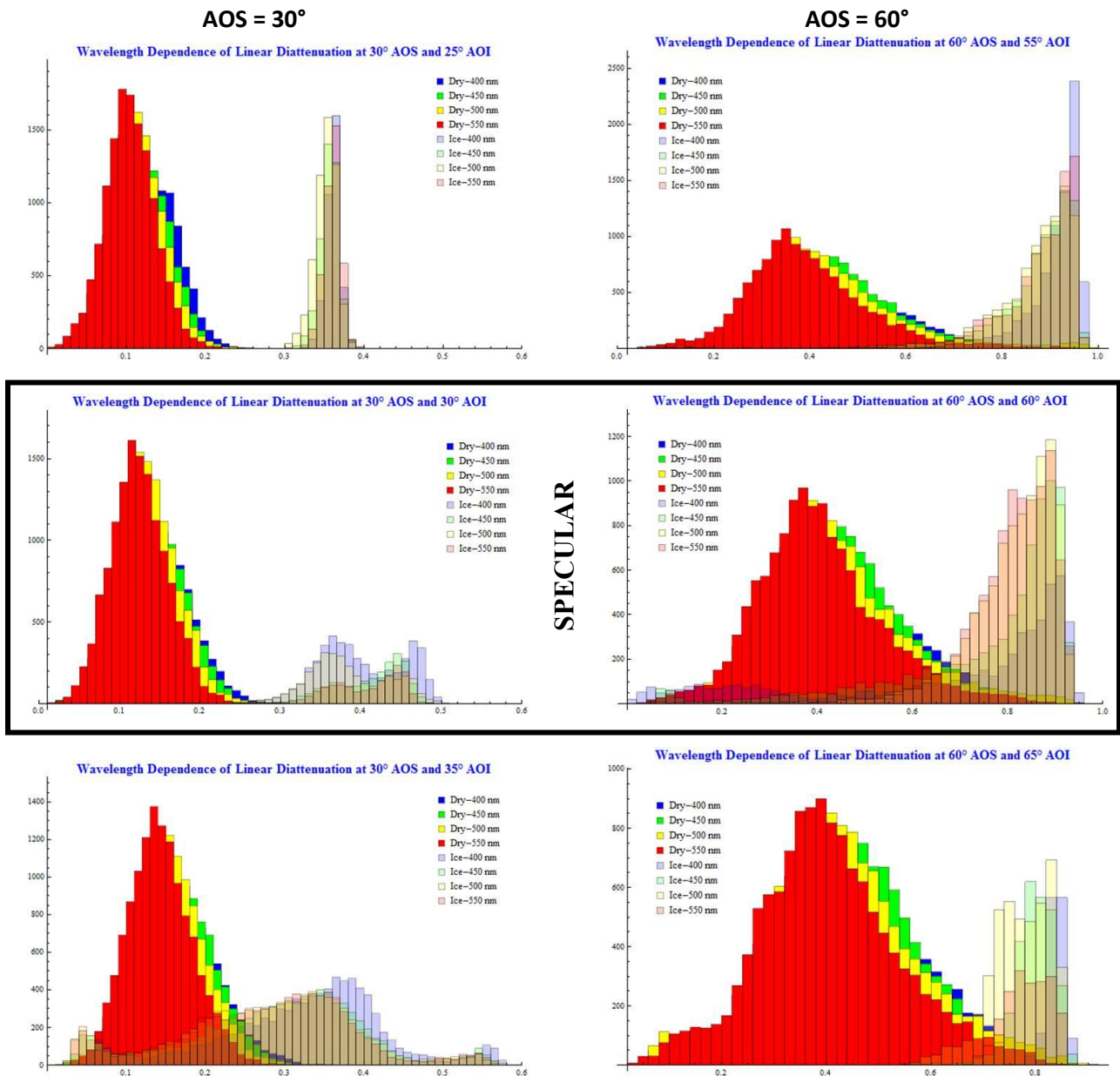


**Figure 3.12: ROC curves for the Linear Retardance property for asphalt sample B-1:** LR angle of incidence dependence (left) at 500 nm, and LR wavelength dependence (right) at respective minimum AOS and AOI.



## Linear Diattenuation

The sample seen in Figure 3.13 is asphalt sample A-2. Measurements for the dry asphalt increase in magnitude slightly as the AOI increases, meaning the LD appears to have a small direct relationship with AOI. LD measurements for the dry asphalt increase in magnitude as wavelength decreases, meaning there appears to be an inverse relationship between LD and wavelength; iced asphalt does not appear to share this relationship.



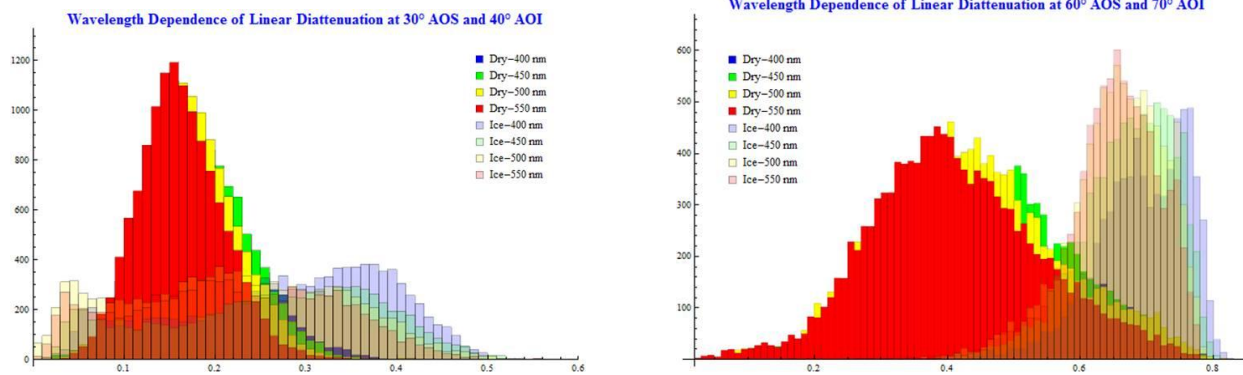


**Figure 3.13: Linear Diattenuation response for asphalt sample A-2:** Asphalt sample A-2's Linear Diattenuation property

responses as the angle of incidence is increased (moving from top to bottom) for a 30° angle of scatter (left column) and a 60° angle of scatter (right column).

LD measurements for the iced asphalt are clearly larger than dry asphalt within specular (AOI 30°, AOI 35°), however, at other AOI's the LD has a much broader FWHM and is difficult to distinguish from dry asphalt. Within specular, the majority of LD values for iced asphalt are found in a small range, meaning the distribution of LD values is limited to a smaller region of LD, also note that the measurements outside of specular, have more counts, which might have occurred from a larger reflectance response above the noise floor (i.e. more light reflected towards camera).

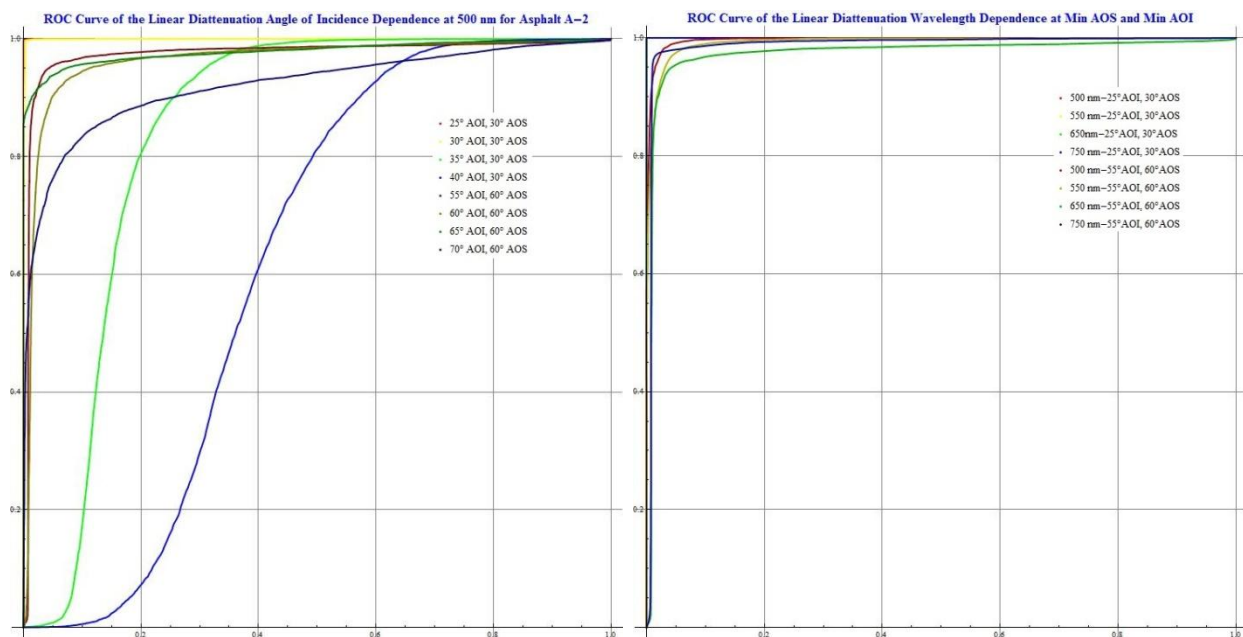


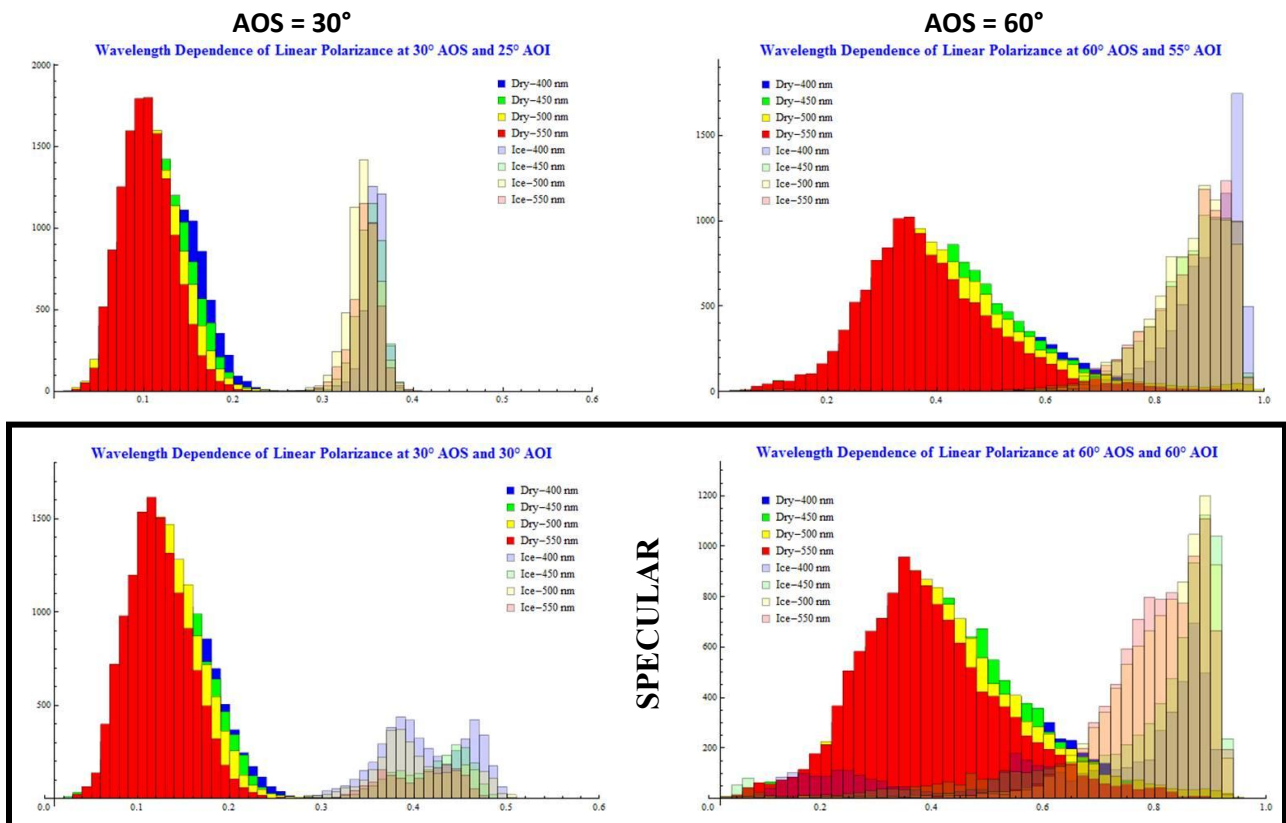
**Figure 3.14: ROC curves for the Linear Diattenuation property for asphalt sample A-2:** LD angle of incidence dependence (left)

at 500 nm, and LD wavelength dependence (right) at respective minimum AOS and AOI.



## Linear Polarizance

The sample seen in Figure 3.15 is asphalt sample A-2. Measurements for the dry asphalt increase in magnitude slightly as the AOI increases, meaning the LP appears to have a small direct relationship with AOI. LP measurements for the dry asphalt increase in magnitude as wavelength decreases, meaning there appears to be an inverse relationship between LP and wavelength. LP measurements for the iced asphalt are clearly larger than dry asphalt within specular (AOI 30°, AOI 35°), however, at other AOI's the LP is indistinguishable between dry and iced asphalt. At specular, the majority of LP values for iced asphalt are found in a small range, meaning the distribution of LP values is limited to a smaller region of linear polarizance. Also note that the measurements outside of specular, have more counts, which might have occurred from a larger reflectance response above the noise floor (i.e. more light reflected towards camera).



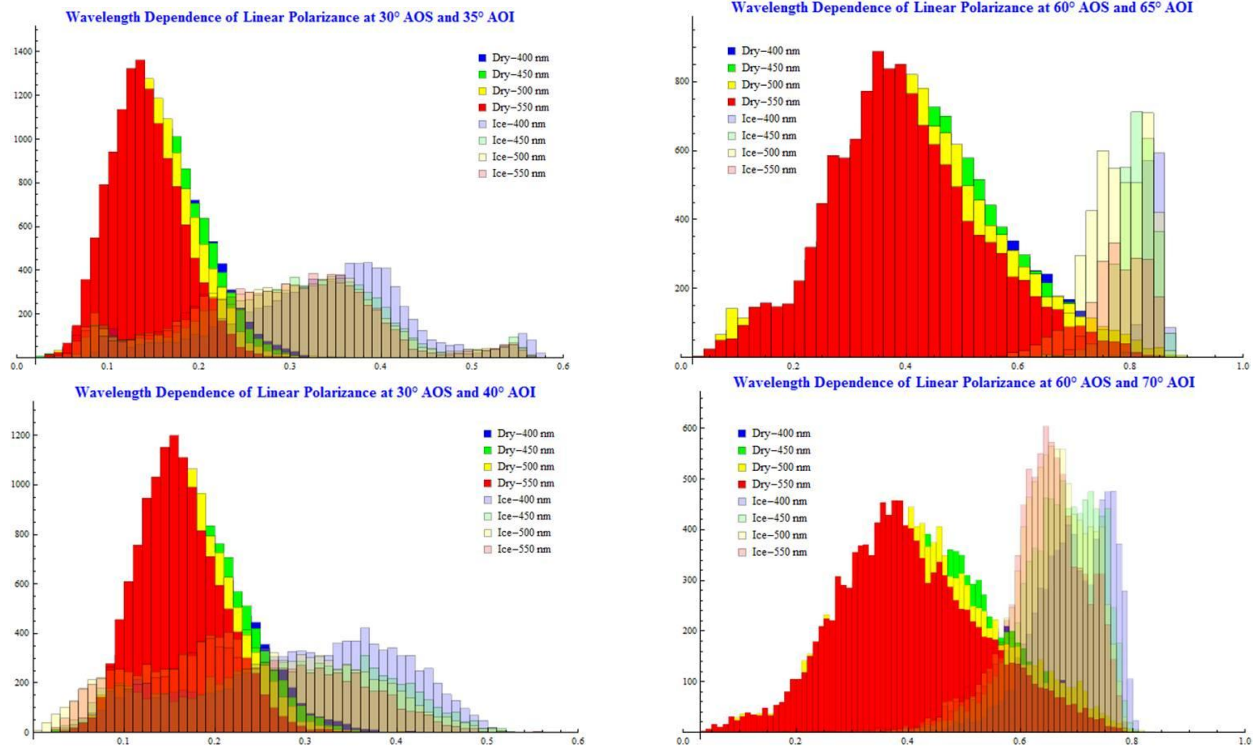


Figure 3.15: Linear Polarization response for asphalt sample A-2: Asphalt sample A-2's Linear Polarization property responses as

the angle of incidence is increased (moving from top to bottom) for a 30° angle of scatter (left column) and a 60° angle of scatter (right column).

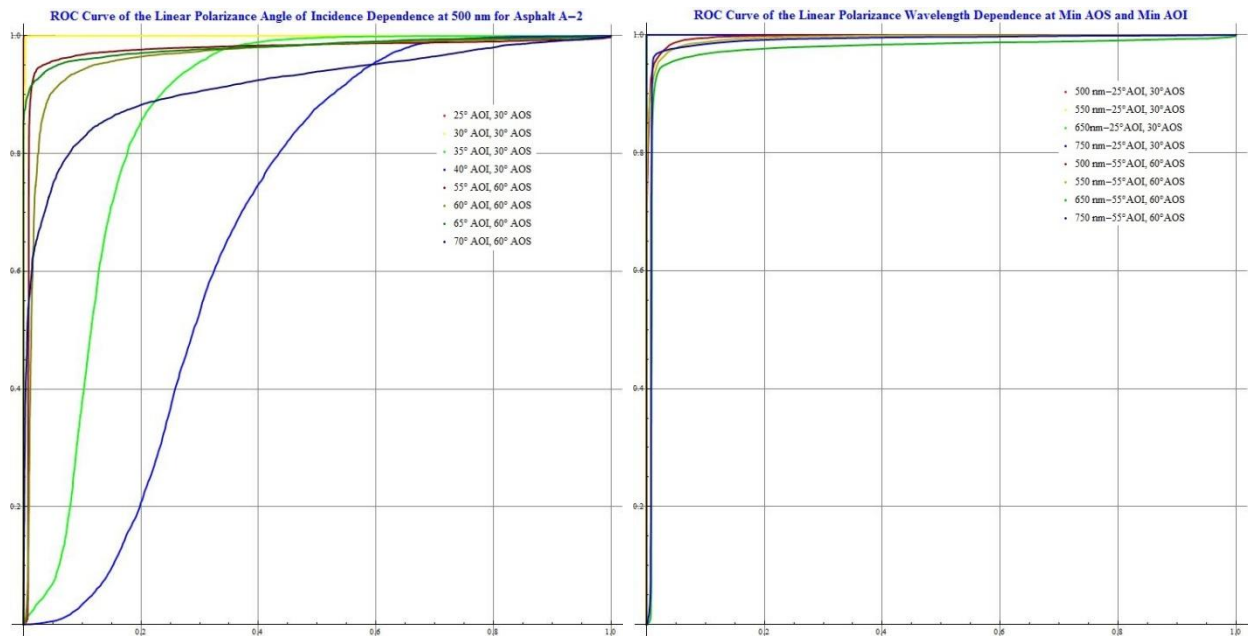
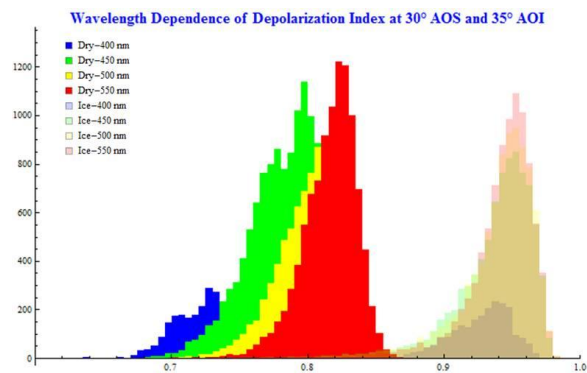
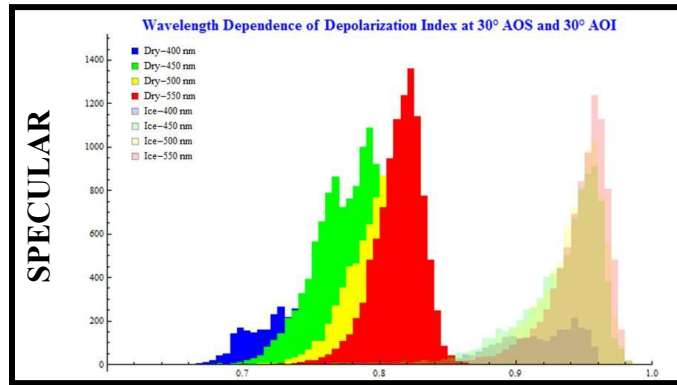
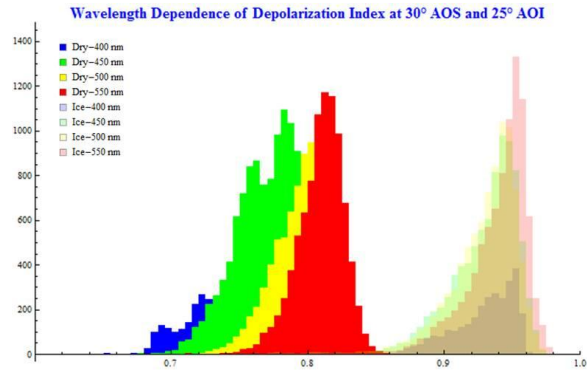


Figure 3.16: ROC curves for the Linear Polarization property for asphalt sample A-2: LP angle of incidence dependence (left) at

500 nm, and LP wavelength dependence (right) at respective minimum AOS and AOI.

### Depolarization Index

The sample seen in Figure 3.17 is concrete sample A-3. For this particular measurement, there is no AOS = 60° data, due to file corruption. However, this particular polarization property (DI) on this concrete measurement produced the strongest ROC curves seen yet.



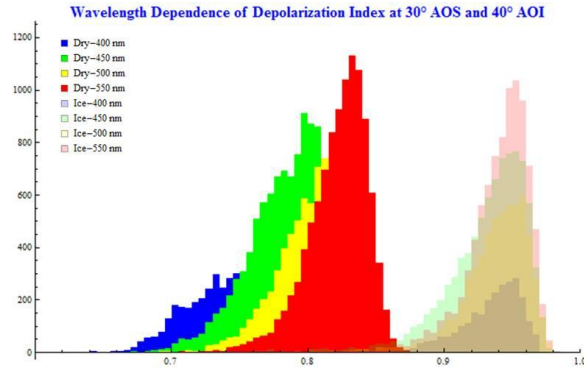


**Figure 3.17: Depolarization Index response for concrete sample A-3:** Concrete sample A-3's Depolarization Index property responses as the angle of incidence is increased (moving from top to bottom) for a 30° angle of scatter.

Iced concrete has a higher DI than dry concrete. Measurements for the dry concrete increase in magnitude slightly as AOI increases, meaning there appears to be a small DI dependence on AOI. DI measurements for the dry concrete slightly decrease as wavelength decreases, meaning there appears to be a slight direct relationship between DI and wavelength.

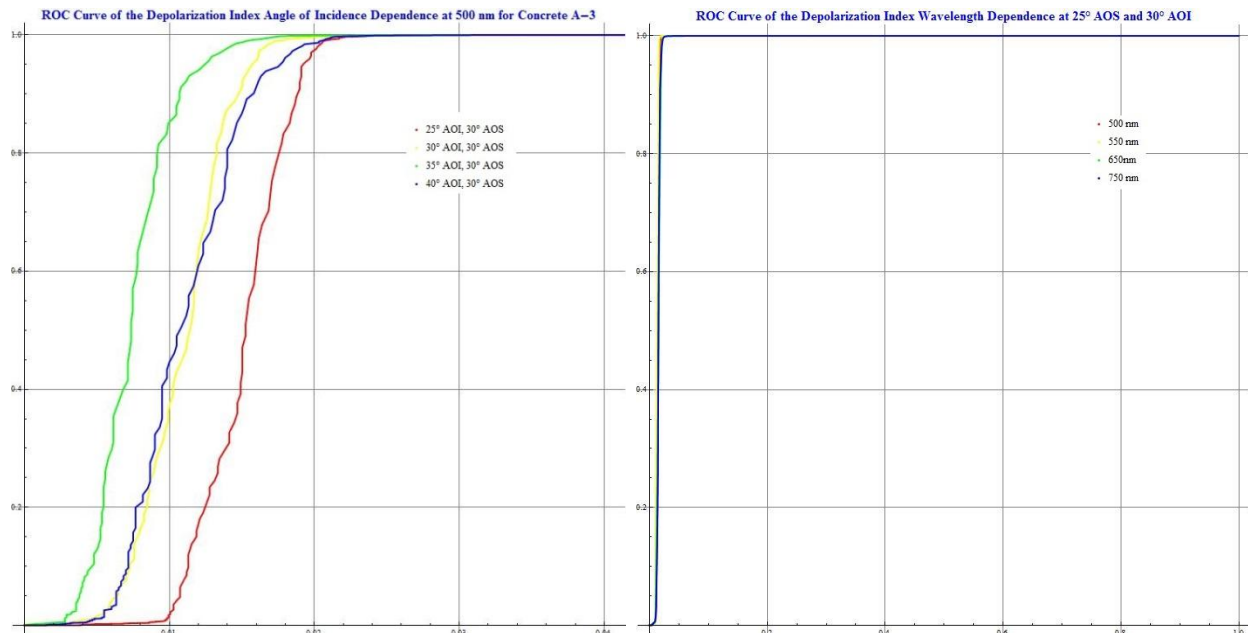


**Figure 3.18: ROC curves for the Depolarization Index property for concrete sample A-3:** DI angle of incidence dependence (left) at 500 nm, and DI wavelength dependence (right) at respective minimum AOS and AOI. Note the scaling differences, i.e. both ROC curves were so sharp that a close up of the elbow of the AOI dependence was used to show the distribution of DI responses.

### **3.3 Campaign 3: NIR Measurement, Wet Sample Measurement, and System Repeatability**

#### **3.3.1 NIR Measurement**

A measurement campaign was taken to characterize road ice polarization responses in NIR and compare it to responses from the rest of the measured spectrum. This was a single measurement of concrete sample A at 820 nm, on the visible polarimeter, shown in Figure 3.19. Collection angles were spread around a specular reflection of 30°. Such conditions were chosen to easily and directly compare NIR test results to a previous measurement of concrete A at lower wavelengths. The following series of histograms shows all of the NIR measurement and includes both dry and ice samples. The NIR measurement showed the same polarization property changes as rest of the measured spectrum.

Data from 820 nm measurement shows excellent ice detection. Iced concrete has a much narrower FWHM than dry concrete. Iced concrete has a higher DI, meaning it preserves the polarization state of incident light much better than dry concrete. Depolarization index showed the largest separation between dry and iced measurements, as seen in Figure 3.20.

Measuring in the near infrared (NIR) shows the same trends in polarization property changes as the rest of the measured spectrum. Discrimination between iced and dry states is once again seen in Linear Diattenuation, Linear Polarizance, and Depolarization Index.

## Linear Polarization Properties

## Circular Polarization Properties

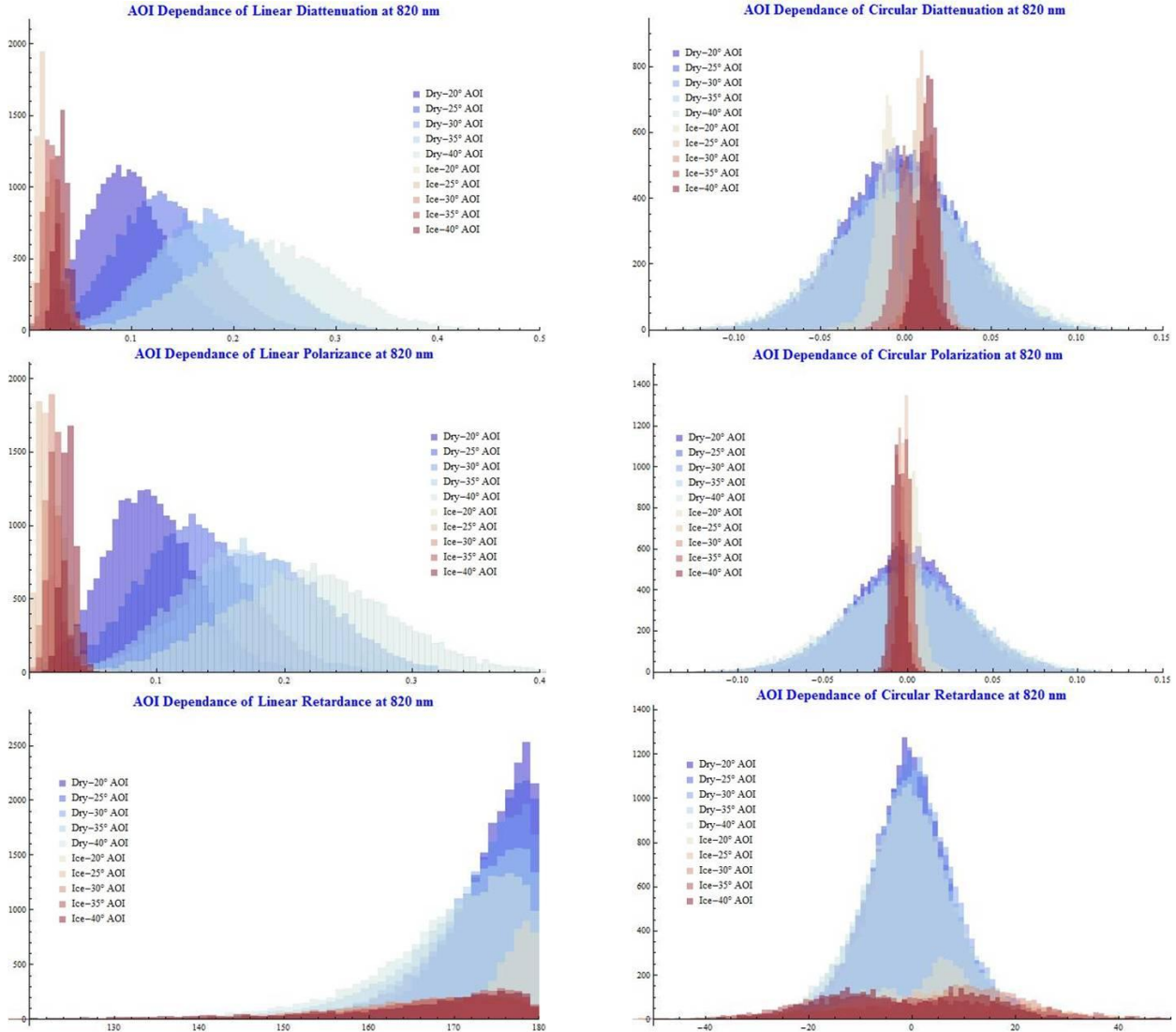


**Figure 3.19: NIR measurement polarization property responses: Concrete sample A's polarization property responses as the angle of incidence is increased for a 30° angle of scatter.**

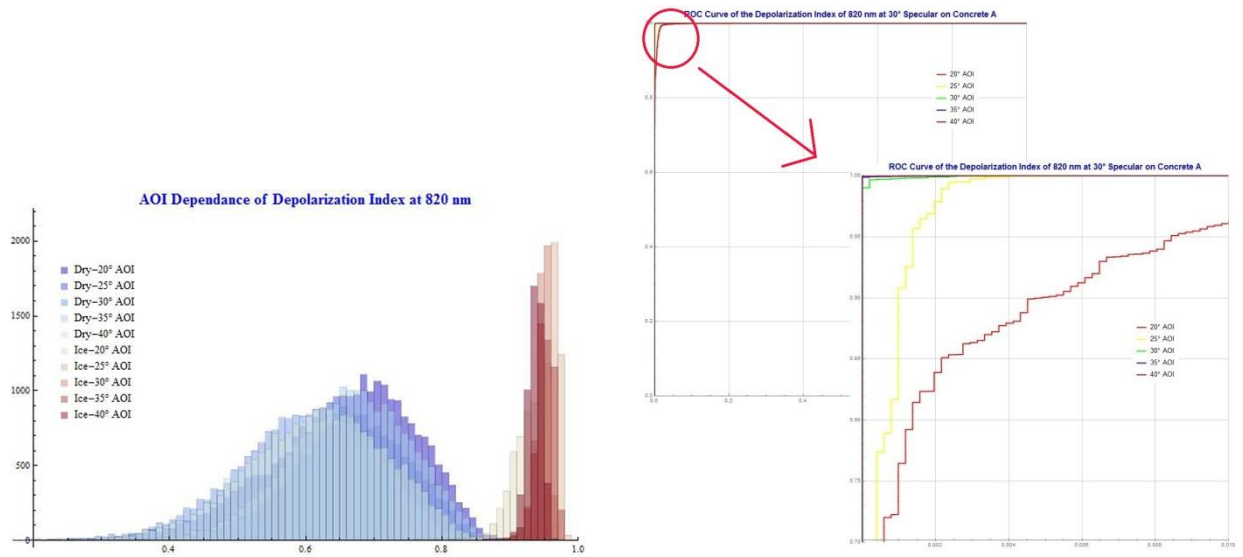


**Figure 3.20: Depolarization Index had highest discrimination:** Concrete sample A's Depolarization Index histogram (left), which shows the largest amount of distinction between the dry concrete (blue) and the iced concrete (red). The corresponding ROC curve (right) shows the AOI dependence of DI at 820 nm and a 30° angle of scatter. Note the detector mask for iced measurement was smaller than mask for dry measurement, resulting in less counts for ice than for dry.

### 3.3.2 Wet Sample Measurement

Ice is not the only danger to roadway travelers. Rain and moisture buildup, even melting ice, on asphalt or concrete greatly reduces surface traction. An investigation into the polarization property changes seen during the presence of liquid water was desired. Ice, water, combinations of ice and water, and dry conditions all have different optical properties. Measuring these fluid conditions became a very different type of process, and required the development of a new testing method, a progression measurement.

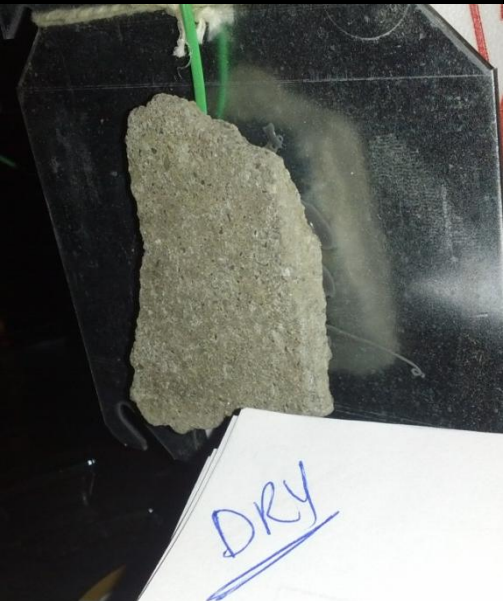

This data is a series of Mueller matrix measurements of a sample as it progresses from dry to wet, back to dry. This measurement was done to evaluate the response of the stronger polarization properties (LD, LP, LR, DI) of the sample surface to the presence of liquid water. A wavelength of 500 nm was chosen, along with an AOS = 30°, AOI = 30°. Four samples were measured. These samples were



mounted in the UV polarimeter using the same setup as described in Campaign 2. A measurement of dry sample was taken. The sample was then wet evenly using a deionized water filled spray bottle.

Measurements of surface temperature and surface resistance were taken and recorded. The Mueller Matrix was then measured. This method was repeated for varying degrees of “wetness” (roughly 2 minutes between steps) and is outlined in Table 3.3.

**Table 3.3: The progression measurement from a dry surface state to a wet surface state back to a dry surface state:** The left column shows images of Concrete sample B as it undergoes this measurement, note the darkening of the surface when it is wet and the lightening as it dries.

 A photograph of a rectangular concrete sample held in a black frame. The sample is light-colored and appears dry. A white card with the word "DRY" written in blue ink is placed in front of the sample. A green string is attached to the top of the sample.	Dry – No water on surface
 A photograph of the same concrete sample, now wet. The surface is dark and glistening with water droplets. A white card with a blue scribble is placed in front of the sample. A red and white spray bottle is visible in the background. A label on the frame reads "CONCRETE - B".	8 Sprays – 8 sprays of the spray bottle were sprayed onto the surface of the sample

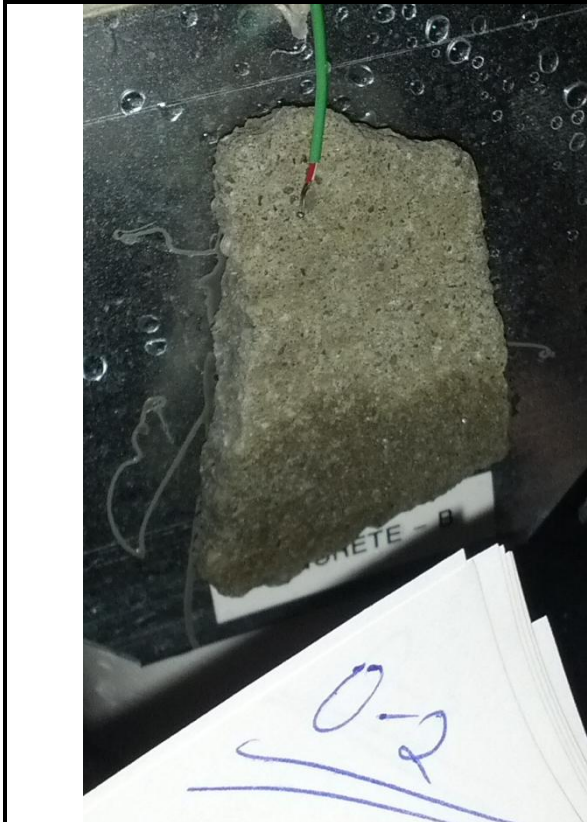




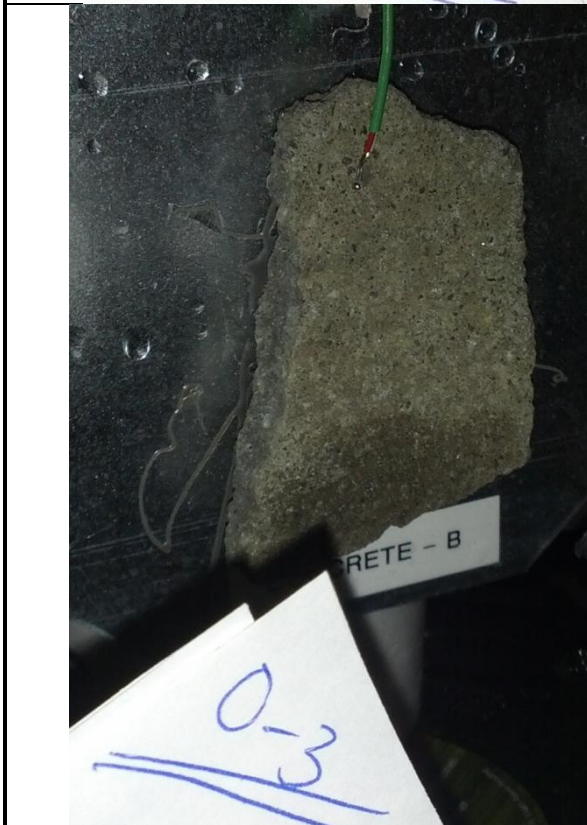
2 Sprays – 2 sprays of the spray bottle were sprayed onto the still wet surface of the sample, this would have a thinner layer of surface water than 8 Sprays, but more than 0 Sprays (1)



0 Sprays (1) – No additional water added to the surface of the sample

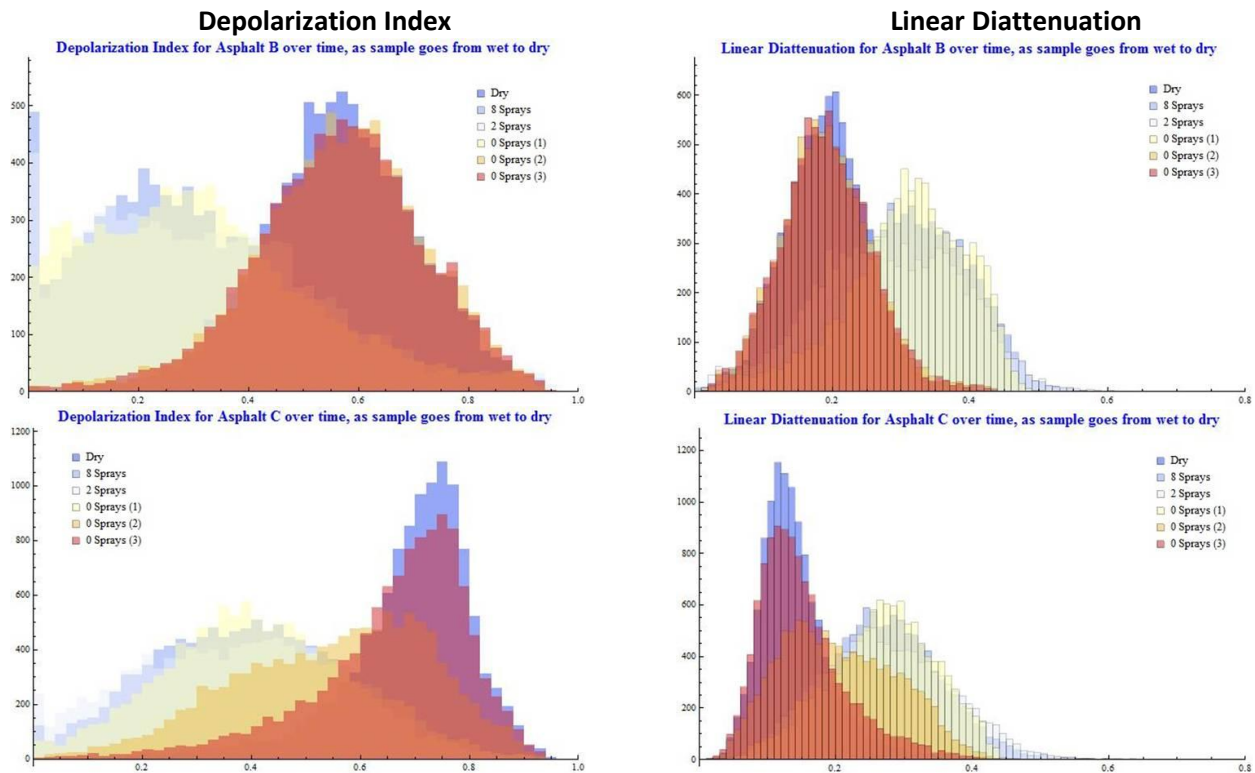


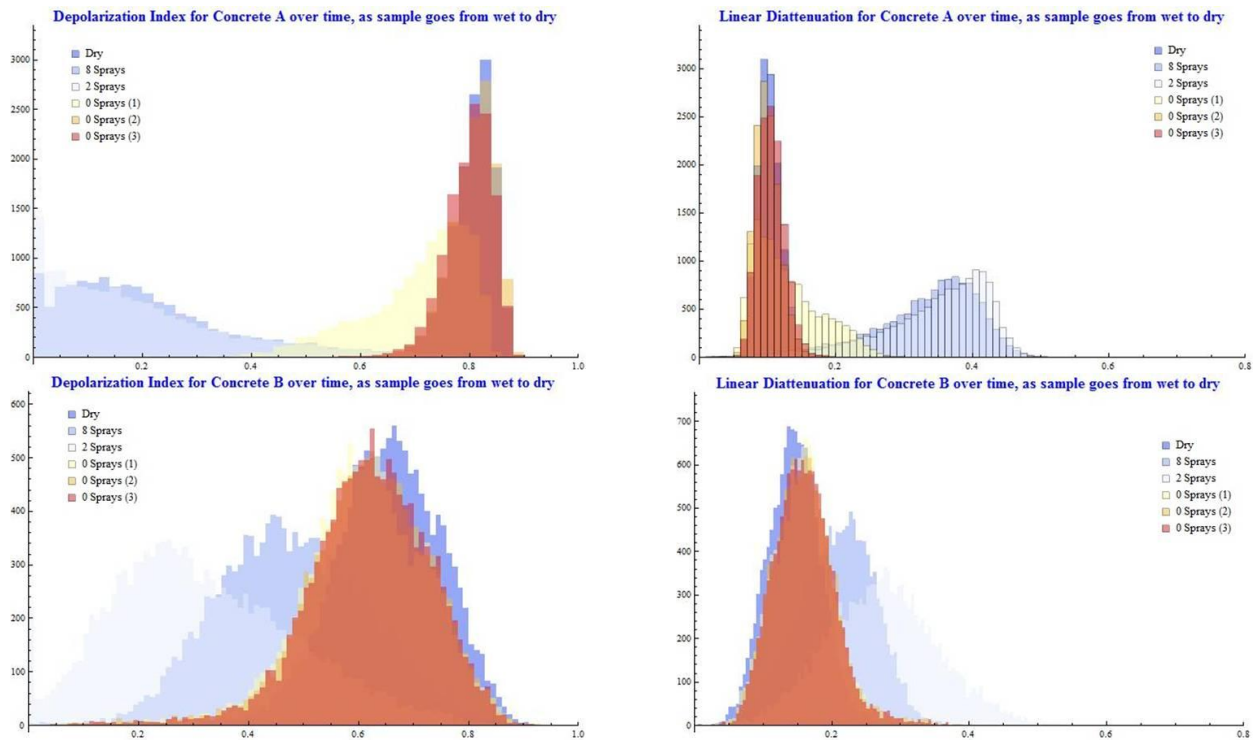
0 Sprays (2) – Second measurement where no additional water is added to the surface of the sample



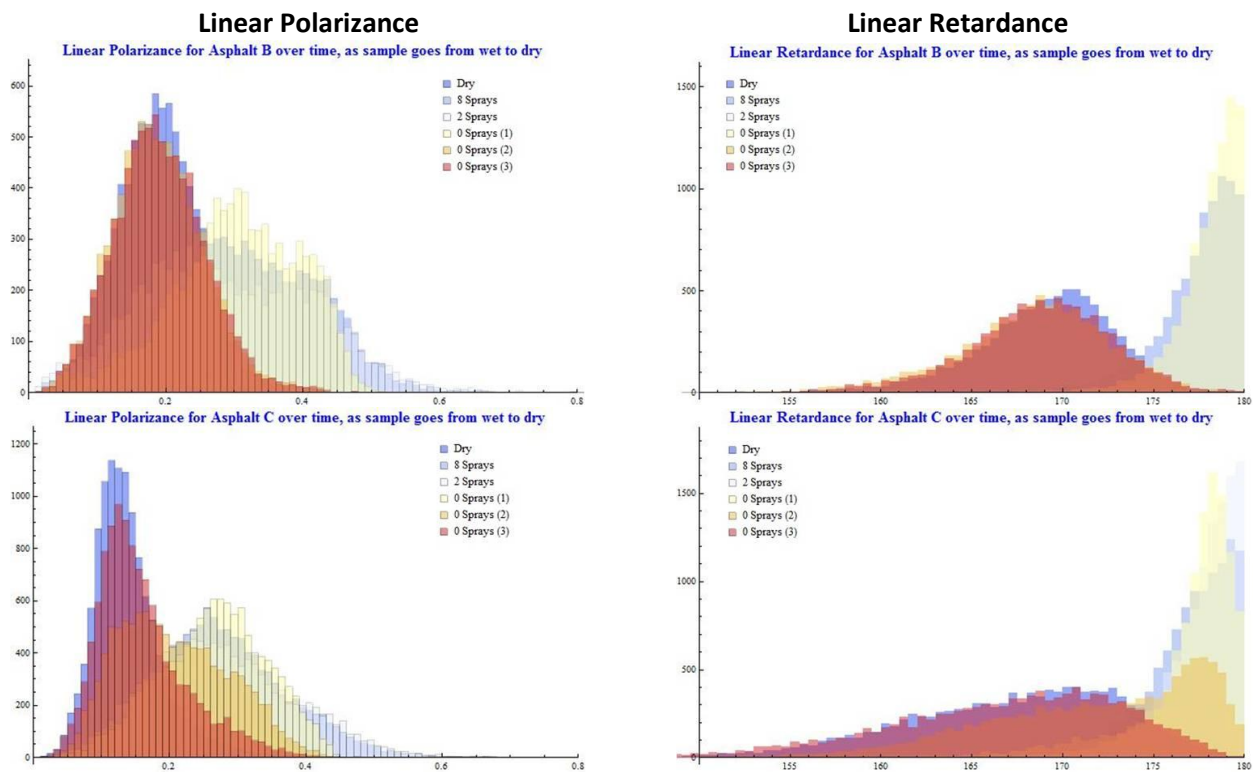
0 Sprays (3) – Third measurement where no additional water is added to the surface of the sample; by this measurement the surface of the sample is dry, a state recognized by the lighter color of the sample surface

New surface variables were recorded in order to better understand and model the water layer present during a measurement. Electrical resistance ( $\Omega$ ) measurements of the surface have been included. Resistance of the sample surface was measured to see if such a metric would provide a good indication of the water layer thickness. However, because the resistances of dry asphalt and concrete are so large, and conducting water layers so thin, changes to surface resistance were hard to measure and only appeared when the sample surface was saturated with a large amount of water. Surface resistance for each of the samples measured is seen in Table 3.4, notice that the large values measured for wet surfaces quickly grow to infinity (or immeasurable by multimeter used) as the surface dries. The histograms below show the surface wetness dependence of each of the polarization properties for each of the samples (excluding sample asphalt A; dry measurement overwritten).





**Figure 3.21: DI and LD responses for wet to dry progression measurement: Depolarization Index (left column) and Linear Diattenuation (right column) responses as the sample surface wetness is changed for a 30° angle of scatter.**



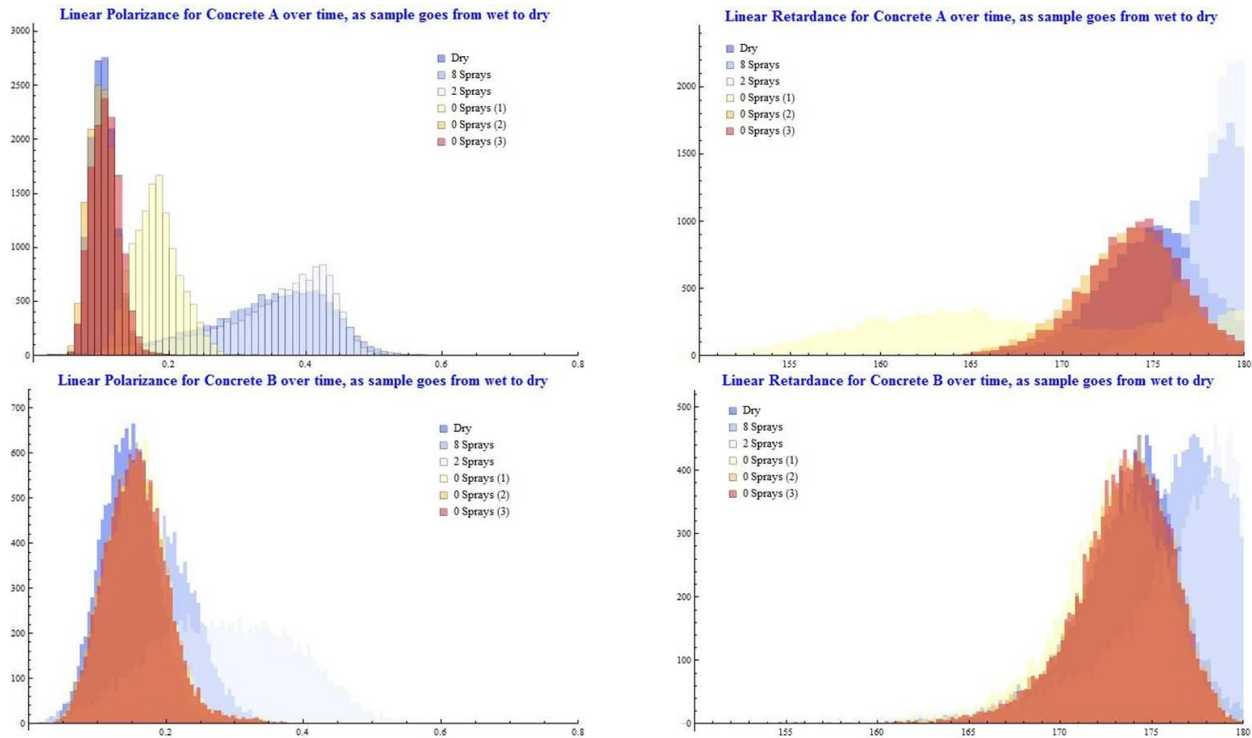


**Figure 3.22: LP and LR responses for wet to dry progression measurement: Linear Polarizance (left column) and Linear**

Retardance (right column) responses as the sample surface wetness is changed (colors) for a 30° angle of scatter.

Many polarization property changes are seen. Figure 3.21 shows that the presence of water decreases the DI in all cases, and that the presence of water increases the LD in all cases. Figure 3.22 shows that the presence of water increases the LP in all cases. The presence of water increases the LR in all cases as well, see in Figure 3.22. As seen before circular polarization properties do not provide distinction between differing surface conditions. No distinction can be made between water coated road, and dry road through CD. No distinction can be made between water coated road, and dry road through CP. No distinction can be made between water coated road, and dry road through CR.

**Table 3.4: Progression measurement surface values:** New surface variables were recorded in order to better understand and model the water layer present during a measurement. Electrical resistance ( $\Omega$ ) measurements of the surface can be used to measure the amount of liquid present, while a temperature measurement can be used to determine if residue water remains after sprays have stopped.

	Dry		8 Sprays		2 Sprays		0 Sprays (1)		0 Sprays (2)		0 Sprays (3)	
	Temperature (°C)	Resistance ( $\Omega$ )	Temperature (°C)	Resistance ( $\Omega$ )	Temperature (°C)	Resistance ( $\Omega$ )	Temperature (°C)	Resistance ( $\Omega$ )	Temperature (°C)	Resistance ( $\Omega$ )	Temperature (°C)	Resistance ( $\Omega$ )
Asphalt A	25.9	inf	23.2	1.78 M	19.3	1.863 M	18.1	inf	20.9	inf	21.3	inf
Asphalt B	24.2	inf	22	inf	18.5	1.90 M	17.7	1.64 M	19.6	inf	20.7	inf
Asphalt C	24.7	inf	19.8	1.34 M	18	1.756 M	17.8	inf	18.6	inf	20.7	inf
Concrete A	24.2	inf	20.9	1.836 M	17	1.51 M	15.7	inf	15.7	inf	15.9	inf
Concrete B	24.4	inf	20.4	1.002 M	17.4	1.901 M	16.2	inf	18.1	inf	19.2	inf

### 3.3.3 System Repeatability

System Repeatability shows the reliability of the polarimeter. This system allows for highly repeatable measurements. One test of how repeatable this polarimetric system is can be done by simply comparing a few measurements in the wet test. Since the wet sample measurement is a progression from dry to wet back to dry, ideally the first dry measurement would exactly match the second dry measurement. Assuming the final dry measurement is truly taken of a completely dry surface, system repeatability can be seen in the complete overlapping of **Dry** measurements with **0 Spray (3)** measurements. With a high enough system repeatability, any changes in polarization property values



between measurements (and between samples) can be attributed to the highly varying surface geometry of each sample.

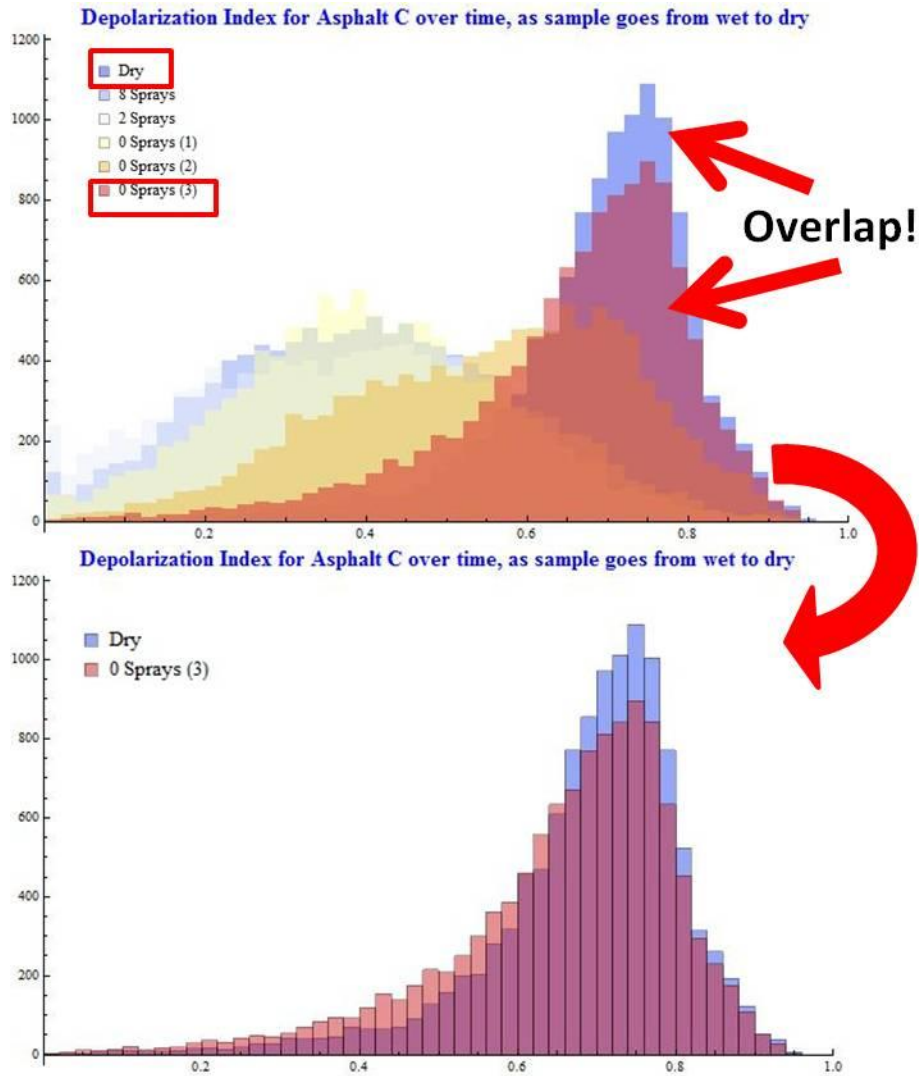


**Figure 3.23: System repeatability:** Progressing from a dry surface state to a wet state back to a dry state, while changing no other variables, should produce exactly overlapping histograms. The overlapping histograms shown here, of the first and last progression steps, show the high level of accuracy of the polarimeter system.

The two measurements seen in Figure 3.23 show a nearly perfect overlap. Differences between these two histograms could come from a not-yet-dry surface for the second measurement (red). A more accurate test would re-measure this surface after hours had passed, and the surface was guaranteed to be completely dry.

## Chapter 4: Discussion

This study is an investigation into using polarimetry to determine road surface conditions. How does the presence of ice make a noticeable difference to the polarization signature of light reflected off a patch of road? Through multiple sample road measurements, interesting polarization property trends have appeared.

Campaign one was an initial survey of the polarization properties of our samples. It gave us an idea of what we could expect in later studies, where we might find interesting polarization responses, and which areas to expand upon. Three polarization properties stood out for having discrimination between dry and iced measurements:

- Depolarization Index
- Linear Diattenuation
- Linear Polarizance.

Campaign two measured the same samples under many more wavelengths and angles, which gave us a larger data library from which to observe trends. It also compared the specular and off-specular reflection responses of each sample, measuring the geometry where most light is scattered. Again, four polarization properties stood out for having high separation between dry and iced measurements:

- Depolarization Index
- Linear Diattenuation
- Linear Polarizance
- Linear Retardance.

Campaign three investigated if the observed polarization property trends hold up at longer wavelengths by measuring in 820 nm. It also investigated if the presence of liquid water could be



determined from a polarimetric measurement. Four polarization properties reacted to the presence of liquid water on the surface:

- Depolarization Index
- Linear Diattenuation
- Linear Polarizance
- Linear Retardance.

A measurement in 1550 nm was desired. This IR wavelength is commonly used in industry which has made it a cheap wavelength to create with a large existing library of 1550 nm optics; great properties for a deployment system. However, our polarimeter capable of measuring 1550 nm resides in a clean room making dirty road samples a contaminant to the room, and has weak intensities in that light range, increasing the measurement time. A summary of the ability of each polarization property as a discriminator is seen in Table 4.1.

**Table 4.1: Polarization Property as a discriminator:** Distinction capabilities of each reported polarization property tabulated for ease of reference. [KEY ○: Polarization property has high contrast, Δ: Polarization property has low contrast, while FWHM difference is large, ×: No distinction is observed]

Condition	Wavelength	Distinction by ROC curves and FWHM of histograms						
		DI	LD	LP	LR	CD	CP	CR
Ice/Dry	500 nm	○	○	○	○	Δ or ×	Δ or ×	Δ or ×
Ice/Dry	820 nm	○	○	○	×	Δ	Δ	Δ
Wet/Dry	500 nm	○	○	○	○	Δ or ×	Δ	×

#### 4.1 Result Implications (Results Viewed in Larger Context)

These results were what we expected. We had expected to find that some polarization properties change with changing surface conditions, while others do not. Dry measurements were expected to behave like a light impenetrable surface, acting as a highly diffuse reflector, scattering rays of light in many directions. Surface smoothness and geometry were expected to be the dominant polarization changing properties. Iced samples were expected to behave more like a specular reflector, reflecting a majority of light in a single direction. The surface ice layer was expected to have a more complex affect on the polarization state of incident light.

Since ice is a transparent solid, in the visible spectrum, we expected some of the incident light to penetrate the ice surface and some of it to be reflected. We expected transmitted light to be manipulated by the H<sub>2</sub>O crystal lattice, and be reflected off the road surface. Pure ice is slightly birefringent, with  $\Delta n = 0.002$  near  $\lambda = 532$  nm. This intrinsic birefringence gives rise to relative phase shift, or retardance, between the two wave components orthogonal to the direction of travel of the incident light. This means that the ice layer acts like a linear retarder, with the retardance,  $\delta$ , being dependent on the ice thickness [Miller]. However, in this experiment the ice measured was polycrystalline, effectively reducing this already small birefringence induced retardance to zero.

We expected the reflected light to behave similar to a specular reflector while also coupling the light into a linearly polarized state (s polarization state, parallel to the ice surface). If light were being transmitted through the ice and being reflected off of the substrate below, we could expect to see differences in Mueller matrix responses due to different substrates. We found that asphalt had better discriminating qualities than concrete, meaning that reflections off concrete were more similar to reflections off ice.

We found that the linear polarization properties tended to show larger differences between dry and iced surfaces, while circular polarization properties showed no measureable distinction. This makes sense because when light hits a specularly reflecting dielectric surface the reflected beam is commonly

partially linearly polarized. Also, when this reflecting surface is transparent, the beam transmitted through the medium is also partially polarized [Chronin]. Since ice is both largely transparent, and capable of strong specular reflections, we would expect it to have a strong influence on linear polarization properties.

Perovich investigated the electromagnetic properties of sea ice by making spectral measurements of the albedo, reflectance, and Stokes vector of the reflected radiance field, in the 400-1000 nm spectrum. Data from this inquiry showed that highest reflected intensities and highest degrees of polarization were found at specular angles [Perovich]. During an investigation of fresh water as well as brined sea water, Sun found that clear (flat) ice polarized more light than ice with air bubbles or sea ice in the visible spectrum, but were similar in NIR wavelengths, implying a significant contribution of polarization derived from specular reflection [Sun]. These results agree with our high linear polarization values found at specular for iced sample measurements. It is interesting to note, for future deployment design, that Sun's experiment also concluded that NIR measurements (beyond 1500 nm) appear to be independent of ice quality (including no obvious change in degree of linear polarization). Meaning ice with bubbles appears spectrally indistinguishable from black (clean and clear) ice [Sun]. Investigating whether or not surface roughness is detectable in NIR would be useful.

Miller conducted a study which measured polarization dependent light scattering in sea ice. They found that the platelets of pure water ice that form are weakly birefringent and show varying degrees of orientation depending on growth conditions [Miller]. Our linear retardance measurements also show a small birefringence in road ice. However, such birefringence is ruled by ice thickness, making it fairly unmeasurable in field conditions where detecting even thin layers of road ice is desired.

Because our ice samples created a smooth air-dielectric boundary, we were expecting to see measurements that indicated iced surfaces were more polarizing than dry, and that is what we saw. Linear diattenuation measurements for iced surfaces were closer to a value of 1, while dry surfaces were

nearer 0.5, meaning that the majority of light reflected off an iced sample had a single linear polarization state.

Depolarization index values also supported this hypothesis. Iced samples had higher DI values than dry samples, indicating a proclivity to preserve the polarity of incident light for icy roads. Because of this we expected to have higher Depolarization Index values for concrete than asphalt. Remember that, larger depolarization index values indicate a proclivity of a surface to preserve the polarization of incident light. If a surface is smooth and uniform, theoretically, reflected rays should all be affected the same way, and in the same direction. If a surface has prominent hills and valleys, much like an asphalt surface, rays will be reflected in different directions causing polarization degradation from multi-path scattering [Chronin]. In fact, in an experiment where the effects of surface roughness were isolated, by artificially roughening part of a 31 cm thick, smooth, young ice sheet, spectral results showed that reflectance and degree of linear polarization were much greater for the smooth surface [Perovich]. This shows that linear polarization or linear diattenuation measurements alone are enough to distinguish rough from smooth surfaces, but might not be enough to distinguish ice from asphalt.

Because our results were not very wavelength dependent, this suggests wavelength can be a degree of freedom during the deployment design process. Eye-safe light sources, such as NIR LEDs, are a good solution to protecting road users from device injury. Wavelengths far from the Sun spectrum are also smart. This would reduce the possible error induced by sunlight in measurements taken during the day, also allowing day and night measurements to be processed the same way.

The FWHM of a measurement is a good indicator of surface roughness. For example, if a measurement has a broad distribution of values, the surface being measured is most likely rough. If a measurement has a narrow spike as its value distribution, the surface is most likely smooth. If the surface is smooth, and each spot illuminated is made of the same substances and thicknesses

(relatively), the Mueller matrix should be fairly uniform, resulting in narrow FWHM histogram. Larger measurement areas could also produce a more uniform polarization response.

Asphalt measurements tend to have higher quality ROCs than concrete. From earlier discussion, part of this results from surface smoothness differences. Since concrete is smoother than asphalt, a property that is closer to the surface geometry of ice, we can expect LD and DI values to have less dry-to-ice separation. Material composition may also be responsible for this better response. For example, the dark shade of asphalt might absorb light normally reflected by ice, or the asphalt's surface roughness may scatter the light much more than ice. Concrete has bulk scattering from transparent sand grain imbedded in the surface, diffusing light and reflecting it away from the detector. This might require changes in deployment method for different surfaces.

## **Chapter 5: Conclusions**

Not only is polarimetric ice detection an exciting and novel use of polarization, it has the potential to improve road safety through real-time ice response measures. Through our investigation polarimetric ice detection is possible. Results show several promising polarization properties which react to the presence of ice. Linear diattenuation, linear polarizance, and depolarization index all consistently have high quality ROC curves, meaning that a measurement of these particular polarization properties distinguished between a safe dry road and a slick iced road in lab experiments. Continued experimentation should provide a method of polarimetric road ice detection.

### **5.1 Summary**

Our study was performed with Mueller matrix imaging polarimeters. Representative road surfaces were illuminated with a series of light polarization states. Reflected and scattered light was collected and its polarization state measured. These measurements covered all possible combinations of

incident and scattered polarization states (Mueller matrices). Receiver operating characteristic (ROC) curves were used to rank each polarization property's ability to detect ice. Several polarization measurements showed excellent performance, the best being linear diattenuation and depolarization index.

## **5.2 Future Considerations**

Evaluating polarimetry as a mode of road condition testing, in a lab and in the field, is a large undertaking with many variables. These variables included observation and incidence angles, wavelength, sample surface, ice type, thickness, temperature, ice cleanliness, etc. In order to streamline this research survey most variables were fixed, including ice manufacturing, ice cleanliness, thickness, temperature, etc. Future lab studies should study the effects of changing these variables which will be uncontrolled in the field.

Different types of ice need to be prepared for lab studies. Many different types of ice exist, each with slightly different optical properties. For example, snow is diffusely reflective while black ice is almost perfectly transparent. Such diversities in ice create a difficulty for ice detection technologies in the field. To improve ice detection in the field, these different types of ice need to be polarimetrically characterized and ice detection algorithms optimized. Once their properties as a polarization element are known, we can see the traces of their existence in field data and react appropriately. One difficulty is growing these different types of ice. Each type of ice requires a specific combination of atmospheric dryness, fluid dynamics (movement), purity, temperature, change in temperature over time, etc. creating a new puzzle for each ice type. It is desirable to have a system capable of not only detecting the presence of ice, but also able to determine the type of ice present. Such knowledge of ice type will further enhance road safety. It could also reduce environmental impact by distinguishing and spraying salt for dangerous black ice and not for less harmful frost.

This investigation focused on the effect of light illumination geometry and spectrum. First, we studied what effect the angles of incidence and scatter had on the quality of ROC curves. Specular angles were found to have the highest levels of reflected light and consistently good ROC curves for the ice detecting polarization properties (linear diattenuation, depolarization index, etc.). Higher levels of reflected light allow for shorter measuring periods, in turn allowing for more measurements to be taken. Higher levels of reflected light also increase the signal-to-noise ratio (SNR), moving the measured intensity away from the noise floor and reducing system error.

The effect of wavelength on the quality of ROC curves was investigated. Wavelengths within the visible spectrum showed little variation; the closer the wavelength is to blue-green, the more light will be absorbed by water. This could be used as an ice indicator in the future, however, because of the low reflectance of asphalt, it would be hard to detect. Testing in the IR and NIR should be pursued. Our measurement in the NIR (850 nm) showed similar behavior to visible light ice detection abilities via ROC curves. It is also a preferred light source for system deployment. Illumination with IR light is eye safe so streets can be illuminated with 1550 nm light without danger to humans, dogs, squirrels, etc. The sun is not as bright at 1550 nm as it is in the visible spectrum, so less daylight interference will be encountered. IR also works at night, and is better at penetrating through dust, fog, and rain. It may penetrate further into samples and scatter less (a characteristic discussed in the previous section).

Active illumination versus passive illumination is also a consideration. Actively providing a light source will ensure consistent illumination of the test surface. Natural sources of illumination, the sun or existing streetlamps, are not constant and reliable. Figure 5.1 shows the possible changes in natural light intensities throughout a period of three days. Firstly, if the sun is being used as a light source, cloud cover, and shadows from roadway structures and buildings would cause fluctuations throughout the day. Measurements couldn't be taken at night after the sun sets, and light pollution from passing cars and streetlamps would cause measurement spikes. Measuring at night is an important ability. Since

nighttime is when temperatures usually drop, it becomes the most likely time for ice to form. Actively illuminating the scene allows for much more control. Not only would there be a consistent source of light, but this light could be a single wavelength, reducing noise from other sources. The light actively illuminating the road surface could be pulsed. Pulsed incident light, with synchronous detection, will allow for lower noise data collection in the day, and reduce the impact of ambient light. It will also decrease the power consumption of such a system.

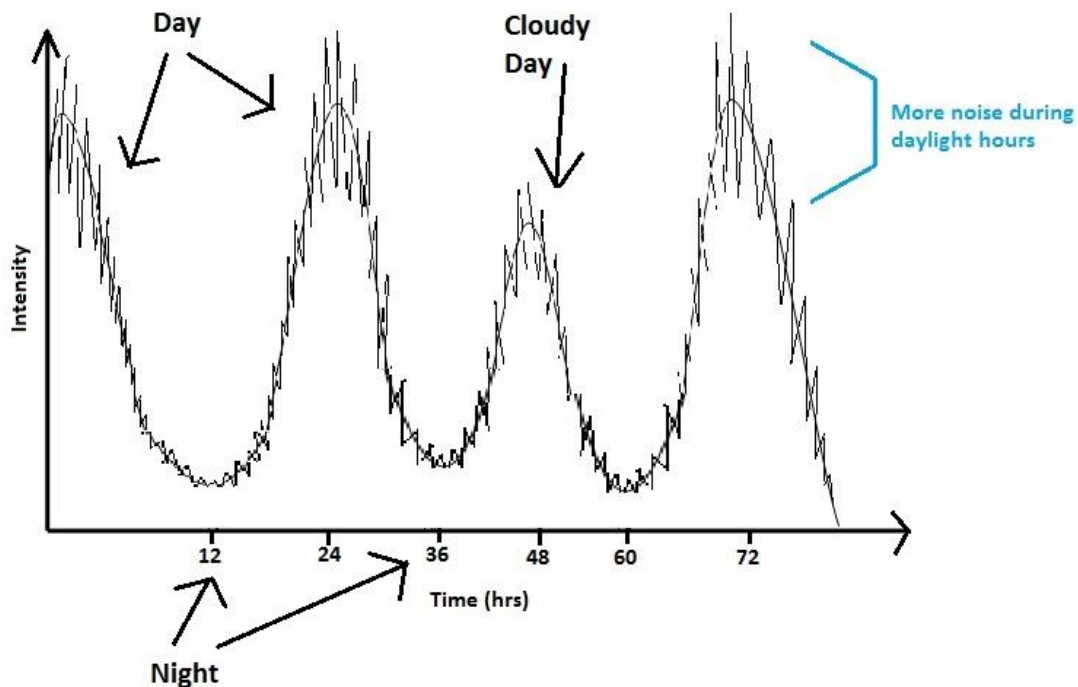


**Figure 5.1: Natural environmental light intensity fluctuates over time:** Daylight has the sun as a source of light, while night has the moon, headlights, and streetlamps as sources. Noise levels are different in each of these cases from the varying nature of these sources. For example, clouds vary sunlight, headlights vary with car speed and direction, etc.

Since this technology will be deployed along roadways, multiple systems are expected to be utilized making cost an important aspect of design. 1550 nm light sources and detectors are produced in high volume for fiber optic communications. It is a commonly used wavelength in many different applications and can be found in multiple energies, sizes, and durability. However, this scientific investigation did not study if 1550 produces good ROC curves with concrete, asphalt and ice.



A combination of discriminating polarization properties could be measured to increase the accuracy of a measurement system. Deployment concepts take into consideration these different design options. One such concept is a two post (source and detection) system. Multiple sources could be mounted to a post at different heights, focused on a section of roadway. Different heights will allow for different specular angles to be measured, and different sources allow for multiple wavelengths to be used. There will also be a detection post, equipped with polarization cameras at heights to match respective sources. These polarization cameras could be a single pixel detector equipped with optical elements needed to capture a particular polarization property, or it could be a more complex polarization imaging system, such as a polarimeter. Figures 5.2 and 5.3 show examples of conceptual two-pole deployment systems.

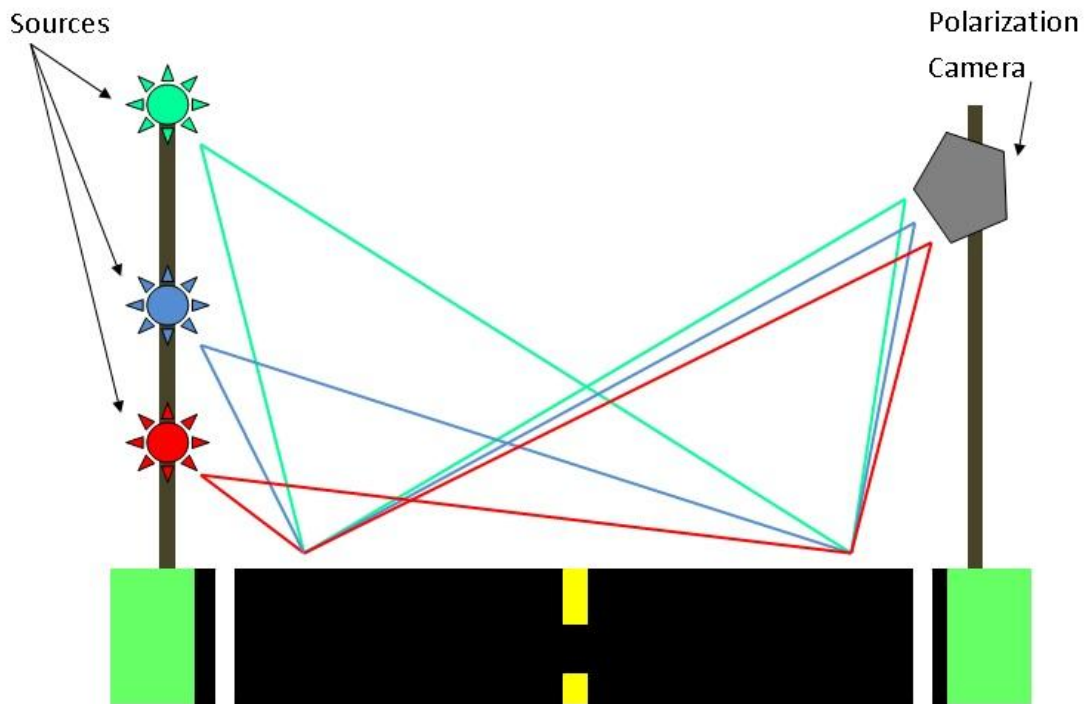


**Figure 5.2: Multiple source, single detector, two-pole system:** An example two-pole system with three sources, multiple wavelengths, and a single detector. Each of the sources is mounted to a pole at different heights, creating differing angles of incidence.

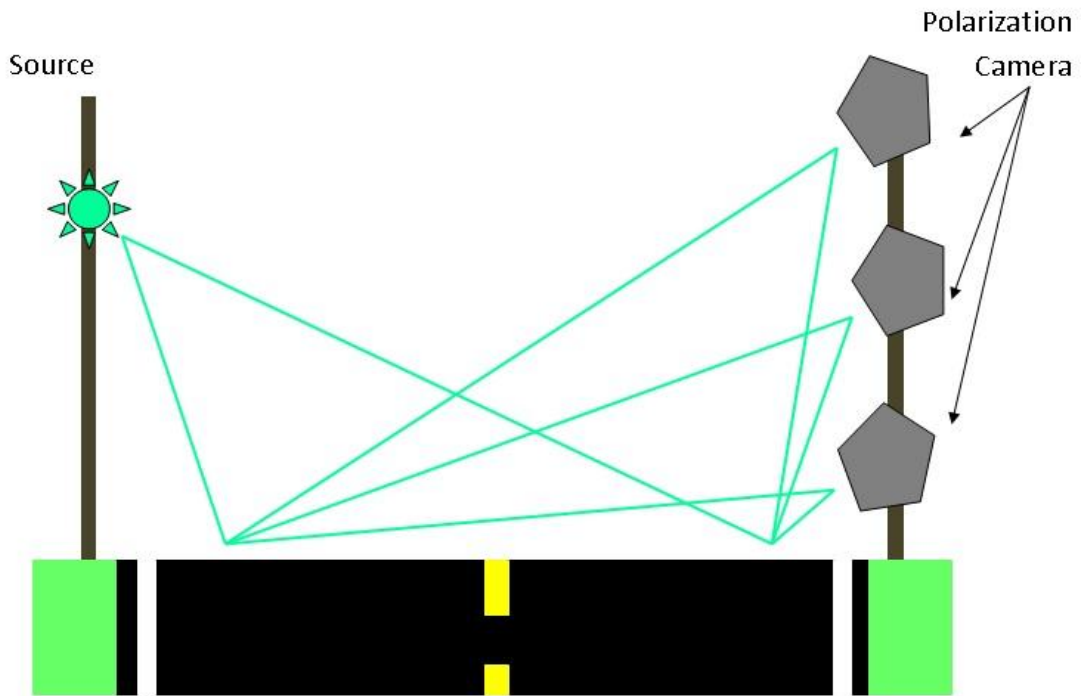


**Figure 5.3: Single source, multiple detector, two-pole system:** An example two-pole system with a single source, and three detectors mounted to a pole at different heights, creating differing angles of scatter.

## **APPENDIX A – SUPPLEMENTAL DATA**





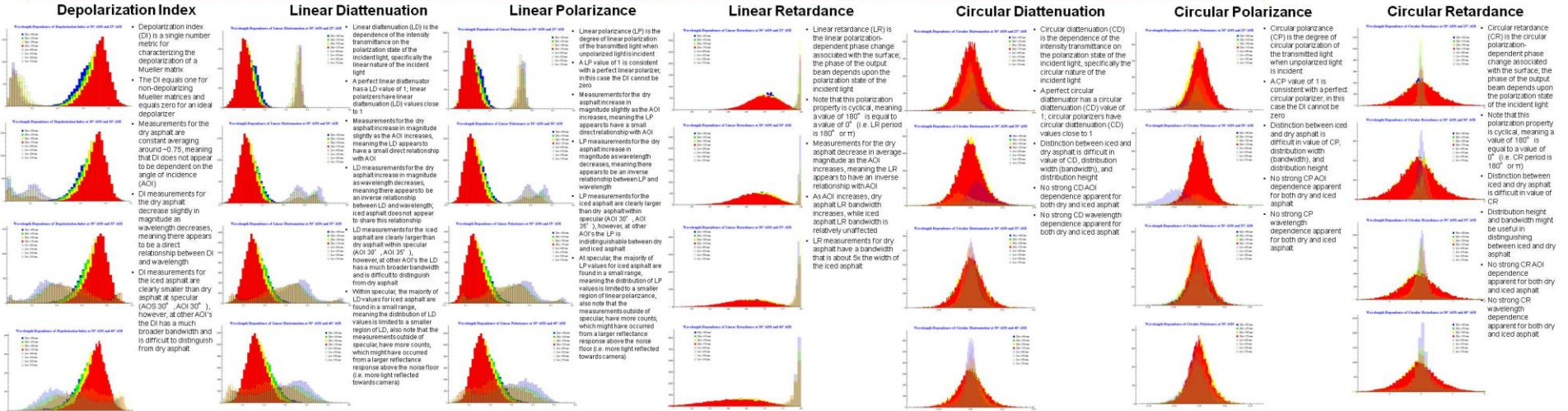
# Detecting Road Conditions with Polarimetry

Krista Drummond, Russell A. Chipman, Karlton Crabtree  
University of Arizona College of Optical Sciences

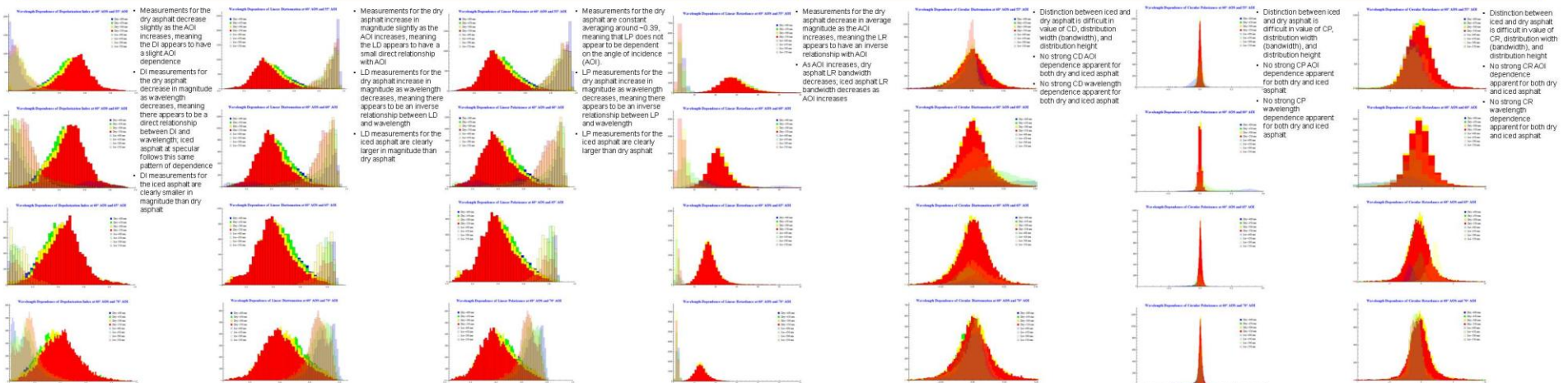


## Asphalt (Measurement AsphA2) – UltraViolet Spectrum

Angle of Scatter 30°



Angle of Scatter 60°



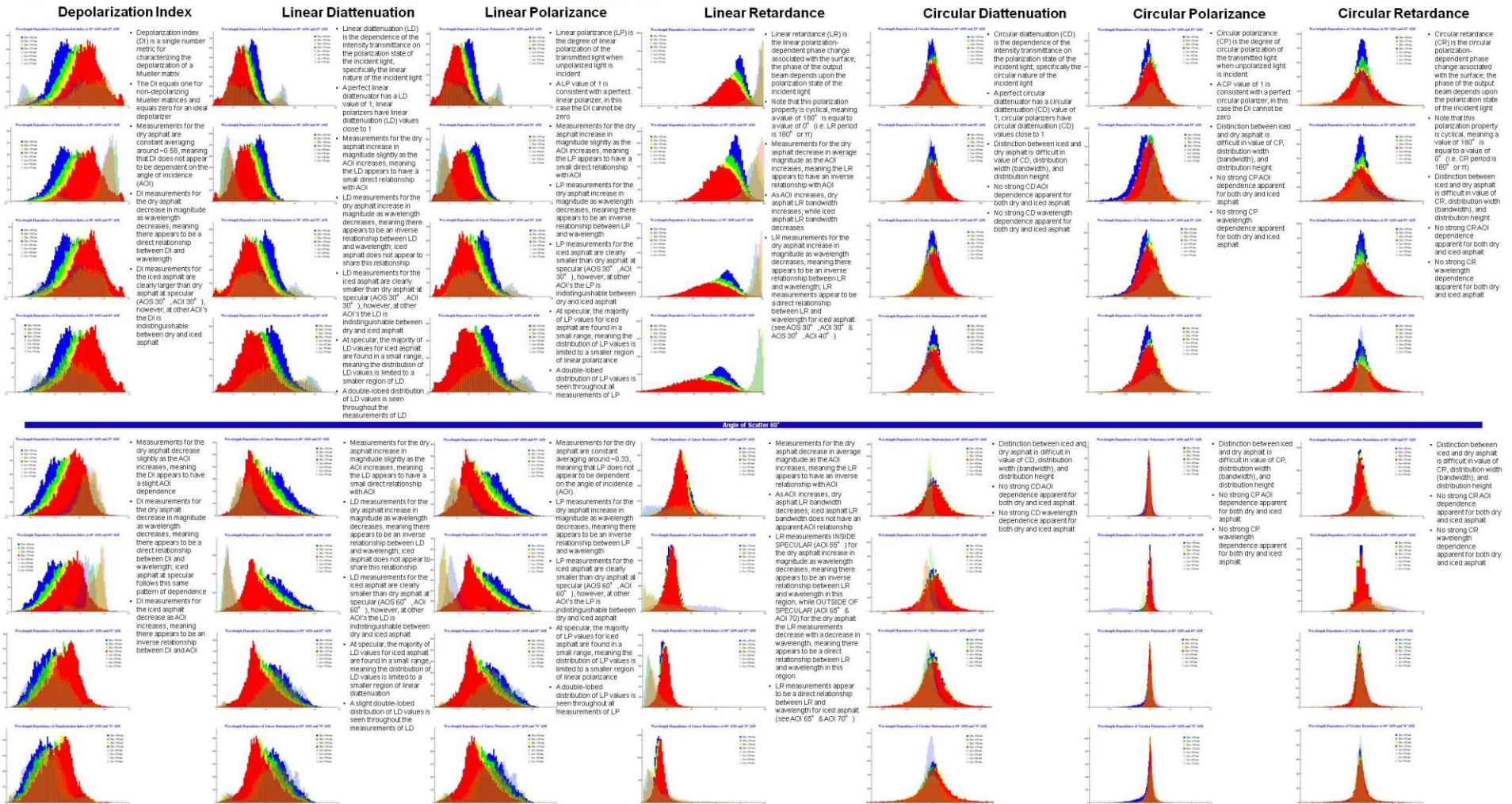


# Detecting Road Conditions with Polarimetry

Krista Drummond, Russell A. Chipman, Karlton Crabtree  
University of Arizona College of Optical Sciences



## Asphalt (Measurement AsphB1) – UltraViolet Spectrum



# Detecting Road Conditions with Polarimetry

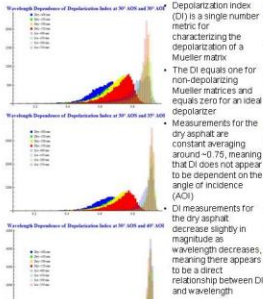
Krista Drummond, Russell A. Chipman, Karlton Crabtree  
University of Arizona College of Optical Sciences



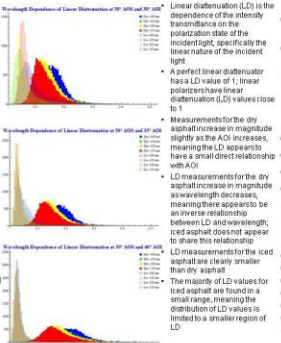
## Asphalt (Measurement Asphalt1) – UltraViolet Spectrum

Angle of Scatter 30°

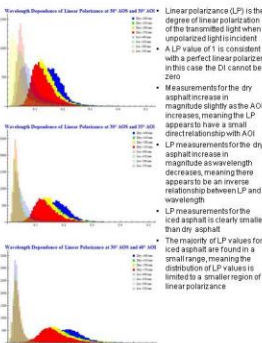
### Depolarization Index



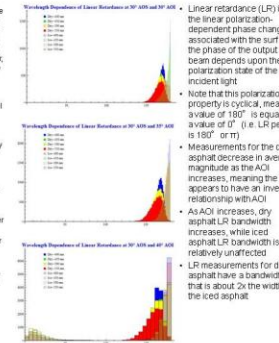
### Linear Diattenuation



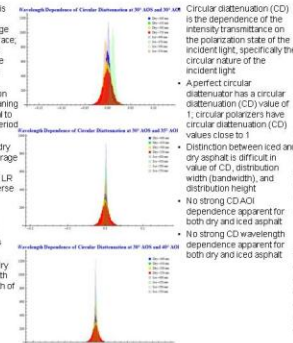
### Linear Polarization



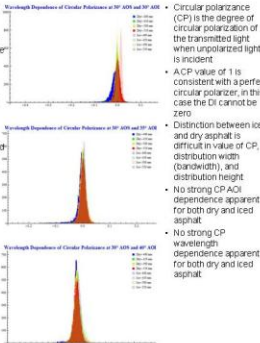
### Linear Retardance



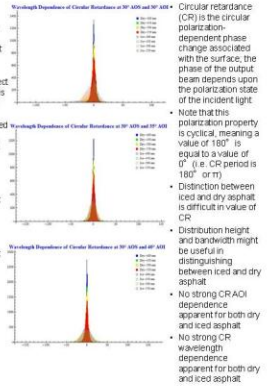
### Circular Diattenuation



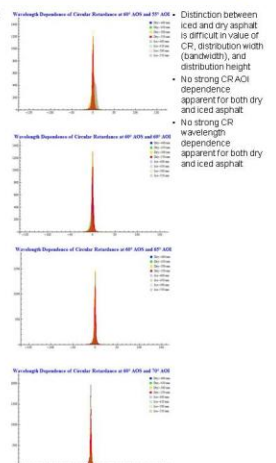
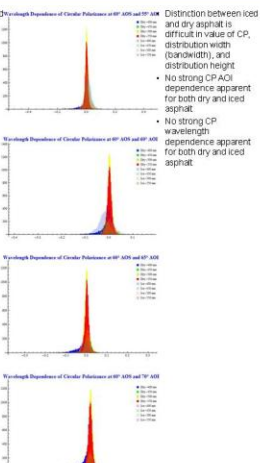
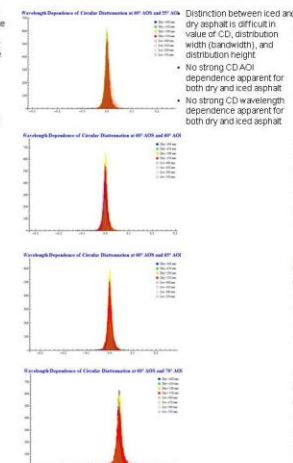
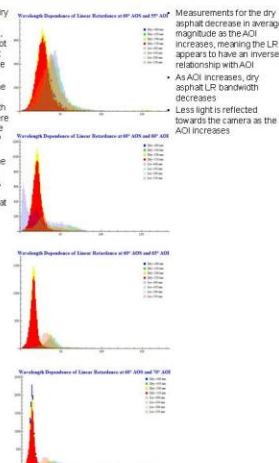
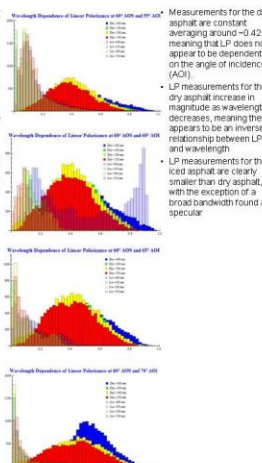
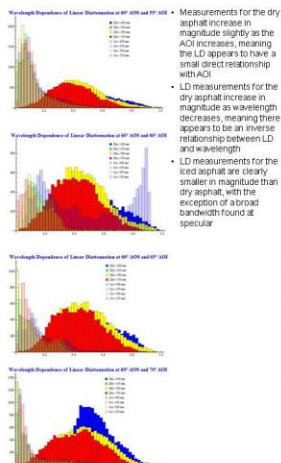
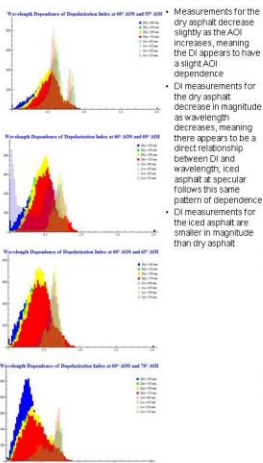
### Circular Polarization



### Circular Retardance



Angle of Scatter 65°



Note: This measurement does not include the AOS 30° AOI 25° due to a file corruption



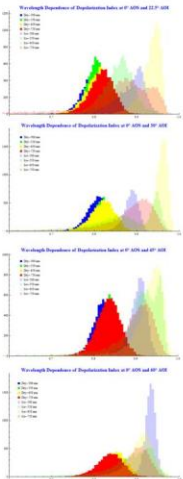
# Detecting Road Conditions with Polarimetry

Krista Drummond, Russell A. Chipman, Karlton Crabtree  
University of Arizona College of Optical Sciences



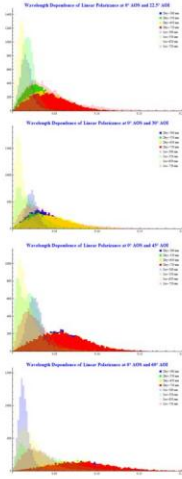
## Concrete (Measurement ConcA1) - Visible Spectrum

### Depolarization Index



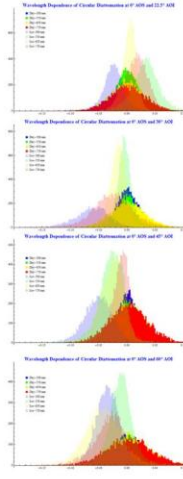
- Depolarization index (DI) is a single number metric for characterizing the depolarization of a Mueller matrix
- The DI equals one for non-depolarizing Mueller matrices and equals zero for an ideal depolarizer
- Iced concrete has a higher DI than dry concrete
- Measurements for the dry concrete increase in magnitude slightly as AOI increases, meaning there appears to be a small DI dependence on AOI
- DI measurements for the dry concrete slightly decrease as wavelength decreases, meaning there appears to be a slight direct relationship between DI and wavelength
- DI measurements for the iced concrete increase as the angle of incidence (AOI) increases, causing the different wavelengths to group together

### Linear Polarizance



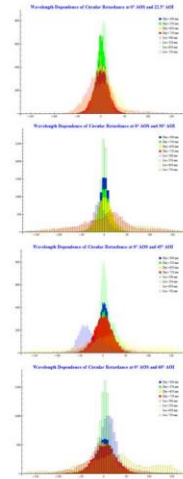
- Linear polarizance (LP) is the degree of linear polarization of the transmitted light when unpolarized light is incident
- A LP value of 1 is consistent with a perfect linear polarizer, in this case the DI cannot be zero
- Average value for the dry concrete LP increases as the AOI increases, meaning the LP appears to have a small angular dependence
- LP Measurements for the dry concrete increase in bandwidth as the AOI increases
- Iced concrete has a lower LP than dry concrete, and has about half of the bandwidth (in LP) than dry concrete

### Circular Diattenuation



- Circular diattenuation (CD) is the dependence of the intensity transmittance on the polarization state of the incident light, specifically the circular nature of the incident light
- A perfect circular diattenuator has a circular diattenuation (CD) value of 1; circular polarizers have circular diattenuation (CD) values close to 1
- Distinction between iced and dry concrete is difficult in value of CD, distribution width (bandwidth), and distribution height

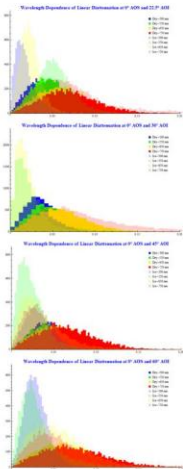
### Circular Retardance



- Circular retardance (CR) is the circular polarization-dependent phase change associated with the surface; the phase of the output beam depends upon the polarization state of the incident light
- Note that this polarization property is cyclical, meaning a value of  $180^\circ$  is equal to a value of  $0^\circ$  (i.e. CR period is  $180^\circ$  or  $\pi$ )
- Distinction between iced and dry concrete is difficult in value of CR, distribution width (bandwidth), and distribution height
- No strong CR AOI dependence apparent for both dry and iced concrete
- No strong CR wavelength dependence apparent for both dry and iced concrete

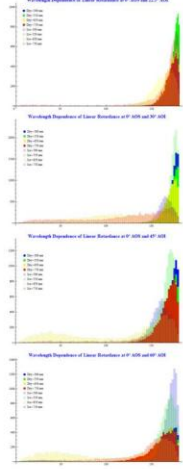
### Linear Diattenuation

- Linear diattenuation (LD) is the dependence of the intensity transmittance on the polarization state of the incident light, specifically the linear nature of the incident light
- A perfect linear diattenuator has a linear diattenuation (LD) value of 1; linear polarizers have linear diattenuation (LD) values close to 1
- Measurements for the dry concrete stay fairly constant at about  $\sim 0.06$  across the full AOI spectrum, meaning there appears to be no LD dependence on AOI
- Iced concrete has a lower LD than dry concrete, and has about half of the bandwidth (in LD) than dry concrete



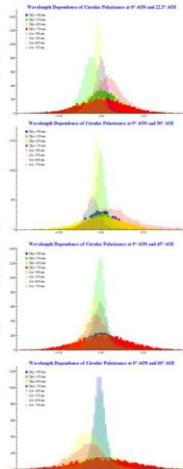
### Linear Retardance

- Linear retardance (LR) is the linear polarization-dependent phase change associated with the surface; the phase of the output beam depends upon the polarization state of the incident light
- Note that this polarization property is cyclical, meaning a value of  $180^\circ$  is equal to a value of  $0^\circ$  (i.e. LR period is  $180^\circ$  or  $\pi$ )
- Both the dry and iced concrete have a linear retardance (LR) of  $\sim 180^\circ$  ( $\pi/2$  radians)
- Iced concrete has a much broader bandwidth in the higher wavelengths (650 nm and 750) than dry concrete
- No strong LR AOI dependence apparent for both dry and iced concrete



### Circular Polarizance

- Circular polarizance (CP) is the degree of circular polarization of the transmitted light when unpolarized light is incident
- A CP value of 1 is consistent with a perfect circular polarizer, in this case the DI cannot be zero
- Dry concrete has a much broader bandwidth than iced concrete; dry concrete has a CP bandwidth  $\sim 3\times$  larger than iced concrete
- No strong CP AOI dependence apparent for both dry and iced concrete
- No strong CP wavelength dependence apparent for both dry and iced concrete



### Measurement Summary

- Note: This measurement set is missing data from wavelength 750 nm at AOI of  $30^\circ$

### Acknowledgements

1. Chipman, Russell A. "Depolarization Index and the Average Degree of Polarization." *Applied Optics* 44:13 (2005): 2600-2608. <https://doi.org/10.1364/AO.44.13.02600>  
 2. Chipman, Russell A. "Chapter 22. Polarimetry." *Handbook of Optical Devices, Measurements, & Properties* 2nd ed. Vol. 2. N.p.: McGraw-Hill, 1995. N. pag. 1116.



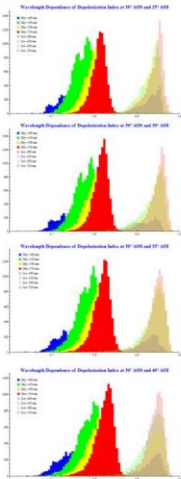
# Detecting Road Conditions with Polarimetry

Krista Drummond, Russell A. Chipman, Karlton Crabtree  
University of Arizona College of Optical Sciences



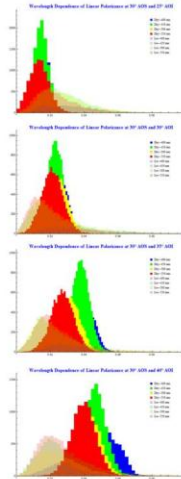
## Concrete (Measurement ConcA3) - Ultraviolet Spectrum

### Depolarization Index



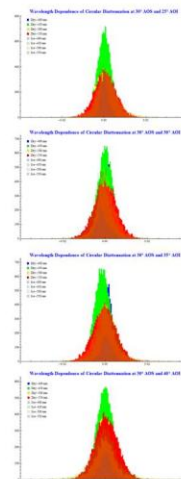
- Depolarization index (DI) is a single number metric for characterizing the depolarization of a Mueller matrix
- The DI equals one for non-depolarizing Mueller matrices and equals zero for an ideal depolarizer
- Iced concrete has a higher DI than dry concrete
- Measurements for the dry concrete increase in magnitude slightly as AOI increases, meaning there appears to be a small DI dependence on AOI
- DI measurements for the dry concrete slightly decrease as wavelength decreases, meaning there appears to be a slight direct relationship between DI and wavelength

### Linear Polarizance



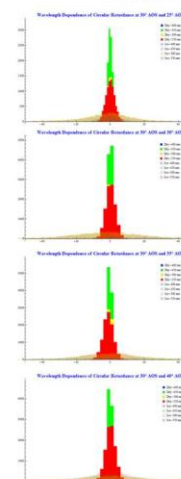
- Linear polarizance (LP) is the degree of linear polarization of the transmitted light when unpolarized light is incident
- A LP value of 1 is consistent with a perfect linear polarizer, in this case the DI cannot be zero
- Average value for the dry concrete LP increases as the AOI increases, meaning the LP appears to have a small angular dependence
- LP Measurements for the dry concrete increase in bandwidth as the AOI increases
- Iced concrete has a lower LP than dry concrete, and has about half of the bandwidth (in LP) than dry concrete

### Circular Diattenuation



- Circular diattenuation (CD) is the dependence of the intensity transmittance on the polarization state of the incident light, specifically the circular nature of the incident light
- A perfect circular diattenuator has a circular diattenuation (CD) value of 1; circular polarizers have circular diattenuation (CD) values close to 1
- Distinction between iced and dry concrete is difficult in value of CD, distribution width (bandwidth), and distribution height

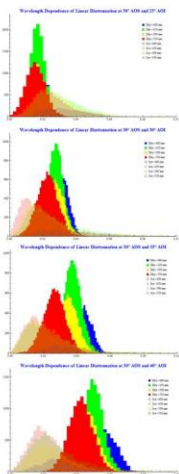
### Circular Retardance



- Circular retardance (CR) is the circular polarization-dependent phase change associated with the surface; the phase of the output beam depends upon the polarization state of the incident light
- Note that this polarization property is cyclical, meaning a value of  $180^\circ$  is equal to a value of  $0^\circ$  (i.e. CR period is  $180^\circ$  or  $\pi$ )
- Dry concrete has a narrow CR magnitude bandwidth while iced concrete has a CR magnitude bandwidth about 5x larger
- No strong CR AOI dependence apparent for both dry and iced concrete
- No strong CR wavelength dependence apparent for both dry and iced concrete

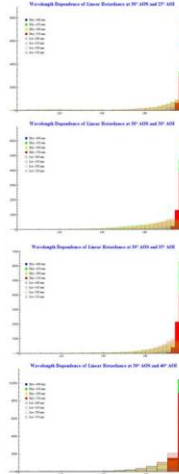
### Linear Diattenuation

- Linear diattenuation (LD) is the dependence of the intensity transmittance on the polarization state of the incident light, specifically the linear nature of the incident light
- A perfect linear diattenuator has a linear diattenuation (LD) value of 1; linear polarizers have linear diattenuation (LD) values close to 1
- Measurements for the dry concrete slightly increase as AOI increases, meaning there appears to be a slight direct LD dependence on AOI
- Iced concrete has a lower LD than dry concrete
- LD magnitude for the dry concrete slightly increase as wavelength decreases, meaning there appears to be a slight inverse relationship between DI and wavelength



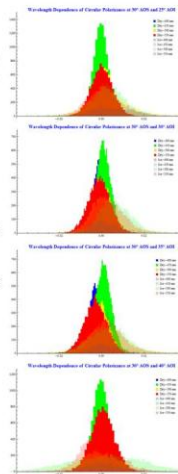
### Linear Retardance

- Linear retardance (LR) is the linear polarization-dependent phase change associated with the surface; the phase of the output beam depends upon the polarization state of the incident light
- Note that this polarization property is cyclical, meaning a value of  $180^\circ$  is equal to a value of  $0^\circ$  (i.e. LR period is  $180^\circ$  or  $\pi$ )
- Both the dry and iced concrete have a linear retardance (LR) of  $\sim 180^\circ$  ( $\pi/2$  radians)
- Iced concrete has a much broader than dry concrete
- No strong LR AOI dependence apparent for both dry and iced concrete



### Circular Polarizance

- Circular polarizance (CP) is the degree of circular polarization of the transmitted light when unpolarized light is incident
- A CP value of 1 is consistent with a perfect circular polarizer, in this case the DI cannot be zero
- Both dry and iced concrete have almost no CP
- No strong CP AOI dependence apparent for both dry and iced concrete
- No strong CP wavelength dependence apparent for both dry and iced concrete



## Measurement Summary

## Acknowledgements

1. Chipman, Russell A. "Depolarization Index and the Average Degree of Polarization." *Applied Optics* 44:13 (2005): 2600-2605. <https://doi.org/10.1364/AO.44.13.02600>  
 2. Chipman, Russell A. "Chapter 22. Polarimetry." *Handbook of Optical Devices, Measurements, & Properties* 2nd ed. Vol. 2. N.p.: McGraw-Hill, 1995. N.p. pag. 1116.

# Detecting Road Conditions with Polarimetry

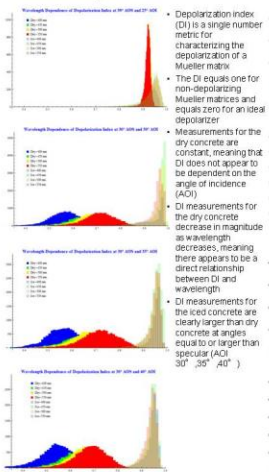
Krista Drummond, Russell A. Chipman, Karlton Crabtree  
University of Arizona College of Optical Sciences



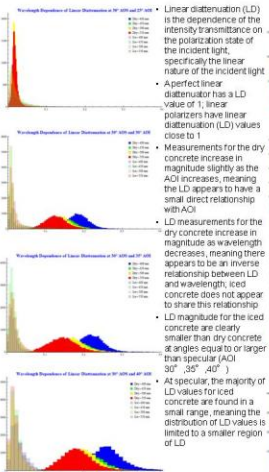
## Concrete (Measurement ConcB1) – Ultra Violet Spectrum

Angle of Scatter: 90°

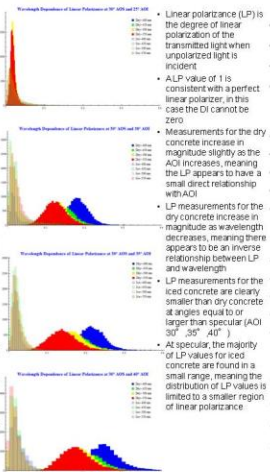
### Depolarization Index



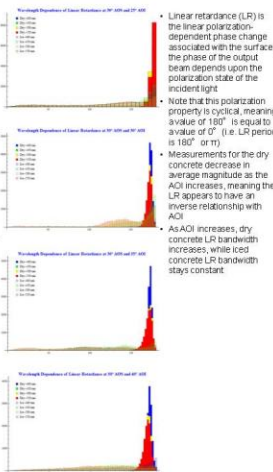
### Linear Diattenuation



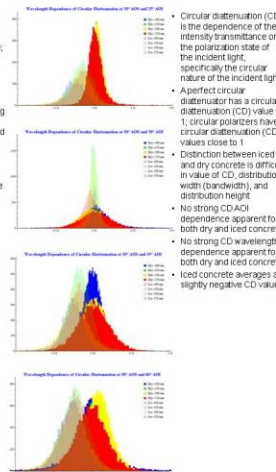
### Linear Polarization



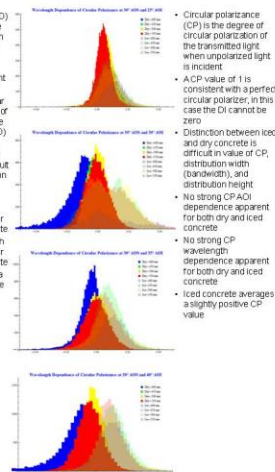
### Linear Retardance



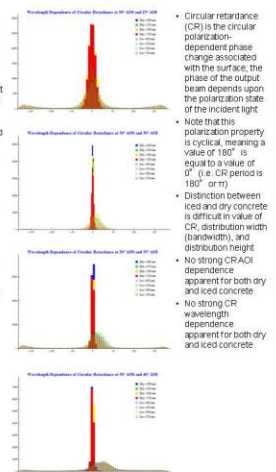
### Circular Diattenuation



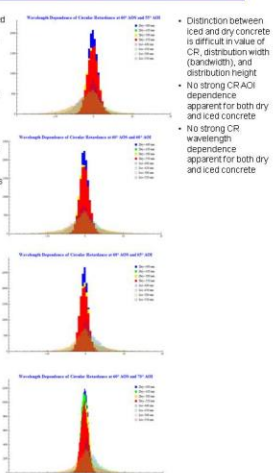
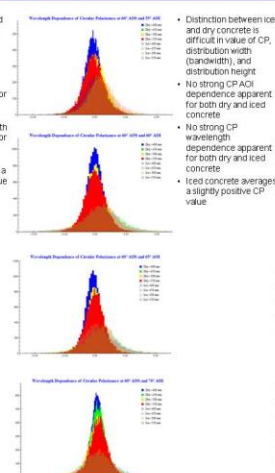
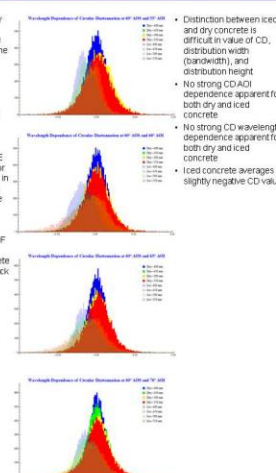
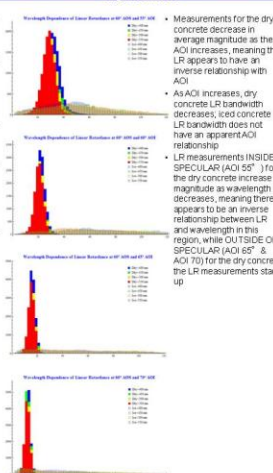
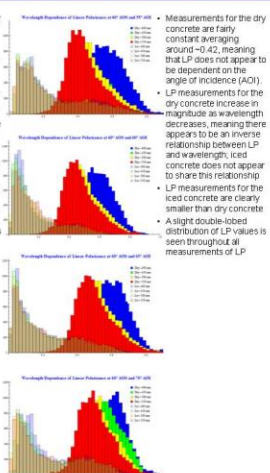
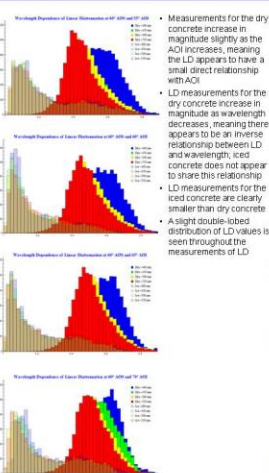
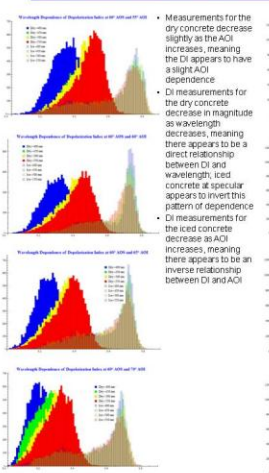
### Circular Polarization



### Circular Retardance



Angle of Scatter: 60°





# Detecting Road Conditions with Polarimetry

Krista Drummond, Russell A. Chipman, Karlton Crabtree  
University of Arizona College of Optical Sciences

## Wet Sample Polarimetric Survey – 500 nm, Spectral 30° Imaging

### Measurement

- Progression Measurement**, meaning this series of measurements will be measuring the Mueller matrix of a wet sample as it progresses from dry to wet, back to dry.
- This measurement was done to evaluate the response of the polarization properties of the sample surface to the presence of liquid water
- System Repeatability**, meaning this series of measurements shows the reliability of the polarimeter
- Compare the Dry measurement to the 0 Sprays (3) measurement

### Method

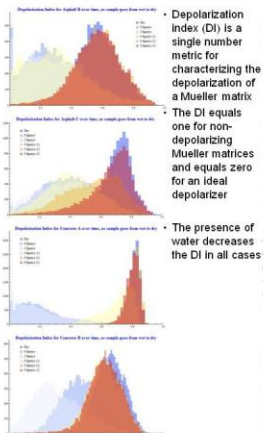
- Wavelength: 500 nm, AOS: 30°, AOI: 30°
- Samples were mounted in the UV polarimeter using the same setup as described in Campaign 2
- Measurement of dry sample taken
- Sample was then wet evenly using a deionized water filled spray bottle
- Measurements of surface temperature and surface resistance were measured
- Mueller Matrix was then measured
- Method repeated for varying degrees of "wetness":
  - Dry – No water on surface
  - 8 Sprays – 8 sprays of the spray bottle were sprayed onto the surface of the sample
  - 2 Sprays – 2 sprays of the spray bottle were sprayed onto the still wet surface of the sample, this would have a thinner layer of surface water than 8 Sprays, but more than 0 Sprays (1)
  - 0 Sprays (1) – No additional water added to the surface of the sample
  - 0 Sprays (2) – Second measurement where no additional water is added to the surface of the sample
  - 0 Sprays (3) – Third measurement where no additional water is added to the surface of the sample; by this measurement the surface of the sample is dry, a state recognized by the lighter color of the sample surface

### Data

- New surface variables were recorded in order to better understand and model the water layer present during a measurement – Resistance ( $\Omega$ ) measurements of the surface have been included
- Resistance of the sample surface should give us a good indication of the water layer thickness
- The histograms below show the surface wetness dependence of each of the polarization properties for each of the samples (excluding sample Asphalt A; dry measurement overwritten)

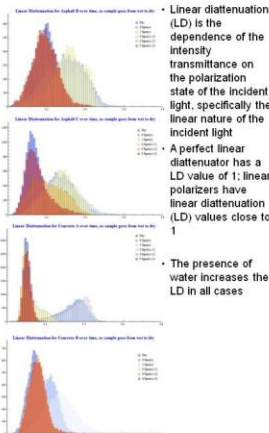
	Dry		0 Sprays		2 Sprays		0 Sprays (1)		0 Sprays (2)		0 Sprays (3)	
	Temperature e (°C)	Resistance (Ω)	Temperature e (°C)	Resistance (Ω)	Temperature e (°C)	Resistance (Ω)	Temperature e (°C)	Resistance (Ω)	Temperature e (°C)	Resistance (Ω)	Temperature e (°C)	Resistance (Ω)
Asphalt A	25.9	inf	23.2	1.78 M	19.3	1.863 M	18.1	inf	20.9	inf	21.3	inf
Asphalt B	24.2	inf	22	inf	18.5	1.90 M	17.7	1.64 M	19.6	inf	20.7	inf
Asphalt C	24.7	inf	19.8	1.34 M	18	1.756 M	17.8	inf	18.6	inf	20.7	inf
Concrete A	24.2	inf	20.9	1.836 M	17	1.51 M	15.7	inf	15.7	inf	15.9	inf
Concrete B	24.4	inf	20.4	1.002 M	17.4	1.901 M	16.2	inf	18.1	inf	19.2	inf

### Depolarization Index



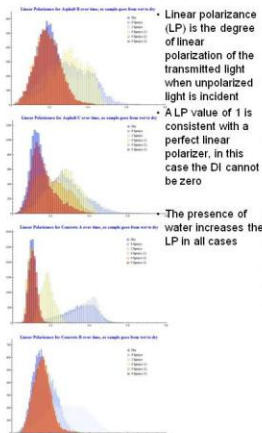
- Depolarization Index (DI) is a single number metric for characterizing the depolarization of a Mueller matrix
- The DI equals one for non-depolarizing Mueller matrices and equals zero for an ideal depolarizer
- The presence of water decreases the DI in all cases

### Linear Diattenuation



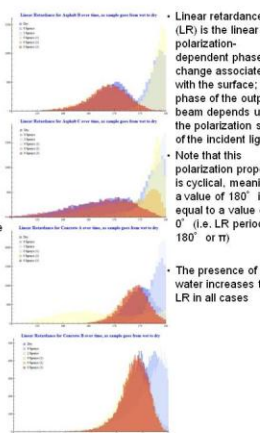
- Linear diattenuation (LD) is the dependence of the intensity transmittance on the polarization state of the incident light, specifically the linear nature of the incident light
- A perfect linear diattenuator has a LD value of 1; linear polarizers have linear diattenuation (LD) values close to 1
- The presence of water increases the LD in all cases

### Linear Polarizance



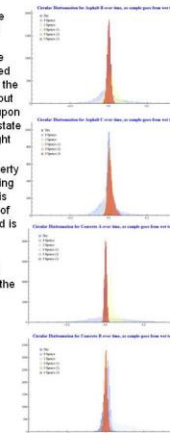
- Linear polarizance (LP) is the degree of linear polarization of the transmitted light when unpolarized light is incident
- A LP value of 1 is consistent with a perfect linear polarizer. In this case the DI cannot be zero
- The presence of water increases the LP in all cases

### Linear Retardance



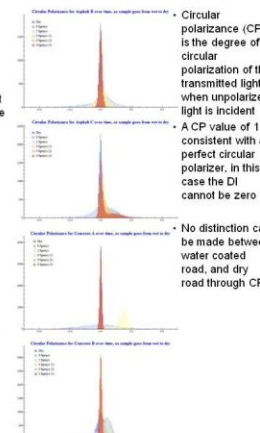
- Linear retardance (LR) is the linear polarization-dependent phase change associated with the surface; the phase of the output beam depends upon the polarization state of the incident light
- Note that this polarization property is cyclical, meaning a value of 180° is equal to a value of 0° (i.e. LR period is 180° or  $\pi$ )
- The presence of water increases the LR in all cases

### Circular Diattenuation



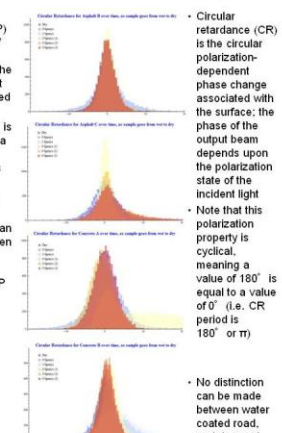
- Circular diattenuation (CD) is the dependence of the intensity transmittance on the polarization state of the incident light, specifically the circular nature of the incident light
- A perfect circular diattenuator has a circular diattenuation (CD) value of 1; circular polarizers have circular diattenuation (CD) values close to 1
- No distinction can be made between water coated road, and dry road through CD

### Circular Polarizance



- Circular polarizance (CP) is the degree of circular polarization of the transmitted light when unpolarized light is incident
- A CP value of 1 is consistent with a perfect circular polarizer. In this case the DI cannot be zero
- No distinction can be made between water coated road, and dry road through CP

### Circular Retardance



- Circular retardance (CR) is the circular polarization-dependent phase change associated with the surface; the phase of the output beam depends upon the polarization state of the incident light
- Note that this polarization property is cyclical, meaning a value of 180° is equal to a value of 0° (i.e. CR period is 180° or  $\pi$ )
- No distinction can be made between water coated road, and dry road through CR

## BIBLIOGRAPHY

- Chipman, Russell A., Pierre-Yves Gerligand, Elizabeth A. Sornsin, and Matthew H. Smith. *Polarization Diversity Active Imaging: Mueller Matrix Imaging Polarimetry of Spheres and Cones*. Rep. N.p.: n.p., n.d. Print.
- Cronin, T. W., and J. Marshall. "Patterns and Properties of Polarized Light in Air and Water." *Philosophical Transactions of the Royal Society B: Biological Sciences* 366.1565 (2011): 619-26. Web. 11 Oct. 2014. <<http://rstb.royalsocietypublishing.org>>.
- Matrosov, Sergey Y., Roger F. Reinking, Robert A. Kropfli, and Bruce W. Bartram. "Estimation of Ice Hydrometeor Types and Shapes from Radar Polarization Measurements." *Journal of Atmospheric and Oceanic Technology* 13 (1996): 85-96. Web.
- Miller, D., M. S. Quinby-Hunt, and A. J. Hunt. "Laboratory Studies of Angle- and Polarization-dependent Light Scattering in Sea Ice." *Applied Optics* 36.6 (1997): 1278-288. Web.
- Najibi, Nasser, and Shuanggen Jin. "Physical Reflectivity and Polarization Characteristics for Snow and Ice-Covered Surfaces Interacting with GPS Signals." *Remote Sensing* 5.8 (2013): 4006-030. Web.
- Perovich, Donald K. "Observations of the Polarization of Light Reflected from Sea Ice." *Journal of Geophysical Research* 103.C3 (1998): 5563-575. Web.
- Sprawls, Perry. "Image Characteristics and Quality." *The Physical Principles of Medical Imaging*. 2nd ed. Madison, WI: Medical Physics Pub, 1995. N. pag. *The Web-based Edition of The Physical Principles of Medical Imaging*. Medical Physics Publishing. Web. 24 Apr. 2014.
- Sun, Zhongqiu, Jiquan Zhang, and Yunsheng Zhao. "Laboratory Studies of Polarized Light Reflection From Sea Ice and Lake Ice in Visible and Near Infrared." *IEEE Geoscience and Remote Sensing Letters* 10.1 (2013): 170-73. Web.